



**HAL**  
open science

# Low fouling membranes for water and bio tech applications

Lucia Benavente

► **To cite this version:**

Lucia Benavente. Low fouling membranes for water and bio tech applications. Chemical and Process Engineering. Université Paul Sabatier - Toulouse III, 2016. English. NNT : 2016TOU30213 . tel-01548291

**HAL Id: tel-01548291**

**<https://theses.hal.science/tel-01548291>**

Submitted on 27 Jun 2017

**HAL** is a multi-disciplinary open access archive for the deposit and dissemination of scientific research documents, whether they are published or not. The documents may come from teaching and research institutions in France or abroad, or from public or private research centers.

L'archive ouverte pluridisciplinaire **HAL**, est destinée au dépôt et à la diffusion de documents scientifiques de niveau recherche, publiés ou non, émanant des établissements d'enseignement et de recherche français ou étrangers, des laboratoires publics ou privés.



Université  
de Toulouse

# THÈSE

En vue de l'obtention du

**DOCTORAT DE L'UNIVERSITÉ DE TOULOUSE**

Délivré par : *l'Université Toulouse 3 Paul Sabatier (UT3 Paul Sabatier)*

---

---

Présentée et soutenue le *03/11/2016* par :

**BENAVENTE LUCÍA**

**Low Fouling Membranes for Water and Bio tech Applications**

---

---

## JURY

CRESPO JOÃO	Professeur, Universidade Nova de Lisboa	Rapporteur
RABILLER MURIELLE	Professeur, Université de Rennes	Rapporteur
BRÉHANT ANNE	Dr., Suez Environnement	Membre du jury
CHANG YUNG	Professeur, Chung Yuan Christian University	Membre du jury
BACCHIN PATRICE	Professeur, LGC Université de Toulouse	Directeur de thèse
AIMAR PIERRE	DR CNRS, LGC, Université de Toulouse	Directeur de thèse

---

### École doctorale et spécialité :

*MEGEP : Génie des procédés et de l'Environnement*

### Unité de Recherche :

*Laboratoire de Génie Chimique de Toulouse*

### Directeur(s) de Thèse :

*AIMAR Pierre et BACCHIN Patrice*

### Rapporteurs :

*CRESPO João et RABILLER-BAUDRY Murielle*





*Cuando creíamos que teníamos todas las respuestas,  
de pronto, cambiaron todas las preguntas.*

*When we thought we had all the answers,  
suddenly, all the questions changed.*

Mario BENEDETTI



---

## Acknowledgments

First of all, I would like to thank the Agence Nationale de la Recherche (ANR, France) for the financial support.

The initial quote is one of my favourite phrases, which reminds me of the continuity of change, a change that includes every aspect of life. Change has been one of the common denominators during this thesis project, combined with the need to adapt in order to continue. Thus, I express my eternal gratitude to my scientific partners and supervisors during this journey: Pierre, Patrice, Christel and Clémence, to whom I will always be grateful for the many meetings, and discussions, that guided me through these three years of hard and constant work, with its many turns and loops.

This journey also gave me the chance into continuing one of my passions: travelling. Visiting Taiwan to meet the partners of the project and working with them was the icing on the cake for a world-hungry person such as myself. Therefore, I thank all the professors and students from the Membrane and Research Center for Membrane Technology of the Chung Yuan Christian University in ChungLi for an unforgettable one and a half months of teachings and learning, particularly, to Prof. Lai, Prof. Chang, Assoc. Prof. Venault, Brian, Jason, and all the other students of the centre that were helping me daily.

Special thanks to the members of the jury: Prof. Rabiller-Baudry, Prof. Crespo, Dr. Brehant, and Prof. Chang, for reviewing my work and being present during the presentation. Your questions and comments were highly appreciated, and helped improving the quality of the work while adding future challenges to be solved. Merci beaucoup! Muito obrigada! Xie xie!

Je voudrais remercier spécialement à Corinne Routaboul du Service commun de spectroscopie infrarouge et Raman - Institut de Chimie de Toulouse - pour votre soutien pour la partie d'analyse de cartographie FTIR.

Je voudrais aussi remercier à tout l'équipe du Laboratoire de Génie Chimique à Toulouse, pour le soutien que j'ai reçu de tous pendant ces trois années. Particulièrement à Sebastian Teychené, Nhat et Dmytro pour tout ce qui concerne la partie de préparation des puces microfluidiques.

---

It will be hard to leave, but the show must go on. I will keep many special memories, memories that involve many other (ex-) doctoral/master candidates (in order of appearance throughout the years and/or my mind): Dima and Iza – my companions on a very international trip since we arrived for our Erasmus Master five years ago –, Makarronis, Arturo I, Alessio, Joseph, Aurelie, Le, Zena, Nhat, Panwana, Waritha, Yandi, Mel G., Meredith, Aamir, Anto, Abi, Arthur II, Johanne, Christian, Flavie, Paul, Hugo, Veysi, Nayan, Shazia, Melissa, Audrey, Anaïs, Samir, Cécilia, Alexis, Florent, Yin, Airy, and Vincent. I hope I am not forgetting anybody, if not you can insert your name in the following blank lines:

Thank you for being my emotional support during all of these years, because carrying on a project for so long does not come free of hurdles, and you made tough times easier and good ones much more enjoyable.

There are two particularly important students to whom I want to dedicate this paragraph: Maithili and Anja. They came from lands far far away and made an exceptional work that was utterly paramount for the fulfillment of this thesis. It was a pleasure working with you and being part of your first steps into research.

These lines go to my Erasmus Mundus family: five years ago we started a gipsy journey together, and even though distance separates us again, I feel like it does not have any effect on us. I hope we will have many more years of get-togethers, international weddings, and crazy trips.

Finalmente, y no menos importante, paso a dedicar unas palabras a mis primeros agentes de cambio: mi familia. A los que se han ido, a los que siguen y a los que han llegado: gracias por todo el apoyo que siempre me dieron, y por siempre darme ese empujón de energía transmitido a través del espacio-tiempo y contra toda ley natural o teoría científica.





---

## Résumé

La pénurie d'eau est devenue un des problèmes clés à résoudre, et pour y faire face, il est nécessaire de disposer d'unités de traitement de l'eau efficaces. Au cours des dernières décennies la technologie des membranes est devenue l'une des techniques les plus prometteuses pour le traitement de l'eau. Néanmoins, les membranes ont une durée de vie limitée et sont, par ailleurs, sujettes à des phénomènes de colmatage - le dépôt, l'adsorption et l'absorption de particules dans la structure de la membrane -, ce qui réduit leur productivité, et augmente les coûts opérationnels. Une approche pour minimiser ce problème consiste à modifier des membranes hydrophobes, mécaniquement et chimiquement stables, en y greffant des matériaux amphiphiles afin de réduire le colmatage. L'objectif principal de ce travail est de caractériser les propriétés anti-colmatage des membranes de PVDF (Polyvinylidène fluoride) modifiées avec différents types de copolymères PS-PEGMA (Polystyrène – Poly(ethylene glycol) methacrylate), tout d'abord par l'utilisation de techniques classiques, puis, par le développement et / ou l'adaptation de techniques microfluidiques couplés à la microscopie à fluorescence et l'utilisation de la cartographie par microspectroscopie infrarouge à transformée de Fourier (IRTF). La cartographie IRTF a permis de quantifier localement le greffage et de mettre en évidence l'hétérogénéité du greffage sur la membrane. Ces cartes, représentant l'importance du greffage sur la membrane, ont par ailleurs été corrélées au dépôt de protéines sur la surface. Des systèmes microfluidiques ont également été développés pour caractériser sous microscope à fluorescence l'adsorption de protéines fluorescentes sur une membrane en présence d'un débit. Cette étude permet de suivre in situ et en dynamique l'adsorption (lors de cycles de filtration) et la désorption (lors de cycles de rinçage) de protéines sur la membrane. Ces mesures locales ont été mises en regard avec des mesures de perméabilité lors de cycles filtrations/rinçage mettant en évidence un rôle anti-fouling en particulier pour les copolymères tri-blocs ou pour les copolymères à enchaînement aléatoire.

## Summary

Water scarcity has become one of the key issues to solve, and efficient water treatment is paramount to treat water sources. In recent decades membrane technology has become one of the promising solutions for water treatment. Nevertheless, membranes are prone to fouling phenomena - the deposition, adsorption, and absorption of particles in the membrane structure -, which hinders their life-span and productivity, and raise operative costs. One approach to minimize this issue is to modify the already mechanically and chemically stable hydrophobic membranes with amphiphilic materials. The main aim of this work is to characterise the anti-fouling properties of PVDF (Polyvinylidene fluoride) membranes modified with different types of PS-PEGMA (Polystyrene – Poly(ethylene glycol) methacrylate) copolymers, firstly by using classical techniques, and then, by developing and/or adapting new ones: microfluidic devices coupled with fluorescence microscopy, and the use of Fourier Transform Infrared microspectroscopy (FTIR mapping). FTIR mapping allowed the local detection of the coating layer and showed its heterogeneous distribution on the surface of the membrane. These maps, that represent the importance of the coating on the membrane, were correlated with the deposit of proteins on the surface. Microfluidic systems were also developed to characterise the adsorption of fluorescent proteins on the membrane under a fluorescent microscope in the presence of a flow. This study allowed the in-situ and dynamic follow-up of the adsorption – during filtration cycles – and of the desorption – during rinsing cycles – of the proteins on the membrane. These local measurements were compared against permeability measurements during the filtration/rinsing cycles evidencing the anti-fouling role of the copolymers used for the modification of the membranes, particularly for the triblock and random copolymers.

# Contents

<b>List of Figures</b>	<b>ix</b>
<b>List of Tables</b>	<b>xv</b>
<b>List of Abbreviations</b>	<b>xvii</b>
<b>1 General Introduction</b>	<b>1</b>
1 A summary on water and crisis . . . . .	3
2 Membrane technology for water treatment . . . . .	5
2.1 Membrane processes . . . . .	7
2.2 Membrane materials . . . . .	8
2.2.1 Polymeric membranes . . . . .	9
3 Membrane fouling . . . . .	11
3.1 Foulants and types of fouling . . . . .	12
3.2 Factors that affect fouling phenomena . . . . .	13
3.2.1 Hydrophilicity . . . . .	13
3.2.2 Roughness . . . . .	14
3.2.3 Charge . . . . .	15
3.2.4 Steric hindrance/repulsion . . . . .	15
4 Management of fouling for membrane filtration processes - Membrane modification . . . . .	17

---

5	Techniques for the characterisation of the modification of membranes and of their anti-fouling properties . . . . .	21
6	Presentation of the SuperNAM project . . . . .	25
7	Objectives . . . . .	26
8	References . . . . .	27
<b>2</b>	<b>Membrane modification and anti-fouling properties assessment</b>	<b>37</b>
1	Introduction . . . . .	39
1.1	Membrane modification with PS-PEGMA copolymers . . . . .	39
1.2	Characterisation methods . . . . .	41
1.3	Objectives . . . . .	42
2	Materials and Methods . . . . .	44
2.1	Materials . . . . .	44
2.2	Methods . . . . .	45
2.2.1	Coating of the membranes . . . . .	45
2.2.2	Determination of the coating density . . . . .	45
2.2.3	Water contact angle . . . . .	46
2.2.4	Hydration capacity . . . . .	46
2.2.5	XPS . . . . .	46
2.2.6	Protein adsorption . . . . .	48
2.2.7	Blood cell adsorption . . . . .	48
2.2.8	Filtration protocol . . . . .	49
2.2.9	Analysis of fouling - Resistances in series . . . . .	51
3	Results and Discussion . . . . .	54
3.1	Physical and chemical properties of the modified membranes . . . . .	54
3.1.1	Coating density . . . . .	55
3.1.2	Water contact angle and hydration capacity . . . . .	58
3.1.3	X-ray photoelectron spectroscopy (XPS) . . . . .	60
3.2	General biofouling tests . . . . .	62
3.2.1	Adsorption of proteins . . . . .	63
3.2.2	Adsorption of blood cells . . . . .	65
3.3	Filtration tests . . . . .	69
3.4	Analysis of fouling - resistances in series . . . . .	72

---

3.5	General discussion . . . . .	73
4	Conclusions . . . . .	77
5	References . . . . .	79
<b>3</b>	<b>Coupling of microfluidic chips with fluorescence microscopy for the study of fouling</b>	<b>81</b>
1	Introduction . . . . .	83
1.1	Objectives . . . . .	85
2	Methodology . . . . .	86
2.1	Materials . . . . .	86
2.2	Chip fabrication . . . . .	87
2.3	Filtration protocol . . . . .	89
2.4	Image analysis protocol . . . . .	93
2.5	Calculations . . . . .	93
3	Results and Discussion . . . . .	96
3.1	Comparison of fluxes in the microchip with dead-end filtration	96
3.2	Coupling of filtration and fluorescence data . . . . .	99
4	Conclusions . . . . .	109
5	References . . . . .	111
<b>4</b>	<b>FTIR mapping for the study of coating and fouling</b>	<b>113</b>
1	Introduction . . . . .	115
1.1	Objectives . . . . .	117
2	Materials and Methods . . . . .	119
2.1	Materials . . . . .	119
2.2	Methods . . . . .	120
2.2.1	Membrane casting . . . . .	120
2.2.2	Coating . . . . .	120
2.2.3	BSA adsorption . . . . .	120
2.2.4	Contact Angle . . . . .	121
2.2.5	Coating density . . . . .	121
2.2.6	FTIR mapping . . . . .	122
3	Methodology for the analysis of FTIR maps . . . . .	124

---

3.1	Measurement of the average grey value . . . . .	124
3.2	Analysis of heterogeneity - Methodology for the definition of coating and adsorption levels . . . . .	125
4	Results and Discussion . . . . .	127
4.1	Variation of copolymer concentration in coating solution . .	127
4.2	Variation of coating time . . . . .	135
5	Conclusions . . . . .	142
6	References . . . . .	143
<b>5</b>	<b>Filtration-rinsing cycles for the assessment of fouling reversibility</b>	<b>147</b>
1	Introduction . . . . .	149
1.1	Objectives . . . . .	149
2	Materials and Methods . . . . .	151
2.1	Materials . . . . .	151
2.2	Methods . . . . .	151
2.2.1	Coating of the membranes . . . . .	151
2.2.2	Water contact angle . . . . .	152
2.2.3	FTIR analysis . . . . .	152
2.2.4	Filtration protocol . . . . .	153
2.2.5	Detection of BSA . . . . .	155
3	Results and Discussion . . . . .	157
3.1	Characterisation of the membranes . . . . .	157
3.2	Evaluation of the coating time in the filtration performance of the membranes . . . . .	161
4	Conclusions . . . . .	171
5	References . . . . .	173
<b>6</b>	<b>General conclusions and perspectives</b>	<b>175</b>
	References . . . . .	181
	<b>Appendix</b>	<b>183</b>
<b>A</b>	<b>Supplementary material on the characterisation of the modified membranes</b>	<b>185</b>

---

1	Scanning electron microscopy (SEM) and Atomic force microscopy (AFM) . . . . .	187
2	Confocal images of the WBC and PRP for the modified membranes	191
<b>B</b>	<b>Supplementary information on the selection of the peaks of interest</b>	<b>193</b>
<b>C</b>	<b>Scientific communication</b>	<b>197</b>



# List of Figures

1.1	World market sales distribution for membranes and membrane equipment per market segment. Adapted from [14]	6
1.2	Example of membrane processes	6
1.3	Pressure-driven membrane processes: pore sizes, TMP, and particle size ranges	8
1.4	Diagram for the different operation modes: cross-flow and dead-end filtration	9
1.5	Structure of the PVDF molecule	10
1.6	Diagram of the factors that affect fouling phenomena	13
1.7	FTIR technique. <b>(A)</b> : Schematics on the stretching of the bonds when irradiated with a beam and the generation of the subsequent spectra. <b>(B)</b> : Regions of the spectrum where the concerned bonds typically absorb (taken from [69])	22
1.8	Comparison of membrane area and filtration volumes necessary for a typical laboratory-scale filtration device (left) and a membrane inserted inside a microfluidic device (right)	24
2.1	Chemical structure of the PS-PEGMA copolymers [1, 2]	39
2.2	Diagram of the structure of the copolymers used in this work	40
2.3	Example of the variation of the peaks for the C1s spectrum	47
2.4	Diagram of the protocol for the filtration	50

---

2.5	Illustration of the parameters taken into account to calculate the reversibility index . . . . .	51
2.6	General chart on the results for this chapter . . . . .	54
2.7	Calculated coating density for the diblock, random and triblock copolymers as a function of copolymer concentration in the coating solution. Top: coating density in mg/cm <sup>2</sup> , bottom: molar coating density in nmol/cm <sup>2</sup> . . . . .	56
2.8	Water contact angle and Hydration capacity for the diblock, random and triblock copolymers as a function of molar coating density . . .	59
2.9	Water contact angle as a function of Hydration capacity for the diblock, random and triblock copolymers . . . . .	61
2.10	Evolution of copolymer present on the membrane surface for the different copolymers as a function of molar coating density, calculated from XPS data . . . . .	63
2.11	Protein adsorption as a function of the molar coating density for the diblock, random, and triblock copolymers. Top: Adsorption of BSA; bottom: adsorption of LYZ . . . . .	64
2.12	Example of confocal microscopy images of RBC for the membranes coated with different concentrations of copolymers . . . . .	66
2.13	Blood cell count of RBC, WBC, and PRP for the membranes coated with different concentrations of copolymers as a function of molar density. Top: RBC; middle: WBC, and bottom: PRP . . . . .	68
2.14	Filtration tests for the unmodified and modified membranes. Top: Permeabilities vs. time; bottom: relative fluxes vs. time . . . . .	71
2.15	Relationship between protein adsorption and hydration capacity. Top: BSA adsorption; bottom: LYZ adsorption . . . . .	75
3.1	Comparison of an Amicon filtration cell with a microfluidics chip .	83
3.2	Schematic representation of the fabrication process of the microfluidic device . . . . .	88

---

3.3	Microfluidic chip. <b>(A)</b> Design of the different layers: 1-retentate, 2-membrane and 3-permeate; <b>(B)</b> 3D diagrams of the layers and chip assembly; and <b>(C)</b> real chip. Each chip has two membranes with two channel per membrane. One channel (blue) has a length, height, and width of 2 cm, 300 $\mu\text{m}$ , and 630 $\mu\text{m}$ , respectively . . . . .	89
3.4	Diagram of the equipment used in combination with the microfluidic chip . . . . .	90
3.5	Protocol of the filtration performed with the microfluidic chips . . .	92
3.6	Image analysis. <b>A:</b> Diagram of the measurement of the GV at different positions of the channel; <b>B:</b> Diagram of the measurement of the GV for the whole channel; and <b>C:</b> Grey value scale for an 8-bit image . . . . .	93
3.7	Permeabilities obtained for the microchip vs Amicon cell for the unmodified membrane (virgin - upper graph) and membranes modified with 5 mg/mL triblock copolymer for two hours (lower graph) . . . . .	97
3.8	Images of the channels taken at different points of the filtration experiments of the unmodified membrane (virgin - upper images) and membranes modified with 5 mg/mL triblock copolymer for two hours (lower images) . . . . .	100
3.9	Measured average grey values at different sites of the channel for the unmodified membrane (virgin) and membranes modified with random and triblock copolymer . . . . .	101
3.10	Image of the channel at the end of the second BSA filtration for the membrane modified with the random copolymer . . . . .	102
3.11	Evolution of the measured average grey values for the whole channel and the permeability of the membranes for the unmodified membrane (virgin) and membranes modified with the random and triblock copolymer . . . . .	103
3.12	Permeability and Relative permeability versus average grey value during the filtration of BSA for the unmodified membrane (virgin) and membranes modified with the random and triblock copolymer .	105

---

3.13	Evolution of the flux and grey value indexes after each filtration/rinsing cycle for the experiments performed in the microfluidic chips. FDR ratio was calculated by dividing the $FDR_{flux}$ by the $FDR_{GV}$ . . . . .	107
4.1	Sample spectra of a coated and fouled membrane with additional information on the peaks of interest, functional groups related to them and to the compounds present in our study . . . . .	123
4.2	Colour (up) and grey (down) scale bars for peak heights between 0.0 and 0.5 . . . . .	124
4.3	Example of FTIR maps obtained for membranes modified with the random copolymer at different concentrations. Each map has an area of $1 \text{ mm}^2$ . . . . .	128
4.4	Example of FTIR maps obtained for membranes modified with the diblock copolymer at different concentrations. Each map has an area of $1 \text{ mm}^2$ . . . . .	129
4.5	Image of the membrane surface modified with the random copolymer and incubated with $1 \text{ g/L}$ BSA solution. Virgin membrane (upper left) and modified with copolymer solution concentration of $1 \text{ mg/mL}$ (upper right), $5 \text{ mg/mL}$ (lower right), and $10 \text{ mg/mL}$ (lower left). The mesh is a consequence of the images taken by the microscope to determine the subsequent surface to be analysed by the FTIR microspectrometer . . . . .	130
4.6	Average peak height of the $1737 \text{ cm}^{-1}$ and $3300 \text{ cm}^{-1}$ peaks as a function of random (RND) and diblock (DB) copolymer concentration . . . . .	131
4.7	Evolution of the foulant adsorbed as a function of the copolymer presence for the different coating concentrations . . . . .	132
4.8	Coverage and adsorption levels for the membranes modified with different random copolymer concentrations and a coating time of 2 h . . . . .	133
4.9	Coverage and adsorption levels for the membranes modified with different diblock copolymer concentrations and a coating time of 2 h . . . . .	134

---

4.10	Measured area percentages for the different coverage and adsorption levels as a function of copolymer concentration. <b>(A)</b> and <b>(B)</b> : Random copolymer; <b>(C)</b> and <b>(D)</b> : Diblock copolymer . . . . .	135
4.11	Water contact angle and average coating densities as a function of coating time. Coating solution: 5 mg of random copolymer per mL of ethanol . . . . .	136
4.12	Example of FTIR maps obtained for membranes modified with the random copolymer at different coating times while keeping the copolymer concentration at 5 mg/mL. Each map has an area of 1 mm <sup>2</sup>	137
4.13	Average peak height of the 1737 cm <sup>-1</sup> and 3300 cm <sup>-1</sup> peaks as a function of coating time for the random and diblock copolymers . . .	138
4.14	Evolution of the foulant adsorbed as a function of the copolymer presence for the different coating times and copolymers . . . . .	139
4.15	Measured area percentages for the different coverage and adsorption levels as a function of coating time. <b>(A)</b> and <b>(B)</b> : Random copolymer; <b>(C)</b> and <b>(D)</b> : Diblock copolymer . . . . .	140
5.1	Diagram of the protocol for the filtration-rinsing cycles . . . . .	154
5.2	Variation of the water contact angle and peak height ratio with coating time for the membranes modified with 5 mg/mL of diblock, random, and triblock copolymer solutions. For the peak height ratio table: standard deviations of the measurements are presented inside the brackets) . . . . .	158
5.3	Variation of the water contact angle with relative peak height for the coating times of 2 and 4 hours for the membranes modified with 5 mg/mL of diblock, random, and triblock copolymer solutions. The peak heights were determined by ATR-FTIR . . . . .	159
5.4	FEG-SEM images of the unmodified membranes and modified with 5 mg/mL random copolymer solution for 4 and 6 hours. The scale bars for the x20k and x50k magnifications correspond to 1 μm and 100 nm, respectively. The images were taken with a Schottky Field Emission Scanning Electron Microscope (JEOL SEM-FEG JSM7800F); samples were metallised with gold . . . . .	160

---

5.5	Evolution of the permeability with time for the unmodified membranes and modified with 5 mg/mL random, triblock, and diblock copolymer solution for 2, 4 and 6 hours . . . . .	162
5.6	PBS and BSA permeabilities vs. coating time for the unmodified membranes and modified with 5 mg/mL random, triblock, and diblock copolymer solution . . . . .	164
5.7	FTIR maps of the retentate and permeate sides for the unmodified membranes and modified with 5 mg/mL random copolymer solution for 2 h and 6 h. The maps were acquired for the membranes used on the filtration-rinsing experiments once the filtration protocol was performed. For the virgin membranes the size of the images are of 400 $\mu\text{m}$ by 400 $\mu\text{m}$ , while for the rest of the maps the size is of 500 $\mu\text{m}$ by 500 $\mu\text{m}$ . . . . .	167
5.8	Diagram of the copolymers adsorbed on the surface of the membrane: (A) side view, (B) upper view . . . . .	169
A.1	Scanning electron microscopy images of the unmodified and modified membranes . . . . .	187
A.2	Atomic force spectroscopy of the surface of the membranes and rugosity values. Each image was taken for an area of 10 $\times$ 10 $\mu\text{m}$ . . . . .	188
A.3	Confocal microscopy images of WBC for the membranes coated with different concentrations of copolymers . . . . .	191
A.4	Confocal microscopy images of PRP for the membranes coated with different concentrations of copolymers . . . . .	192
B.1	ATR and external reflection spectra taken with the same equipment used in the experiments for unmodified and modified membranes, with and without adsorption of BSA . . . . .	195
B.2	BSA adsorbed on a PVDF membrane at different times. From left to right: 10 minutes, 1 h, 2 h and 8 h . . . . .	196

# List of Tables

1.1	Summary of membrane modification performed by researchers . . .	18
2.1	Copolymers used for the modification of the membrane . . . . .	44
2.2	XPS C1s scan: peaks of interest and their associated bonds [4] . . .	47
2.3	Blood cells: types and dimensions . . . . .	49
2.4	Maximum coating density for PS-PEGMA copolymers obtained in this work and others . . . . .	57
2.5	XPS results. Survey scan, C1s and O1s scans . . . . .	62
2.6	Summary of registered fluxes and calculated indexes for the modified membranes . . . . .	72
2.7	Summary of calculated resistances for the modified membranes . . .	73
3.1	Comparison of initial permeabilities between filtrations performed with the microchip (TMP=0.1 bar) and Amicon cells (TMP=2 bar) .	98
4.1	Copolymers used for the modification of the membrane . . . . .	119
4.2	Maximum grey values and calculated peak heights for the different experimental set-ups . . . . .	125
4.3	Definition of coating and adsorption levels. The numbers represent the limiting grey values . . . . .	126

5.1	Main permeability values and calculated indexes for the membranes modified with 5 mg/mL of random, triblock or diblock copolymer solutions and different coating times . . . . .	166
-----	--	-----

# List of Abbreviations

AFM	Atomic force microscopy.
ATR	Attenuated total reflectance.
B.E.	Binding energy.
BSA	Bovine serum albumin.
ED	Electrodialysis.
FDR	Flux decline ratio.
FEG	Field emission gun.
FITC	Fluorescein isothiocyanate.
FRR	Fouling reversibility ratio.
FTIR	Fourier transform infrared spectroscopy.
GV	Grey value.
LIPS	Liquid induced phase separation.
LYZ	Lysozyme.
MF	Microfiltration.
MW	Molecular weight.

---

NF	Nanofiltration.
NMP	N-Methyl-2-pyrrolidone.
NOA 68	Norland optical adhesive 68.
NOM	Natural organic matter.
PA	Polyamide.
PBS	Phosphate buffer saline.
PDMS	Polydimethylsiloxane.
PEGMA	Poly(ethylene glycol) methacrylate.
PEGMA-b-PS-b-PEGMA	Triblock copolymer.
PES	Polyethersulfone.
PI	Polydispersity index.
pI	Isoelectric point.
PP	Polypropylene.
PRP	Platelet-rich plasma, thrombocytes.
PS	Polystyrene.
PS-b-PEGMA	Diblock copolymer.
PSf	Polysulfone.
PS-r-PEGMA	Random copolymer.
PTFE	Polytetrafluoroethylene.
PVDF	Polyvinylidene fluoride.
RBC	Red blood cells, erythrocytes.
RI	Reversibility index.
RMS	Root mean square.
RO	Reverse osmosis.
SEM	Scanning electron microscopy.
TIPS	Temperature induced phase separation.
TMP	Trans membrane pressure.

UF	Ultrafiltration.
VIPS	Vapour induced phase separation.
WBC	White blood cells, leukocytes.
WCA	Water contact angle.
XPS	X-ray photoelectron spectroscopy.



# General Introduction

1



---

## 1 A summary on water and crisis

It is not possible to imagine life on earth without water. Animals, plants, microorganisms and needless to say human beings need water for their development. The total volume of water on Earth is estimated to be 1400 million km<sup>3</sup>, but only 35 km<sup>3</sup> represent fresh water sources (2.5 % of the total volume); approximately 30 % of which is groundwater, 0.3 % accounts for freshwater in lakes and rivers and 70 % of fresh water sources are located in ice and snow in mountainous regions [1]. It is estimated that for 2025, 1800 million people will be living in countries or regions with absolute water scarcity and another two thirds of the population will be living in regions under water-stressed conditions [2].

Water is used domestically, in agriculture and industry. Worldwide water demand for agriculture represents around 70 % of the total water withdrawn, while industrial activity consumes 20 % and the water use in households is only 10 % of total water withdrawals [3].

The benefits for caring about our water sources and ultimately evaluating the treatment of water courses for obtaining drinking water or of industrial and domestic effluents before the re-disposition on rivers and oceans also leads to economic benefits. Polluted water ultimately affects governmental and industrial budgets: several studies and reports inform about the economic costs of polluted water in the public health, agriculture and industrial domains, due to the decrease of working days, costs in the health sector, compensations for crop losses due to pathogenic microorganism outbreaks and millions of euros lost on food and beverage production [4–6].

All of these issues highlight the importance of water at every imaginable level. With the shrinking of potable water resources, population growth, uncertainty of water availability due to climate change and human-commodities production, the approach of water usage has to evolve and involve solutions such as disinfection, decontamination, re-use and/or desalination of water [7]. Therefore, water treatment technology has to be developed accordingly to the needs and environmental dispositions.

Classical water treatment technologies involve different treatment steps depending on the origin, use, contamination type and levels. Typical water treatment

steps for drinking water production can be screening, flocculation, coagulation, sedimentation, flotation, sand filtration, disinfection, sludge treatment, water softening, pH adjustment, fluorination [8]. Wastewater treatment is classically divided in four treatment categories. The preliminary treatment involves the removal of large contaminants by means of screening. Afterwards wastewater goes under the primary treatment, in which the objective is the physical removal of smaller particles by a primary sedimentation and no chemicals are used. In the secondary treatment, contaminants are removed by chemical or biological means such as oxidation of organic matter, nitrification and secondary sedimentation. Finally, the tertiary treatment takes place where the finalising treatments take place and it is also known as effluent polishing, eliminating contaminants that secondary treatment could not accomplish.

Membrane filtration technology is a perfect complement for water treatment facilities, either by replacing one or more treatment steps, by improving the quality of water since less coagulants would be used, or by supplementing water purification steps when needed (for example on the tertiary treatment, purification of water for electronics use).

---

## 2 Membrane technology for water treatment

Membranes play an important role in all of the living organisms on Earth. They could be considered the essence of individual life since they separate organelles, enzymes, proteins, and regulate the passage of nutrients for all living beings; without them no living organism can thrive.

The production and study of synthetic membranes started in the beginning of the 1900s with studies carried out by Bechhold [9] and then continued by Brown [10, 11] in the 1910s. The commercial applications of such membranes systems were limited and it was not until the 1960s that up-scaled commercially interesting desalination membrane systems were possible to produce due to the work of Loeb and Sourirajan [12] on asymmetric membranes. This work is considered the milestone for the modern membrane technology systems and its future applications which also led to further develop ultrafiltration and microfiltration technologies. Industrial membranes for gas separation were developed in the 1980's, particularly for hydrogen and nitrogen separation from air and carbon dioxide separation from natural gas [13].

Since then, membranes have been gaining terrain in water treatment, biotechnological and medicine fields. Reverse osmosis (RO), Ultrafiltration (UF) and Microfiltration (MF) membrane and membrane equipment sales for 2014 went from estimated sales of 7500 million € to a predicted market size of 11 000 million € according to McIlvane Company [14]. Figure 1.1 shows the sales distribution among the different market segments.

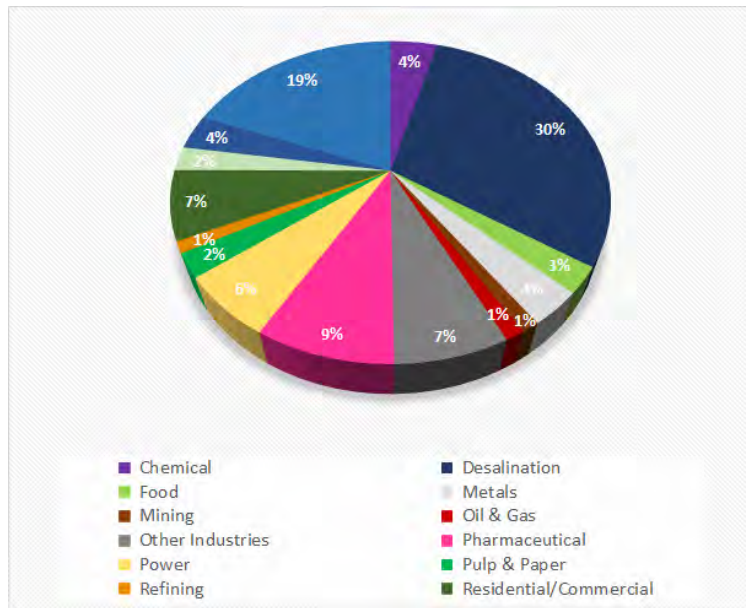


**Figure 1.1:** World market sales distribution for membranes and membrane equipment per market segment. Adapted from [14].

Water, wastewater and desalination application combined account for more than 50 % of the sales market.

What are exactly membranes? They can be defined as a barrier between two separate compartments and will allow or not the selective passage of compounds based on their molecular size, chemical and/or electrochemical properties. This passage is boosted by a driving force. Driving forces are varied and they include differences in temperature, pressure, osmotic pressure, concentration and electric potential. A general diagram of this process can be seen in the following figure (Figure 1.2).

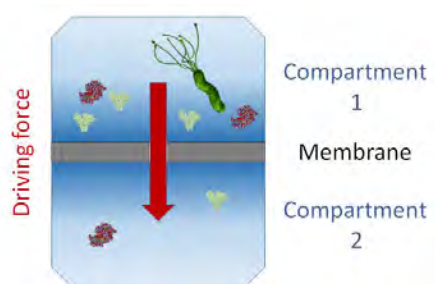


**Figure 1.2:** Example of membrane processes.

Membrane technology allows the separation of components at low temperatures – or lower than the equivalent chemical process-, with little or no use of foreign solvents. Besides, the separation is usually performed without involving a change of state, which would be the case for other separation technologies, i.e., distillation or precipitation. Therefore, energy costs can be lowered and high-quality products can be achieved. Moreover, membrane modules are easily scalable and allow the advanced treatment of water and other fluids covering less area than other technologies available. Some of the disadvantages of membranes are the membrane costs, fouling of the membrane, membrane handling, cleaning, and membrane selectivity- to achieve higher selectivities there is usually a compromise in flux.

## 2.1 Membrane processes

Membrane processes can be classified in different categories, such as by driving force.

Pressure-driven processes are usually divided into four categories: Microfiltration (MF), Ultrafiltration (UF), Nanofiltration (NF) and Reverse osmosis (RO). Figure 1.3 gives more information on these processes, particularly on approximate pore size of the membranes used on each application, required Trans membrane pressure (TMP), and some examples on particle sizes.

Dialysis is a typical membrane process in which the driving force is the concentration difference between two compartments and the diffusion of the concentrated solute will take place from the most to the least concentrated side. Electric potential differences are the main driving forces for Electrodialysis (ED) and electrodeionization procedures. Other membrane processes include pervaporation, membrane distillation and membrane crystallization.

Pressure-driven membrane processes described above plus ED constitute the main industrial applications for membranes as for today.

Membranes are produced as flat sheets, hollow fibres or capillaries, and are arranged into membrane modules to achieve higher filtration areas in a single equipment.

There are two basic operation modes for filtration: dead-end filtration and cross-flow filtration. For the first one the feed stream is perpendicularly fed on the

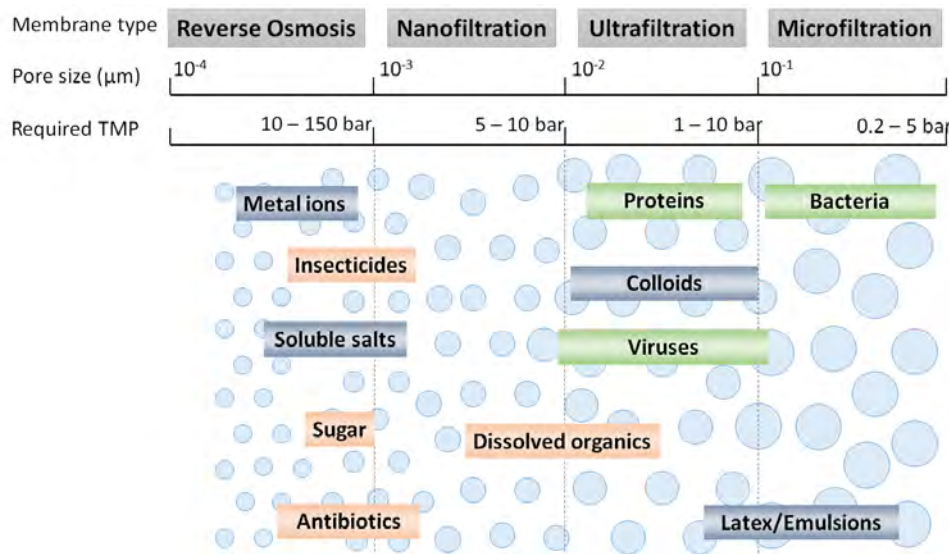


**Figure 1.3:** Pressure-driven membrane processes: pore sizes, TMP, and particle size ranges.

membrane while for other method the feed is passed parallel to the membrane surface (see Figure 1.4). In this case, the feed is separated into concentrate (or retentate) and permeate (or filtrate) streams. Fouling is usually less prominent for cross-flow filtration systems.

## 2.2 Membrane materials

Membranes can be classified as organic or inorganic – polymeric or ceramic, respectively. The main polymers constituting the organic membranes include cellulose acetate, Polyamide (PA), Polysulfone (PSf), Polyethersulfone (PES), Polyvinylidene fluoride (PVDF), and Polypropylene (PP). Polymeric membranes are relatively cheap and easy to produce. However, they tend to be more sensitive against chemicals, pH conditions, or high temperature ranges [15]. On the other hand, inorganic membranes have high mechanical strength and can withstand a wide variety and range of operating conditions. Main materials used are alumina, zirconia and borosilicate glass. Some of the disadvantages of these membranes are the price, their brittleness and the availability is generally limited for UF or MF applications.

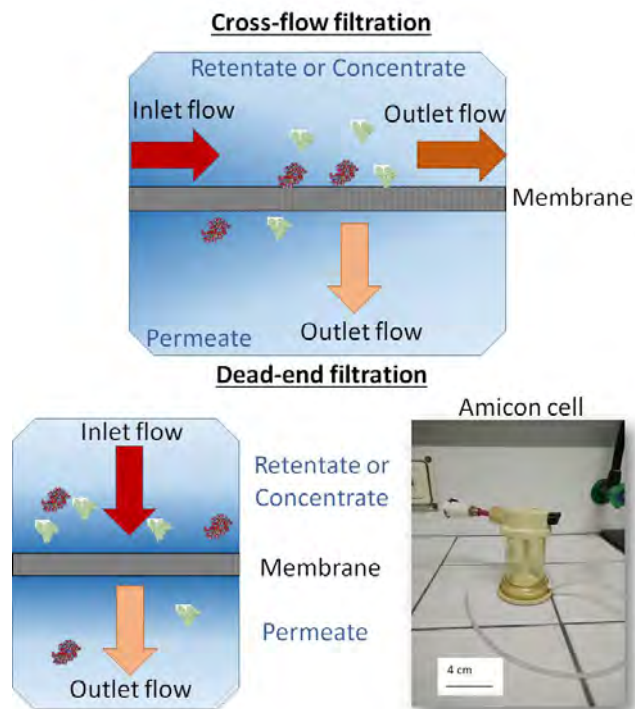


**Figure 1.4:** Diagram for the different operation modes: cross-flow and dead-end filtration.

### 2.2.1 Polymeric membranes

Polymeric membranes can be made out of hydrophilic or hydrophobic materials. Hydrophilic ones include cellulose esters, PSf and PES, while hydrophobic polymers used for membrane applications are PTFE, PVDF, and PP.

The selection of which polymer will be more suitable depends on the application that is needed, the characteristics of the feed stream, pH conditions it has to withstand, cleaning protocols, and sterilisation needs. Nowadays, polymers are also modified with other chemical compounds in order to combine their properties so as to yield a more resistant membrane for the desired application.

Polyvinylidene fluoride (PVDF) is a fluoropolymer, as such it is a very interesting type of material for membrane preparation due to its properties: high thermal stability, chemical resistance and low surface tension. PVDF can be produced as a membrane through a wide variety of techniques, and phase separation methods are the most used commercially [16]. Figure 1.5 shows the structure of

PvDF which contains 59.4 wt% fluorine and 3 wt% hydrogen [17].

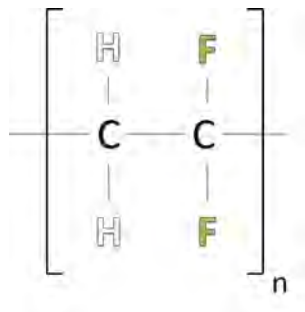


**Figure 1.5:** Structure of the PVDF molecule.

This semicrystalline polymer can be found in at least four phases:  $\alpha$  (the most common),  $\beta$ ,  $\gamma$  and  $\delta$ , and the degree of crystallinity can vary between 35 % to 70 % [18]. Although PVDF is considered thermally stable, it has been shown that it can show degradation – loss of hydrogen fluoride – at high temperatures in vacuum [19]. Its chemical stability is very good, being stable against most chemicals, specially halogens and oxidants, inorganic acids and aliphatic, aromatic and chlorinated solvents; although special care has to be taken when PVDF membranes are in contact with strong base solutions, esters and ketones [18]. PVDF membranes can be prepared by different methods including phase inversion, sintering, track etching and others. Phase inversion methods used for PVDF membrane casting include Temperature induced phase separation (TIPS), Vapour induced phase separation (VIPS), and Liquid induced phase separation (LIPS). For each one of these methods careful control of solvents, evaporation time, room temperature, coagulation bath type and temperature, humidity and other added chemicals have to be taken care of for the reproducibility of the prepared membranes to be ensured.

Due to its hydrophobicity PVDF is prone to fouling. Thus, to avoid this problem more hydrophilic modified PVDF membranes are produced. Some examples include the increase in hydrophilicity by adding polyvinyl pyrrolidone (PVP) or cellulosic materials [20, 21].

### 3 Membrane fouling

Fouling is a phenomena that affects membrane performance and ultimately its longevity. It occurs when particles start being deposited onto the membrane surface and into its pores while carrying out the filtration process. It depends in numerous factors involving membrane properties – chemical composition, surface rugosity, pore size, charge -, effluent composition and properties, and operating conditions – pre-treatment, flow rate, transmembrane pressure, temperature. Metastability of fluids is also a factor to consider, since changes in systems conditions could lead to their destabilization and cause a “slow fouling” phenomenon [22]. The convective flow of a solution that passes through the membrane – permeate – can be generally described as follows:

$$J_V = \frac{\Delta p - \Delta \pi}{\eta * R} \quad (1.1)$$

Where  $J_V$  is the convective flux density in  $\text{m}^3 \text{m}^{-2} \text{s}^{-1}$ ,  $\Delta p$  and  $\Delta \pi$  represent the pressure and osmotic pressure difference respectively (in Pa),  $\eta$  is the dynamic viscosity of the fluid that passes through the membrane (in Pa s), and  $R$  refers to the resistance (in  $\text{m}^{-1}$ ). When a stream of pure water is being filtered, the resistance to passage is only attributed to the membrane, but when a complex solution is being treated additional resistances are created due to the concentration polarization and solute deposition onto and/or into the membrane. Thus, if the pressure difference is kept constant, fouling will affect the flux by decreasing it with time, and if the flux is kept constant the pressure difference will increase in time.

Fouling is not to be considered a static phenomenon; it is a dynamic event in which particles deposit onto the membrane, which will also interact with other particles in the surroundings, being desorbed or re-adsorbed and interact with pore structures depending on their size and chemical characteristics [23, 24].

The extent of fouling determines which type of cleaning procedure can be done to try to reach the previous permeate flux levels. For reversible fouling the permeate flux can be restored by means of a physical washing protocol or eventually by a soft chemical cleaning protocol. When flux is no longer recovered by these means irreversible fouling has occurred. Chemisorption and pore blockage are extremely

difficult to overcome, thus extensive chemical cleaning or membrane replacement are necessary [25].

Although the ideal situation would be to attain zero-fouling conditions, it will probably never be achieved. It is definitely possible to lower fouling by different ways: effluent pretreatment, appropriate selection of operating conditions, membrane module design, membrane modification and cleaning. Each of these solutions involve a deep understanding of the system and more importantly of the fouling phenomenon involved.

Last but not least, fouling constitutes a big – if not the biggest – problem for membrane processes, due to the added pretreatment, cleaning, membrane replacement and power costs.

### 3.1 Foulants and types of fouling

Fluids that are intended to be purified with a membrane system will in fact contain different types of compounds that will cause membrane fouling. They are usually classified as particulates, organic, inorganic and microbiological organisms. Among organic foulants it is possible to find humic substances, proteins, and other hydrophobic and hydrophilic compounds; while inorganic foulants are considered to be metal ions and metal oxides that precipitate due to pH change or oxidation.

The extent of the organic fouling due to proteins depends on pH, ionic strength, and temperature of the fluid. Proteins can also attach to the membrane and start changing their conformation depending on the time they are in contact with the surface [26].

Microbiological foulants are the ones responsible for the biofouling phenomenon, when microorganisms attach to the membrane and form biofilms. The presence of other foulants - particularly the organic ones - can enhance this type of fouling.

Fouling can occur due to pore blocking, cake formation, concentration polarization, organic adsorption, inorganic precipitation and biological fouling [25, 27]. Each one of these phenomena will add an extra resistance against fluid flow through the membrane.

Fouling caused by cake formation could be considered to be reversible for microfiltration and ultrafiltration processes, and is weakly dependent on membrane

surface characteristics, while irreversible fouling is highly dependent on surface chemistry [28].

In this work, we will consider reversible fouling as the particles and colloids that can be removed by rinsing at room temperature, while irreversible fouling will be when harsher cleaning protocols have to take place, with the use of chemicals and higher temperatures. The success of the rinsing or cleaning protocol can be assessed by comparing the initial flux, and the recovered flux after the filtration and rinsing/cleaning protocol are performed. When rinsing protocols are done, the reversibility of the fouling can be assessed.

### 3.2 Factors that affect fouling phenomena

In order to try to minimise fouling, it is necessary to know which factors can affect it, particularly with the one concerning the membrane material. How these factors interact with each other and with the foulants will affect how reversible the fouling will be. The following figure depicts some of the factors that affect fouling phenomena that will be explained in the lines below (Figure 1.6).

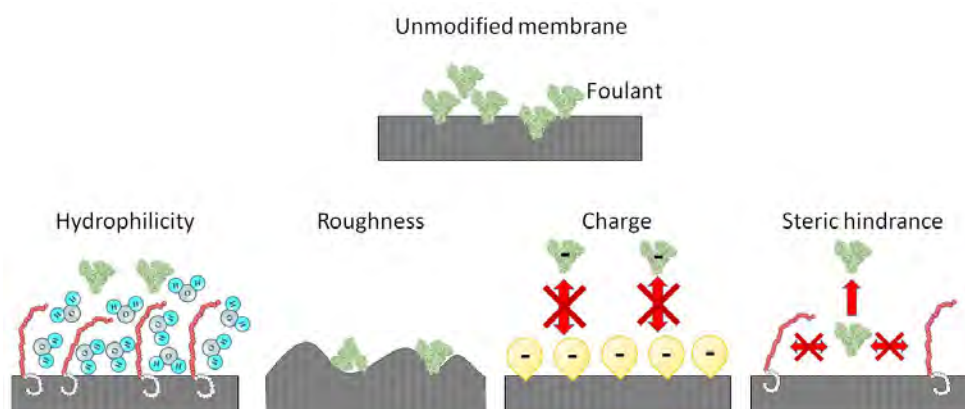


**Figure 1.6:** Diagram of the factors that affect fouling phenomena.

#### 3.2.1 Hydrophilicity

There seems to be a general consensus among membrane researchers that fouling would be largely avoided by modifying the surface of the membrane in a way of making it more hydrophilic. Most of the organic and biological compounds –

proteins, humic substances, bacteria - exhibit mostly hydrophobic characteristics, thus it is reasonable to believe that by achieving “water-loving” surfaces on “super-strong” hydrophobic materials the anti-fouling properties of a membranes would be greatly improved. Several groups have reached some degree of surface hydrophilization [29–33]. Nevertheless, some works show that hydrophobic surfaces could be less fouled than hydrophilic ones [34]. In this particular case, polyethersulfone (PES) membranes were prepared with the addition of amphiphatic macromolecules, and filtration tests were performed with humic acids. The authors found that with an increase of hydrophobicity - more modifying agent present in the membrane -, the deposition of the foulants decreased.

Water contact angle measurement is used to assess hydrophilicity; a decrease in water contact angle is considered to indicate an increase in the hydrophilicity of the surface. The measurements are easy to obtain and process. Nevertheless, changes or differences in pore size, surface roughness, surface patterns, porosity and pore size distribution, will also affect contact angle measurements [35], which makes it a difficult parameter for comparison purposes in spite of its easy measurement protocol.

Another approach of trying to understand foulant interactions with membranes in a wider sense is through force analysis. Atomic force microscopy (AFM) using colloid probes is a useful tool for measuring the surface-particle interactions. Basically, the force of particles that are attached to the cantilever tip are measured while they are approaching the membrane surface on a liquid media [36–40]. This technique, while highly efficient, requires an experienced technician and accurate protocols for its implementation.

### 3.2.2 Roughness

As happens with water contact angle measurements, surface roughness measurements are widely spread as a tool to try to understand and explain fouling phenomena.

On one hand, the rougher the membrane the more area it will have, therefore permeation flows could be higher due to the larger contact area [41]. Nevertheless, it is generally agreed that rougher membranes are more prone to be fouled by particles [42]. The enhancement of available contact area that would improve flux values would be also responsible of the particle-membranes interaction enhancement,

therefore, fouling would increase as surface roughness became higher [43]. Besides, particles – depending on their size - could be even physically trapped alongside the surface topography due to the valleys and peaks found on rougher membranes.

Roughness is usually quantified by AFM analysis, which yields values that can be compared between samples, although the scanning area could not be very significant compared to the general membrane surface – in the  $\mu\text{m}$  order for the  $(x, y)$  axis, and height detections down to nm or  $\mu\text{m}$  level.

The idea of taking membrane roughness as the sole parameter that could determine fouling properties is a limited approach, since fouling most probably depends on the particle-surface interactions that can occur for a specific system [38], thus contradictory data can be found throughout the literature.

### 3.2.3 Charge

Surface charge can also be a factor that affects fouling. Since most proteins have a negative charge at neutral pH [44] it is reasonable to assume that a negatively charged membrane would repel protein-fouling at such conditions. Other water colloidal components such as Natural organic matter (NOM) are also negatively charged [45]. The “most” approach does not cover the myriad of possible particles present in water or other aqueous systems, since some proteins can exhibit positive charges too. Therefore, some membrane modifications done by research groups involve the use of zwitterionic charged materials whose effectiveness against fouling could be even better [46–49].

### 3.2.4 Steric hindrance/repulsion

When attaching polymer chains onto membrane surfaces polymer brush-like structures can be created that can also prevent fouling steric interactions. Steric forces are the consequence of approaching two polymers which were moving freely in a certain solvent and when approached these movements are somehow limited [50]. Kang et al. detected this non-electrostatic and non-specific interaction force while measuring the force curves with BSA colloid probes against PAN-g-PEO/PAN modified membranes. They registered a range of interaction

forces much higher than the ones expected for electrostatic forces and whose decay was independent of the ionic strength of the solution [51].

Steric hindrance is affected by several factors such as the distribution density and the chain length of polymer chains [52–54], solvent quality, bulk protein concentration, temperature, shape and dimension of particles [50, 55, 56]. The solvent quality will determine the state of the brush or “brush health”. On a good solvent the brush will be swollen and large particles will not be able to penetrate the brush while the opposite effect could take place if the polymer is in contact with a bad solvent [55].

The theoretical background that tries to explain the protective properties of polymer brushes against foulants are still under development. Some initial approaches involve using the Flory and the scaling arguments [57]. Szleifer developed also a theory for explaining adsorption of proteins onto polymer brushes using the single-chain mean-field theory [58] while Halperin et al. studied the solvent quality effect on the interactions between colloids and neutral polymer brushes [55].

## 4 Management of fouling for membrane filtration processes - Membrane modification

As seen before, fouling is an unavoidable phenomena that is affected by several parameters. Since attaining zero fouling is an utopian idea, we can definitely try to manage it.

The management of fouling involves different - yet complementary - strategies: improvement of pre-treatment processes, optimisation of cleaning protocols, amelioration of membrane module design, and development and modification of membranes.

Since membranes are the ultimate barrier in the campaign to reduce fouling, special attention has been drawn to the development of new membrane materials, or the modification of existing ones, aiming at making fouling less irreversible, so even if particles adsorb to the membrane, they will be easily removed on the cleaning step.

In the following paragraph, a selection of the research work in the modification of polymeric materials will be presented. It includes many membrane preparation techniques as well as different types of modifying agents and characterisation methods.

Tuning of polymeric membrane anti-fouling properties can be achieved by basically three methods: coating, blending and grafting.

Coating is the most simple of the three. It consists of the physical adsorption of a particular polymer onto a pre-formed polymeric membrane. Usually, the modifying polymer is an amphiphilic copolymer while the membrane is made out of a hydrophobic polymer. Although its easy manipulation makes it an ideal method for industrial scale applications, concerns of the stability of the coating limit its popularity [59].

Polymer blending is another modification method found on the literature. It expands the classic membrane casting techniques to a system with two or more different types of polymers. For our interests, a hydrophobic polymer can be mixed with a hydrophilic one - or with an amphiphilic copolymer - and during phase inversion the hydrophilic groups will tend to move towards the air outside the blend at the membrane surface or pore walls. Nanoparticules can also be used for blending

purposes. Blending is also a potentially interesting technique for scale-up, nevertheless, many factors influence the final structure and properties of the membrane, and it could be costly to produce blended membranes, due to relatively high amounts of modifying agent needed in the blend.

Grafting involves a chemical attachment of a group onto the membrane [60]. This method is usually divided into two groups: ‘grafting from’ and ‘grafting to’. ‘Grafting to’ approaches involve the use of preformed polymer chains that contain reactive groups while with the ‘grafting from’ one the surface is activated and initiate the polymerization of monomers from the surface toward the bulk phase [61, 62]. Covalently bonded species can’t be easily detached from the surface and denser surfaces coverage can be obtained. Nevertheless, grafting techniques are not easy to set up at an industrial scale.

Examples of researchers working on this subject can be easily found in literature. Researchers at the R&D Center for Membrane Technology of the Chung Yuan Christian University in Taiwan have carried out extensive research on polymeric membrane modification using practically all of the modification techniques described before. Some examples of their work can be found in the table below (Table 1.1).

**Table 1.1:** Summary of membrane modification performed by researchers.

Membrane material	Modification molecules	Modification method	WCA (°)		Ref.
			Virgin	Modified	
PVDF	<i>SBMA</i>	ATRP grafting	82 ± 3	51 ± 2	[63]
PVDF	<i>PEGMA</i>	ATRP grafting	82 ± 1	60 ± 2	[31]
PSf	<i>PEO – PPO – PEO</i>	VIPS	85 ± 4	58 ± 5	[64]
		LIPS	77 ± 4	57 ± 2	
PVDF	<i>PEO – PPO – PEO</i>	VIPS	132 ± 3	41 ± 6	[65]
PVDF	<i>PS<sub>55</sub> – b – PEGMA<sub>30</sub></i>	Coating	116 ± 2	106 ± 2	[30]

Abbreviations: Polysulfone (PSf), Polyethylene oxide (PEO), Polyphenylene oxide (PPO), Sulfobetaine methacrylate (SBMA), Atom-transfer Radical-polymerization (ATRP); block (b) copolymers

The group of Mayes-Elimelech has also carried out interesting work in the field of membrane modification and the study of fouling. A research paper from Akthakul et al. explored some of the fouling behaviours when preparing PVDF

membranes with PVDF-g-POEM – polyoxyethylene methacrylate – by two methods: coating and blending [66]. For the coated membrane the water contact angle decreased from 95° (virgin membrane) to 68°. Filtration capabilities were assessed by using an oily feed solution and also several dye solutions; results were comparable in terms of rejections but the blended membrane showed lower flux values. For a subsequent research, the group continued to study these PVDF membranes coated with PVDF-g-POEM graft copolymer in more depth keeping in mind a possible application in membrane bioreactor (MBR) systems [32]. They found that the modified membrane showed better flux behaviour for BSA, sodium alginate and humic acid solutions filtrations against the PVDF base membrane for 10-day filtrations. AFM colloid probe technique was also used to study interaction forces between foulants and unmodified/modified membranes; the analysis showed the presence of repulsive steric interactions for the modified membranes that are probably the ones responsible for the anti-fouling properties seen in previous results.

The use of natural hydrophilic polymers such as chitosan was also reported [33]. On this work three coating techniques were tested and stable anti-fouling chitosan-PVDF membranes were obtained with similar molecular weight cut-offs (MWCO). Ultimately the coating of chitosan inside the pores of the membrane led to lower fluxes, however this led to achieving less in-pore fouling since initial fluxes could be re-established after cleaning.

Nanoparticules are also being used as hydrophilic modifying materials by some. Blending of inorganic alumina ( $\text{Al}_2\text{O}_3$ ) nano-sized particles with PVDF led to composite membranes with uniformly dispersed nanoparticles with enhanced water fluxes, lower contact angles, and improved anti-fouling performance [67]. A very popular nanoparticle used for composite membrane formation is titanium dioxide ( $\text{TiO}_2$ ) due to its stability and potential antibacterial and catalytic properties. Cao et al. prepared blended PVDF- $\text{TiO}_2$  membranes and better anti-fouling membranes were obtained when compared with a PVDF one [68]. More interestingly, in this case they did not find a correlation between water contact angle measurements and anti-fouling properties; instead fouling was more influenced by the surface roughness of the membranes.

All of these examples show only a small selection of the work done in the field. The addition of modifying agents is intended to affect the properties of the

membranes either by increasing hydrophilicity, creating steric repulsion interactions, and/or creating a hydration layer in the vicinity of the surface of the membrane, among others. How can we study these effects will be summarised in the following section.

## 5 Techniques for the characterisation of the modification of membranes and of their anti-fouling properties

No matter how we approach the membrane modification issue, we need to be able to properly characterise, first, the modification that has been carried out, and then the anti-fouling properties of these membranes.

Several techniques are widely used to assess the presence of the modifying agent, hydrophilicity of the membrane, and adsorption of the foulant. The most direct method to determine the hydrophilicity of the membrane is the water contact angle analysis. It is a quite simple method, with an easy sample preparation and results do not require a big expertise for their processing. However, results can be affected by changes in pore size, roughness, porosity and pore size distribution.

For the membranes modified by coating or grafting, the presence of the modifying agent can be estimated by calculating the coating density, which involves a mass balance between the initial - unmodified - state, and the final one, so that the difference in weight is mainly due to the presence of the modifying molecule. This values are usually expressed as the mass or moles of the agent by membrane area or volume. This estimation does not help to elucidate if the grafted copolymers are on top of the membrane surface, on the pore walls, or inside the matrix (for the membranes prepared by blending). The ability of a membrane to adsorb water can be estimated in a similar way, by calculating the hydration capacity. The initial state would be the dry modified membrane, while the final weight will be determined after the membrane was put in contact for a certain period of time in water.

Fourier-transform infrared spectroscopy (FTIR) has been used to qualitatively assess the modification process and sometimes of the foulants. When a sample is irradiated with infrared light some bonds vibrate. This vibration can be detected and represented as a spectrum (see Figure 1.7). An infrared spectrometer measures the frequencies of infrared light absorbed by a compound, whereas a Fourier-transform infrared spectrometer uses an interferometer creating an interferogram which contains all the information from the spectrum and is converted to a frequency or wavenumber graph by applying the Fourier transform algorithm [69]. The peaks that can be measured on these spectra correspond to a particular bond vibration, allowing the identification of the chemical species on the sample [70, 71]. IR spectra provide

information on the presence of functional groups, if the structure of the molecule should be elucidated, other techniques should be used. Sample preparation and data analysis is quite simple, although the technique is limited to the analysis of the surface of the membrane.

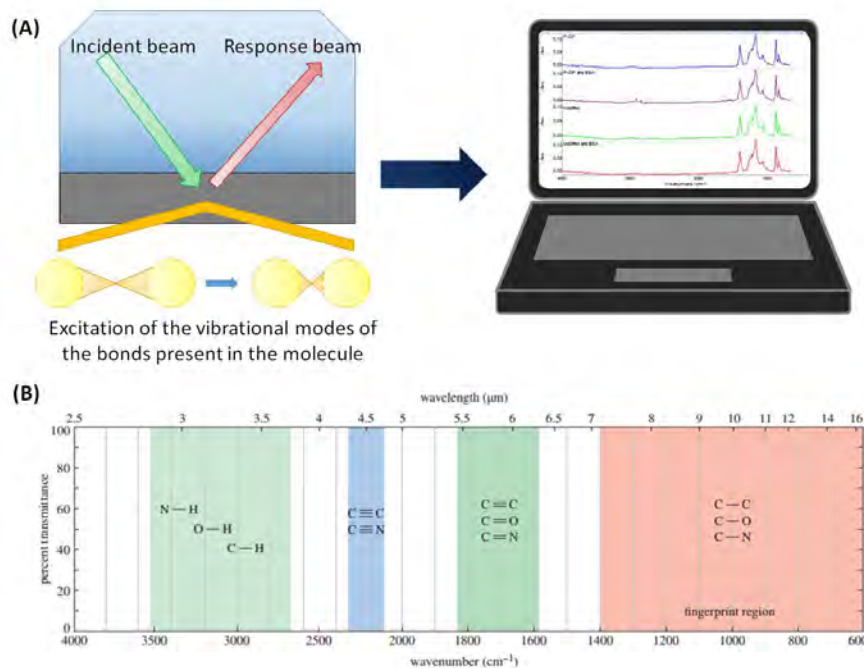


**Figure 1.7:** FTIR technique. **(A):** Schematics on the stretching of the bonds when irradiated with a beam and the generation of the subsequent spectra. **(B):** Regions of the spectrum where the concerned bonds typically absorb (taken from [69]).

Atomic force microscopy (AFM) can be used to measure surface roughness. When used in force spectroscopy mode specific particles are attached to the probe, and it is possible to measure surface-particle interaction forces [51]. These particles can be very varied depending on which kind of system researchers want to study, and the experience the team has with attaching them to the probe. A drawback of AFM is that it is a very local measurement. If the surface of membrane is not perfectly homogeneous, as it is generally assumed when membranes are produced, it might not be possible to get a realistic view of the coating homogeneity.

The adsorption of foulant species can be determined by several methods, depending on the type of foulant. UV spectrophotometry is widely used for the

detection of the adsorbed proteins, or their presence in the retentate and permeate flows, by measuring the absorbance at a wavelength of 280 nm [30]. Confocal microscopy takes advantage of the natural fluorescence of natural agents, therefore it can be used to acquire images of blood cells and bacteria present on the surface of the membrane, which can later be counted with a software [52]. X-ray photoelectron spectroscopy (XPS) is used to chemically detect the presence of proteins and other biofoulants [52]. In the case of bacteria or other bigger biofouling agents, scanning electron microscopy (SEM) can also be used to directly detect and count their presence on the surface of the membranes [72].

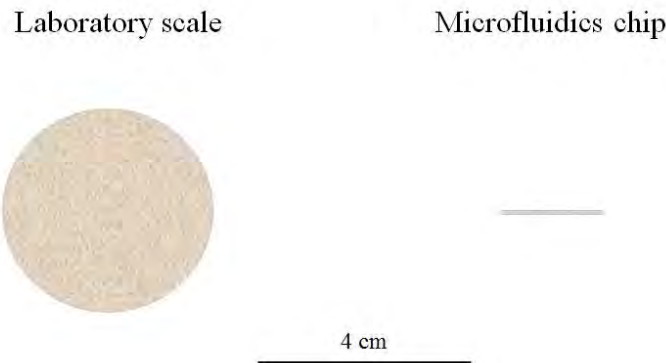
The determination of fouling by most of these techniques can be regarded as static, foulants reach the surface by diffusion and adsorb, and then its presence and concentration is determined. It is an indication of the behaviour and properties of the system but they have not to be regarded as the absolute truth. These membranes are supposed to be used for filtration set-ups or in systems that there will be a flow, thus final fouling behaviour can be different.

To better assess the effect of the modification in the anti-fouling properties of the membrane it is always necessary to perform filtration tests. They normally involve one filtration and cleaning cycle with the determination of pure water fluxes and evolution of the foulant solution flux. More interesting data can be obtained when more than one fouling-cleaning cycle is performed, since it emulates the way membranes are operated in reality. Some of the previously-mentioned analytical techniques can be applied to analyse the fouled membranes after filtration has been carried out to complement the obtained results.

Is it possible to improve the study of fouling? One interesting approach is the development of direct ways to observe fouling [73, 74], more particularly with the combination of microfluidic devices with fluorescence microscopy [75]. Microfluidic devices rely on the miniaturisation of processes by fabricating systems that handle small volumes ( $10^{-9}$  to  $10^{-18}$  litres) at a scale of tens to hundreds of micrometres [76]. These devices have the advantages of being portable, on the flexibility of their design, and choice of materials that can be used for their fabrication. Due to their reduced size, the consumption of chemicals, generated waste, and fabrication costs are also reduced. The following figure (Figure 1.8) compares the sizes of the membranes used for typical laboratory filtration

experiments against the size of the membranes that can be inserted inside microfluidic chips, and an estimation of volume of fluid necessary for a filtration protocol, assuming same membrane, same permeabilities, and operating conditions.

### Membrane size



### Volume of solution

95 mL

0.95 mL

**Figure 1.8:** Comparison of membrane area and filtration volumes necessary for a typical laboratory-scale filtration device (left) and a membrane inserted inside a microfluidic device (right).

For membrane processes and the study of fouling, the integration of membranes inside the microfluidic chips is of great interest [77, 78]. With these kind of chips, the advantages of static tests - determination of adsorption properties on the surface of the membrane - could be combined with those of filtration systems - determination of filtration parameters - at the same time for those experimental conditions. When the chips are assembled with transparent materials, microscopy techniques can be used for the direct observation of the fouling on the surface of the membrane.

Another option for the improvement of the study of fouling would be the application of FTIR-mapping techniques, that would yield interesting chemical maps of the surfaces in which the modification and fouling layers could be simultaneously detected.

These techniques will be presented in the following chapters of this manuscript.

## 6 Presentation of the SuperNAM project

The present PhD project has been fully funded by the SuperNAM project. The Super Non-Adhesive Membranes for Sustainable Water Treatment project (SuperNAM) is a project performed in close international collaboration between two research groups: the Laboratoire de Génie Chimique (UMR 5503, Université de Toulouse, CNRS, INPT, UPS, Toulouse, France) and the Research and Development Center for Membrane Technology (Chung Yuan Christian University, ChungLi, Taiwan).

This project aims at developing a series of polymer membranes for the filtration of water or waste waters, and bearing super non-adhesive properties. This would lead to make membrane fouling very reversible, hence to save energy, productivity, cleaning agents and membrane lifetime.

Its general objective is the creation of a full generation of non adhesive membranes, which can be produced by simple and easily up-scalable processes. Specifically, this involves the synthesis of new additives that would be miscible with the chosen PVDF membrane, followed by the development of an efficient membrane preparation method to yield low-fouling membranes at large scales. The third target is to fully characterize the membrane physico-chemical and functional properties and to find correlations between structural, chemical and antifouling properties. The study of fouling and its reversibility is also among the objectives of the project, to finalise use these low-fouling membranes in water treatment applications.

The total budget of the project is of 400 000 €, half of this amount is funded by the Agence Nationale de la Recherche (ANR, ANR-12-IS08-0002, France) and the other half by the Ministry of Science and Technology (MOST 102-2923-E-033-001-MY3, Taiwan).

## 7 Objectives

The main objective of this manuscript is to study the anti-fouling properties of modified membranes.

The base membranes used are made of PVDF, and the modifying agents concern PS-PEGMA copolymers with three different conformations: diblock, triblock, or random.

Firstly, this study will be performed using most the usual techniques found in bibliography (see Chapters 2 and 5, pages 37 and 147, respectively).

Then, new techniques will be developed or adapted to our system. On the one hand, novel microfluidic chips that contain the membranes will be developed and the fouling will be detected using fluorescence microscopy while performing filtration tests (see Chapter 3, page 81). On the other hand, FTIR-mapping techniques will be applied to the study of our system to see how coating and fouling relate (see Chapter 4, page 113).

---

## 8 References

- [1] UN Water. Water Security and the Global Agenda: A UN-Water Analytical Brief. *United Nations University, Institute for Water, Environment & Health (UNU-INWEH), Hamilton, Ontario, Canada, 2013.*
- [2] UN Water. Policy brief: Water quality, 2011.
- [3] WWAP (World Water Assessment Programme). *The United Nations World Water Development Report 4: Managing Water under Uncertainty and Risk.* UNESCO, Paris, 2012.
- [4] Mark Sanctuary, Laurence Haller, and Hakan Tropp. *Making water a part of economic development: the economic benefits of improved water management and services.* SIWI, 2004.
- [5] Guy Hutton, Laurence Haller, et al. *Evaluation of the costs and benefits of water and sanitation improvements at the global level.* Water, Sanitation, and Health, Protection of the Human Environment, World Health Organization, 2004.
- [6] D Flynn. Germany's E. coli outbreak most costly in history, Food safety news, 2011.
- [7] Mark A Shannon, Paul W Bohn, Menachem Elimelech, John G Georgiadis, Benito J Marinas, and Anne M Mayes. Science and technology for water purification in the coming decades. *Nature*, 452(7185):301–310, 2008.
- [8] Donald R Rowe and Isam Mohammed Abdel-Magid. *Handbook of wastewater reclamation and reuse.* CRC Press, 1995.
- [9] Heinrich Bechhold. Kolloidstudien mit der Filtrationsmethode. *Zeitschrift für Elektrochemie und angewandte physikalische Chemie*, 13(32):527–533, 1907.
- [10] William Brown. On the preparation of collodion membranes of differential permeability. *Biochemical Journal*, 9(4):591, 1915.
- [11] William Brown. Further Contributions to the Technique of preparing Membranes for Dialysis. *Biochemical Journal*, 11(1):40, 1917.

- 
- [12] Sidney Loeb and Srin Sourirajan. *Sea water demineralization by means of a semipermeable membrane*. University of California, Department of Engineering, 1963.
- [13] R.W. Baker. *Membrane Technology and Applications*. John Wiley & Sons, 2 edition, 2004.
- [14] The McIlvaine Company. RO, UF, MF World Markets. Technical report, The McIlvaine Company, 2011-2016.
- [15] ZF Cui and HS Muralidhara. *Membrane technology: a practical guide to membrane technology and applications in food and bioprocessing*. Elsevier, 2010.
- [16] Zhaoliang Cui, Enrico Drioli, and Young Moo Lee. Recent progress in fluoropolymers for membranes. *Progress in Polymer Science*, 39(1):164–198, 2014.
- [17] Bruno Ameduri. From vinylidene fluoride (VDF) to the applications of VDF-containing polymers and copolymers: recent developments and future trends. *Chem. Rev.*, 109(12):6632–6686, 2009.
- [18] Fu Liu, N Awanis Hashim, Yutie Liu, MR Moghareh Abed, and K Li. Progress in the production and modification of PVDF membranes. *Journal of Membrane Science*, 375(1):1–27, 2011.
- [19] SL Madorsky. Fluorocarbon and chlorocarbon polymers. *Thermal degradation of organic polymers*, John Wiley & Sons Inc, pages 130–172, 1964.
- [20] Flemming F Stengaard. Characteristics and performance of new types of ultrafiltration membranes with chemically modified surfaces. *Desalination*, 70(1):207–224, 1988.
- [21] Dongliang Wang, K Li, and WK Teo. Preparation and characterization of polyvinylidene fluoride (PVDF) hollow fiber membranes. *Journal of Membrane Science*, 163(2):211–220, 1999.
- [22] Pierre Aimar and Patrice Bacchin. Slow colloidal aggregation and membrane fouling. *Journal of Membrane Science*, 360(1):70–76, 2010.

- 
- [23] Kuo-Jen Hwang and Chan-Li Hsueh. Dynamic analysis of cake properties in microfiltration of soft colloids. *Journal of Membrane Science*, 214(2):259–273, 2003.
- [24] Lihan Huang and Michael T Morrissey. Fouling of membranes during microfiltration of surimi wash water: roles of pore blocking and surface cake formation. *Journal of Membrane Science*, 144(1):113–123, 1998.
- [25] Wenshan Guo, Hui-Hao Ngo, and Jianxin Li. A mini-review on membrane fouling. *Bioresource technology*, 122:27–34, 2012.
- [26] ME Soderquist and AG Walton. Structural changes in proteins adsorbed on polymer surfaces. *Journal of Colloid and Interface Science*, 75(2):386–397, 1980.
- [27] Robert Field. Fundamentals of fouling. *Membranes for water treatment*, 4:1–23, 2010.
- [28] Nidal Hilal, Oluwaseun O Ogunbiyi, Nick J Miles, and Rinat Nigmatullin. Methods employed for control of fouling in MF and UF membranes: a comprehensive review. *Separation Science and Technology*, 40(10):1957–2005, 2005.
- [29] Antoine Venault, Yi-Hung Liu, Jia-Ru Wu, Hui-Shan Yang, Yung Chang, Juin-Yih Lai, and Pierre Aimar. Low-biofouling membranes prepared by liquid-induced phase separation of the PVDF/polystyrene-*b*-poly (ethylene glycol) methacrylate blend. *Journal of Membrane Science*, 450:340–350, 2014.
- [30] Nien-Jung Lin, Hui-Shan Yang, Yung Chang, Kuo-Lun Tung, Wei-Hao Chen, Hui-Wen Cheng, Sheng-Wen Hsiao, Pierre Aimar, Kazuo Yamamoto, and Juin-Yih Lai. Surface self-assembled PEGylation of fluoro-based PVDF membranes via hydrophobic-driven copolymer anchoring for ultra-stable biofouling resistance. *Langmuir*, 29(32):10183–10193, 2013.
- [31] Yung Chang, Chao-Yin Ko, Yu-Ju Shih, Damien Quémener, André Deratani, Ta-Chin Wei, Da-Ming Wang, and Juin-Yih Lai. Surface grafting control

- of PEGylated poly (vinylidene fluoride) antifouling membrane via surface-initiated radical graft copolymerization. *Journal of Membrane Science*, 345(1):160–169, 2009.
- [32] Ayse Asatekin, Adrienne Menniti, Seoktae Kang, Menachem Elimelech, Eberhard Morgenroth, and Anne M Mayes. Antifouling nanofiltration membranes for membrane bioreactors from self-assembling graft copolymers. *Journal of Membrane Science*, 285(1):81–89, 2006.
- [33] Somnuk Boributh, Ampai Chanachai, and Ratana Jiraratananon. Modification of PVDF membrane by chitosan solution for reducing protein fouling. *Journal of Membrane Science*, 342(1):97–104, 2009.
- [34] L Zhang, G Chowdhury, C Feng, T Matsuura, and R Narbaitz. Effect of surface-modifying macromolecules and membrane morphology on fouling of polyethersulfone ultrafiltration membranes. *Journal of applied polymer science*, 88(14):3132–3138, 2003.
- [35] D Rana and T Matsuura. Surface modifications for antifouling membranes. *Chemical reviews*, 110(4):2448–2471, 2010.
- [36] W Richard Bowen, Nidal Hilal, Robert W Lovitt, and Chris J Wright. A new technique for membrane characterisation: direct measurement of the force of adhesion of a single particle using an atomic force microscope. *Journal of Membrane Science*, 139(2):269–274, 1998.
- [37] Jonathan A Brant and Amy E Childress. Assessing short-range membrane–colloid interactions using surface energetics. *Journal of Membrane Science*, 203(1):257–273, 2002.
- [38] Ingmar H Huisman, Pedro Prádanos, and Antonio Hernández. The effect of protein–protein and protein–membrane interactions on membrane fouling in ultrafiltration. *Journal of Membrane Science*, 179(1):79–90, 2000.
- [39] Jeffrey A Koehler, Mathias Ulbricht, and Georges Belfort. Intermolecular forces between a protein and a hydrophilic modified polysulfone film with relevance to filtration. *Langmuir*, 16(26):10419–10427, 2000.

- 
- [40] Sangyoup Lee and Menachem Elimelech. Relating organic fouling of reverse osmosis membranes to intermolecular adhesion forces. *Environmental science & technology*, 40(3):980–987, 2006.
- [41] Masahiko Hirose, Hiroki Ito, and Yoshiyasu Kamiyama. Effect of skin layer surface structures on the flux behaviour of RO membranes. *Journal of Membrane Science*, 121(2):209–215, 1996.
- [42] Eric M Vrijenhoek, Seungkwan Hong, and Menachem Elimelech. Influence of membrane surface properties on initial rate of colloidal fouling of reverse osmosis and nanofiltration membranes. *Journal of membrane science*, 188(1):115–128, 2001.
- [43] Menachem Elimelech, Xiaohua Zhu, Amy E Childress, and Seungkwan Hong. Role of membrane surface morphology in colloidal fouling of cellulose acetate and composite aromatic polyamide reverse osmosis membranes. *Journal of membrane science*, 127(1):101–109, 1997.
- [44] Mathias Ulbricht. Advanced functional polymer membranes. *Polymer*, 47(7):2217–2262, 2006.
- [45] Seungkwan Hong and Menachem Elimelech. Chemical and physical aspects of natural organic matter (NOM) fouling of nanofiltration membranes. *Journal of membrane science*, 132(2):159–181, 1997.
- [46] Antoine Venault, Wen-Yu Huang, Sheng-Wen Hsiao, Arunachalam Chinnathambi, Sulaiman Ali Alharbi, Hong Chen, Jie Zheng, and Yung Chang. Zwitterionic Modifications for Enhancing the Antifouling Properties of Poly (vinylidene fluoride) Membranes. *Langmuir*, 32(16):4113–4124, 2016.
- [47] Qing Shi, Yanlei Su, Wei Zhao, Chao Li, Yaohui Hu, Zhongyi Jiang, and Shiping Zhu. Zwitterionic polyethersulfone ultrafiltration membrane with superior antifouling property. *Journal of Membrane Science*, 319(1):271–278, 2008.
- [48] Haijun Yu, Yiming Cao, Guodong Kang, Jianhui Liu, Meng Li, and Quan Yuan. Enhancing antifouling property of polysulfone ultrafiltration membrane

- by grafting zwitterionic copolymer via UV-initiated polymerization. *Journal of Membrane Science*, 342(1):6–13, 2009.
- [49] Mingyan Zhou, Hongwei Liu, James E Kilduff, Robert Langer, Daniel G Anderson, and Georges Belfort. High-throughput membrane surface modification to control NOM fouling. *Environmental science & technology*, 43(10):3865–3871, 2009.
- [50] Yuncheng Liang, Nidal Hilal, Paul Langston, and Victor Starov. Interaction forces between colloidal particles in liquid: Theory and experiment. *Advances in colloid and interface science*, 134:151–166, 2007.
- [51] Seoktae Kang, Ayse Asatekin, Anne M Mayes, and Menachem Elimelech. Protein antifouling mechanisms of PAN UF membranes incorporating PAN-g-PEO additive. *Journal of Membrane Science*, 296(1):42–50, 2007.
- [52] Peter Kingshott, Helmut Thissen, and Hans J Griesser. Effects of cloud-point grafting, chain length, and density of PEG layers on competitive adsorption of ocular proteins. *Biomaterials*, 23(9):2043–2056, 2002.
- [53] Lingyan Li, Shengfu Chen, and Shaoyi Jiang. Protein interactions with oligo (ethylene glycol)(OEG) self-assembled monolayers: OEG stability, surface packing density and protein adsorption. *Journal of Biomaterials Science, Polymer Edition*, 18(11):1415–1427, 2007.
- [54] Yung Chang, Yu-Ju Shih, Chao-Yin Ko, Jheng-Fong Jhong, Ying-Ling Liu, and Ta-Chin Wei. Hemocompatibility of poly (vinylidene fluoride) membrane grafted with network-like and brush-like antifouling layer controlled via plasma-induced surface PEGylation. *Langmuir*, 27(9):5445–5455, 2011.
- [55] A Halperin, M Kroger, and EB Zhulina. Colloid-brush interactions: The effect of solvent quality. *Macromolecules*, 44(9):3622–3638, 2011.
- [56] Angus Hucknall, Srinath Rangarajan, and Ashutosh Chilkoti. In pursuit of zero: polymer brushes that resist the adsorption of proteins. *Advanced Materials*, 21(23):2441–2446, 2009.

- 
- [57] ST Milner, TA Witten, and ME Cates. Theory of the grafted polymer brush. *Macromolecules*, 21(8):2610–2619, 1988.
- [58] I Szleifer. Protein adsorption on surfaces with grafted polymers: a theoretical approach. *Biophysical Journal*, 72(2 Pt 1):595, 1997.
- [59] Yen-Che Chiag, Yung Chang, Wen-Yih Chen, and Ruoh-chyu Ruaan. Biofouling resistance of ultrafiltration membranes controlled by surface self-assembled coating with PEGylated copolymers. *Langmuir*, 28(2):1399–1407, 2011.
- [60] A Bhattacharya and BN Misra. Grafting: a versatile means to modify polymers: techniques, factors and applications. *Progress in polymer science*, 29(8):767–814, 2004.
- [61] Koichi Kato, Emiko Uchida, En-Tang Kang, Yoshikimi Uyama, and Yoshito Ikada. Polymer surface with graft chains. *Progress in Polymer Science*, 28(2):209–259, 2003.
- [62] Victor M Kochkodan and Virender K Sharma. Graft polymerization and plasma treatment of polymer membranes for fouling reduction: A review. *Journal of Environmental Science and Health, Part A*, 47(12):1713–1727, 2012.
- [63] Yen-Che Chiang, Yung Chang, Akon Higuchi, Wen-Yih Chen, and Ruoh-Chyu Ruaan. Sulfobetaine-grafted poly (vinylidene fluoride) ultrafiltration membranes exhibit excellent antifouling property. *Journal of Membrane Science*, 339(1):151–159, 2009.
- [64] Antoine Venault, Yung Chang, Da-Ming Wang, Denis Bouyer, Akon Higuchi, and Juin-Yih Lai. PEGylation of anti-biofouling polysulfone membranes via liquid-and vapor-induced phase separation processing. *Journal of membrane science*, 403:47–57, 2012.
- [65] Antoine Venault, Yung Chang, Da-Ming Wang, and Juin-Yih Lai. Surface anti-biofouling control of PEGylated poly (vinylidene fluoride) membranes via vapor-induced phase separation processing. *Journal of membrane science*, 423:53–64, 2012.

- [66] Ariya Akthakul, Richard F Salinaro, and Anne M Mayes. Antifouling polymer membranes with subnanometer size selectivity. *Macromolecules*, 37(20):7663–7668, 2004.
- [67] Lu Yan, Yu Shui Li, and Chai Bao Xiang. Preparation of poly (vinylidene fluoride)(pvdf) ultrafiltration membrane modified by nano-sized alumina ( $Al_2O_3$ ) and its antifouling research. *Polymer*, 46(18):7701–7706, 2005.
- [68] Xiaochun Cao, Jun Ma, Xuehua Shi, and Zhijun Ren. Effect of  $TiO_2$  nanoparticle size on the performance of PVDF membrane. *Applied Surface Science*, 253(4):2003–2010, 2006.
- [69] L.G. Wade. *Organic Chemistry*. Pearson, 2013.
- [70] Shuang Xue, Qing-Liang Zhao, Liang-Liang Wei, and Nan-Qi Ren. Behavior and characteristics of dissolved organic matter during column studies of soil aquifer treatment. *Water Research*, 43(2):499–507, 2009.
- [71] S Belfer, R Fainchtain, Y Purinson, and O Kedem. Surface characterization by FTIR-ATR spectroscopy of polyethersulfone membranes-unmodified, modified and protein fouled. *Journal of Membrane Science*, 172(1):113–124, 2000.
- [72] Jing Jin, Wei Jiang, Jie Zhao, Jinghua Yin, Paola Stagnaro, et al. Fabrication of PP-g-PEGMA-g-heparin and its hemocompatibility: From protein adsorption to anticoagulant tendency. *Applied Surface Science*, 258(15):5841–5849, 2012.
- [73] Seok-Tae Kang, Arun Subramani, Eric MV Hoek, Marc A Deshusses, and Mark R Matsumoto. Direct observation of biofouling in cross-flow microfiltration: mechanisms of deposition and release. *Journal of Membrane Science*, 244(1):151–165, 2004.
- [74] H Li, AG Fane, HGL Coster, and S Vigneswaran. Direct observation of particle deposition on the membrane surface during crossflow microfiltration. *Journal of Membrane Science*, 149(1):83–97, 1998.
- [75] Zenamarkos B Sendekie and Patrice Bacchin. Colloidal jamming dynamics in microchannel bottlenecks. *Langmuir*, 32(6):1478–1488, 2016.

- 
- [76] George M Whitesides. The origins and the future of microfluidics. *Nature*, 442(7101):368–373, 2006.
- [77] David Erickson and Dongqing Li. Integrated microfluidic devices. *Analytica Chimica Acta*, 507(1):11–26, 2004.
- [78] Mario Cabodi, Nak Won Choi, Jason P Gleghorn, Christopher SD Lee, Lawrence J Bonassar, and Abraham D Stroock. A microfluidic biomaterial. *Journal of the American Chemical Society*, 127(40):13788–13789, 2005.



Membrane modification and  
anti-fouling properties  
assessment

2



## 1 Introduction

Extensive research has been made in the field of membrane modification in order to avoid fouling phenomena. Tuning of membranes in order to affect their hydrophilicity, charge, and hydration capacity has led to the production of resistant membranes and the subsequent study of the success of the modification has improved the understanding of fouling.

In this chapter we will focus on the classical study of the modification of membranes modified with copolymers made of Polystyrene (PS) and Poly(ethylene glycol) methacrylate (PEGMA) chains with different conformations: diblock, random, and triblock.

### 1.1 Membrane modification with PS-PEGMA copolymers

In the previous chapter the work of the R&D Center for Membrane Technology of the Chung Yuan Christian University in Taiwan was mentioned. They developed the production of PS-PEGMA copolymers with different chain lengths and structural conformations. The chemical structure of such copolymers is shown in the following figure (Figure 2.1).

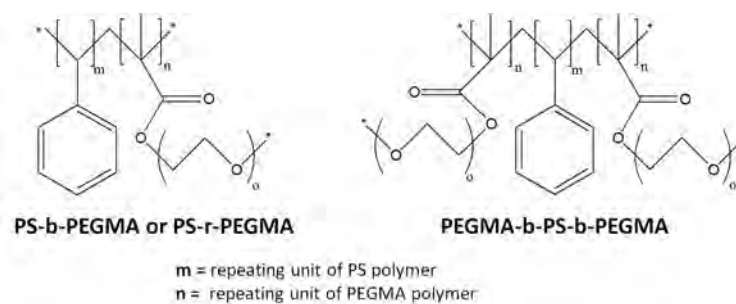


**Figure 2.1:** Chemical structure of the PS-PEGMA copolymers [1, 2].

The PS chain is more hydrophobic, which would be the anchor to the hydrophobic membrane material. The more hydrophilic PEGMA chain would be the one providing the anti-fouling properties to the membrane.

The different structures in which the repeating units of PS and PEGMA can be arranged - that are the ones used in this work - are presented in Figure 2.2. Diblock

PS-*b*-PEGMA, random PS-*r*-PEGMA, and triblock PEGMA-*b*-PS-*b*-PEGMA can be synthesised with varying repeating units of PS and PEGMA.

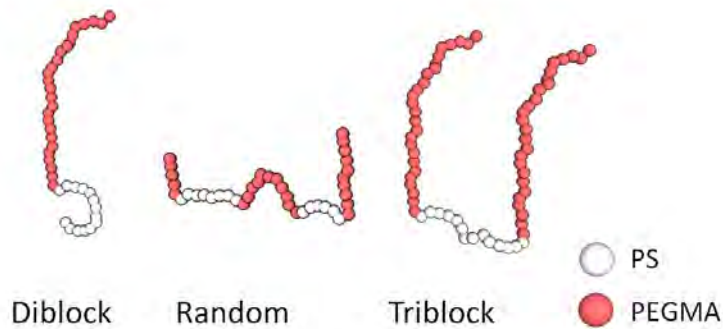


**Figure 2.2:** Diagram of the structure of the copolymers used in this work.

There is a comprehensive amount of research carried out on the modification of membranes with these copolymers - and others - when different modification methods are applied, and their impact on anti-fouling properties.

The chemical grafting on PVDF UF membranes was carried out by Chang et al. [3]. Different grafting techniques were assessed in this work and BSA adsorption and filtration studies were carried out as well. From this study, it was clear that anti-fouling properties were highly influenced by the polymeric structures that could be achieved during modification and were not necessarily dependent on the surface coverage itself nor on the decrease in water contact angle achieved.

Blending techniques - LIPS and VIPS - have also been used by the group with the concerned copolymers. LIPS was used for the preparation of PVDF membranes blended with diblock copolymers - PS-*b*-PEGMA - in [4]. Membranes were prepared with different copolymer concentration in the blend - from 0 wt% to 5 wt% - and the Water contact angle (WCA) were found to decrease with increasing copolymer concentration. The increase of copolymer content in the blend caused a decrease of both protein-adsorption and bacterial adhesion onto the membranes.

More recently, VIPS process was used for the production of PVDF membranes blended with PS-PEGMA triblock copolymers [1]. Excellent anti-biofouling capabilities were obtained, and flux recovery was good, particularly when compared with the recovery for a commercial membrane.

Regarding coating techniques, membranes modified with random and diblock copolymers with different PS and PEGMA chain lengths were studied in [2]. Diblock copolymer coated membranes showed better protein anti-adsorption and bacterial anti-adhesive properties, and the ideal PS/PEGMA ratio for the block copolymer was of about 2.1. In this study PEGMA chains never surpassed 52 repeating units while the PS could go from 20 to 96 repeating units.

On another work, solutions with different concentrations of diblock copolymers with same PS chain length and varying PEGMA chain length were prepared and coated onto commercial PvDF microfiltration membranes (0.1  $\mu\text{m}$  of pore size) [5]. For each copolymer type, when using a copolymer coating solution concentration higher than 5 mg/mL there was no apparent increase on the copolymer packing density. Relative protein fouling resistance was almost the same for most of the modified membranes for the different concentrations used – but much lower than for the pure PVDF membranes. As mentioned before, the physical anchoring of coated copolymers is usually considered as a possible issue for this type of modification, however on this work the authors found that there was good stability with no more than 6 % of the coating was detached after 60 days of soaking the membranes in water (no filtration test done). Further testing on a real system – a Membrane Bioreactor (MBR) with domestic wastewater, cyclic filtrations performed for 12 days – showed an improvement of the process by using the coated membranes, with Trans membrane pressure (TMP) not increasing significantly with the modified membranes after each cleaning cycle.

A remark to be done here involves the coating time used in each of the research papers. It is normally not the same, varying from 30 min to 24 h. This factor could affect the interpretation of results and their comparison between research papers.

## 1.2 Characterisation methods

The analytical techniques used for the characterisation of the modified membranes and their anti-fouling properties are quite varied.

To evaluate the physical or physico-chemical properties of the membranes, the determination of coating density, hydration capacity, hydrophilicity, roughness, and/or force spectrometry can be used.

The first two methods involve the determination of the weight difference between an initial state - unmodified or dry membrane - and a final state - modified or wet for coating density or hydration capacity, respectively. This methods are considered as a first approach on detecting the presence of the copolymer, or of a hydration layer.

The measurement of water contact angle for the determination of hydrophilicity was discussed in Chapter 1 (section 3.2.1, page 13).

Atomic force microscopy (AFM) can be a very useful technique to determine surface roughness and attractive/repulsive forces profiles.

Chemical properties of the surfaces are usually determined with Fourier transform infrared spectroscopy (FTIR) and X-ray photoelectron spectroscopy (XPS) techniques. FTIR can be a very easy-to-apply technique, with little to no sample preparation, and there is plenty of information available on peak positioning regarding to the chemical species of interest.

General (bio)fouling tests involve the static attachment of organic or biological species on the membrane and their detection with the appropriate techniques. For instance, UV absorption at 280 nm can be used for the detection of proteins, such as Bovine serum albumin (BSA) and Lysozyme (LYZ). For bacteria and blood cells, confocal microscopy can be chosen for their detection and counting. Also Scanning electron microscopy (SEM) has been used for this purpose [6].

Finally, filtration tests should also be carried out to test the efficiency of the membranes against fouling. This dynamic testing provides very important and useful information on optimal operational parameters and the behaviour of the system when multiple filtration-cleaning cycles are performed.

The study of the modification of the membranes to enhance their anti-fouling properties requires the application of multiple analytical techniques in order to understand the process. This chapter is mainly dedicated to apply these classical techniques into the study of our membrane-copolymer system.

### 1.3 Objectives

The objectives of this chapter are to apply some of the techniques that are widely used by researchers to assess the success of the modification process in terms of the anti-fouling properties of the membranes in our membrane-copolymer system. The

base membrane being a commercial MF PVDF one, and the copolymers comprised of different PS-PEGMA structures.

Except for the filtration tests, the experiments shown in this chapter were performed at the R&D Center for Membrane Technology and Department of Chemical Engineering of the Chung Yuan Christian University, in Taiwan, during an exchange visit.

## 2 Materials and Methods

### 2.1 Materials

The ethanol ( $\text{EtOH}_{abs}$ ) used to dissolve the copolymers was provided by VWR Prolabo Chemicals (AnalaR NORMAPUR). Phosphate buffered saline solutions (PBS 1x, pH=7.4) were prepared from concentrated PBS 10x bulk solution from Fisher BioReagents (BP399). The molar composition (mol/L) of the concentrated PBS solution are the following: 1.37 M sodium chloride, 0.027 M potassium chloride, and 0.119 M phosphate buffer. Ultrapure water used in the experiments was purified from the osmotic water obtained from an ELGA PURELAB Prima purification system with an ELGA PURELAB Classic water purification system (final minimum resistivity of 18  $\text{M}\Omega \text{ cm}$ ).

Bovine serum albumin (BSA), which has a MW of 66 000 Da, was purchased from Sigma® (A4378). It was used for the static adsorption and filtration experiments. Lysozyme (LYZ) from chicken egg white with a MW of 14 300 Da (L6876 Sigma®) and used for the static adsorption experiments.

Polystyrene (PS) and Poly(ethylene glycol) methacrylate (PEGMA) copolymers were synthesized by the R&D Center for Membrane Technology and Department of Chemical Engineering of the Chung Yuan Christian University in Chung-Li, Taiwan. Random (PS-r-PEGMA or RND), diblock (PS-b-PEGMA or DB), and triblock (PEGMA-b-PS-b-PEGMA or TB) copolymers were used with the repeated units of PS and PEGMA shown in the table below (Table 2.1), and their general structure on Figures 2.1 and 2.2. More detailed information on how these copolymers are synthesized can be found in [2].

**Table 2.1:** Copolymers used for the modification of the membrane.

Copolymer type	Formula	MW (Da)*	PI	PEGMA molar ratio
Random	$PS_{61} - r - PEGMA_{121}$	66,950	1.83	0.66
Diblock	$PS_{53} - b - PEGMA_{124}$	63,850	2.10	0.70
Triblock	$PEGMA_{124} - PS_{54} - PEGMA_{124}$	125,930	2.04	0.82

\* 1 Da = 1  $\text{g mol}^{-1}$

Unless otherwise specified, PVDF microporous membranes (VVHP04700, Millipore Co.) were used as received for the experiments. They have an average pore size of 0.1  $\mu\text{m}$ , and a thickness of approximately 110  $\mu\text{m}$ . With the exception of the filtration tests, 1  $\text{cm}^2$  membrane disks were cut and used for all the analysis.

## 2.2 Methods

### 2.2.1 Coating of the membranes

Copolymer solutions were prepared adding  $\text{EtOH}_{abs}$  to weighed amounts of copolymer and stirring overnight to ensure complete dissolution. The concentrations ranged from 1 to 10 mg of copolymer per mL of ethanol.

The procedure to modify the virgin membranes was as follows. The Polyvinylidene fluoride (PVDF) membranes were left in contact with the corresponding copolymer solutions for 2 hours at room temperature. Then they were rinsed three times with PBS solution to remove non-adsorbed copolymer. The coating solutions concentrations were of 0.5 mg, 1 mg, 5 mg and 10 mg of copolymer per mL of ethanol. Virgin membranes were taken as blank and were treated the same way as the coated ones but using a pure ethanol solution instead of a copolymer one.

### 2.2.2 Determination of the coating density

Coating density was determined by performing a mass balance between the unmodified and modified membranes. First, the membranes were dried overnight at 37 °C and their dry weights were registered ( $W_D$ ). The coating was performed as specified by the experimental parameters and the membranes were dried at 37 °C overnight. Modified membranes weights were then registered ( $W_M$ ). Coating density with respect of membrane area ( $A_{membrane}$ ) was calculated as follows:

$$\text{Coating density} = \frac{W_M - W_D}{A_{membrane}} \quad (2.1)$$

For each experimental condition, the final coating density is an average of five independent dry weight measurements. The average experimental uncertainty was of  $\pm 0.02 \text{ mg/cm}^2$ .

### 2.2.3 Water contact angle

Contact angle measurements were carried out by dropping 4  $\mu\text{L}$  water droplets on a dry membrane at 10 different sites and measuring the contact angle at 25  $^{\circ}\text{C}$  with an angle-meter (Automatic Contact Angle Meter, Model CA-VP, Kyowa Interface Science Co., Ltd., Japan).

### 2.2.4 Hydration capacity

The modified membranes were dried overnight at 37  $^{\circ}\text{C}$  and their dry weights were registered ( $W_M$ ). 1 mL of deionized water was added to each membrane and membranes were left in contact with the water for 6 hours at 37  $^{\circ}\text{C}$ . Then the superficial water was gently removed by adsorbing it with a tissue and wet weight were registered ( $W_W$ ). Hydration capacity was calculated as follows:

$$\text{Hydration capacity} = \frac{W_W - W_M}{A_{\text{membrane}}} \quad (2.2)$$

For each modification condition, five independent measurements were carried out. The average experimental uncertainty was of around  $\pm 0.21 \text{ mg/cm}^2$ .

### 2.2.5 XPS

X-ray photoelectron spectroscopy (XPS) was performed using a PHI Quantera SXM/Auger spectrometer with a monochromated Al KR X-ray source (1486.6 eV photons) [3]. The energy of emitted electrons was measured with a hemispherical energy analyzer at pass energies ranging from 50 to 150 eV. All the data were collected at photoelectron take off angles of 45 $^{\circ}$  with respect to the sample surface. The Binding energy (B.E.) scale was referenced by setting the peak maximum in the C1s spectrum to 284.6 eV. A high-resolution C1s spectrum was fitted using a Shirley background subtraction and a series of Gaussian peaks. The data analysis software was from Service Physics, Inc.

The membranes were dried at 37  $^{\circ}\text{C}$  prior to analysis. For our samples, general peaks for fluorine, carbon and oxygen can be detected on the survey spectrum at binding energies of 687 eV, 285 eV and 531 eV, respectively - F1s, C1s, and O1s, respectively. Then, high-resolution spectra can be acquired from the components of interest, which in our case it involves the C1s spectrum, and the peaks can be

associated with different carbon bonds according to the binding energy. The following table (Table 2.2) shows the peaks of interest in the C1s spectrum as well as the O1s one.

**Table 2.2:** XPS C1s scan: peaks of interest and their associated bonds [4].

C1s scan	Peak (eV)	Bonds	Copolymer	PVDF
A	286	$\underline{C}H_2, \underline{C}-O, \underline{C}-O-H, \underline{C}-O-C$	Yes	Yes
B	290	$\underline{C}F_2, -CH_2CF_2-$	x	Yes
C	284	$\underline{C}-C, \underline{C}-H$	Yes	x
<b>O1s scan</b>				
	531.5-532	organic $C-O$	Yes	x
	533	organic $C=O$	Yes	x

Peak B on the C1s core-level is associated to CF<sub>2</sub> bonds present in PVDF, and while peak A could be as well associated to PVDF and the copolymer, it increases with the presence of copolymer (Figure 2.3). The O1s core-level scan is there to confirm that the detected amounts of oxygen in the survey spectrum correspond to the sample, and it is not a result of foreign oxygen, such as oxygen in air.

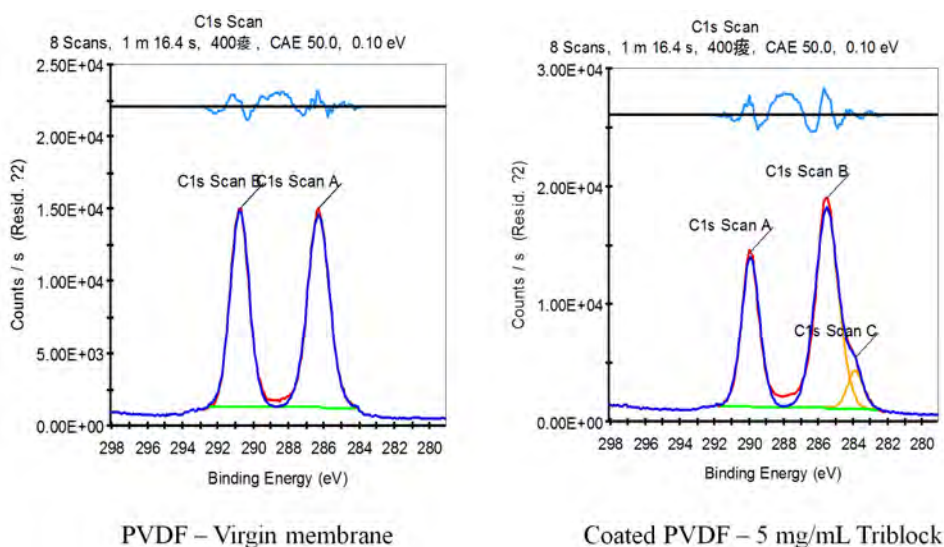


**Figure 2.3:** Example of the variation of the peaks for the C1s spectrum.

From the information on atom percentages of the C1s scan, it is possible to calculate peak ratios to express the amount of copolymer present on the membrane in relation to the virgin membrane (Copolymer surface coverage index - *CSCI*).

$$CSCI = \frac{\frac{A+C}{B} \text{ copolymer}}{\frac{A+C}{B} \text{ virgin}} \quad (2.3)$$

### 2.2.6 Protein adsorption

For the preparation of 1 g/L BSA, the albumin was weighed, dissolved in 1x PBS and stirred for 1 hour.

The adsorption of bovine serum albumin (BSA,  $MW = 66000 \text{ Da}$ , Sigma®) was performed. The membranes were placed in a 24-well plate and immersed in 1 mL of phosphate-buffered saline (PBS 1x) solution for 20 h at 37 °C. then the PBS was removed and the membranes were incubated in 1 mL of 1 g/L BSA for 2 h at 37 °C. The absorbance at 280 nm was measured using a UV-Vis spectrophotometer (PowerWave XS, Biotech). The final absorption value corresponds to the average of three independent absorbance measurements. The same methodology was used for lysozyme from chicken egg white (LYZ,  $MW = 14300 \text{ Da}$ , Sigma®).

### 2.2.7 Blood cell adsorption

The extraction, adsorption procedure and analysis of the blood cell adsorption (Red blood cells, erythrocytes (RBC), White blood cells, leukocytes (WBC), Platelet-rich plasma, thrombocytes (PRP)) were carried out according to [7]. Briefly, the different types of blood cells were isolated from the blood from a healthy human volunteer. Erythrocytes were isolated by centrifugating 250 mL of fresh blood for 10 min at 1200 rpm and extracting 1 mL of the bottom layer. Leukocytes were obtained by centrifugating 250 mL of fresh blood for 30 min at 500 rpm and extracting 1 mL of the intermediate layer from the three visible phases (top: platelets, bottom: red blood cells). Thrombocytes were isolated by centrifugating 250 mL of fresh blood for 10 min at 1200 rpm.

For each blood cell type (RBC, WBC, and PRP) the following adsorption method was carried out. 1 mL of the specific blood cell type was poured onto the membrane disks (diameter of 0.4 cm<sup>2</sup>) placed in a 24-well tissue culture plate and previously

equilibrated for 24 h at 37 °C using 1 mL of PBS. The incubation of the blood cells with the membranes was carried out for 2 h at 37 °C. Membranes were then washed six times with 1 mL of PBS. Thereafter, they were soaked for 10 h into a 2.5 % (v/v) glutaraldehyde solution in PBS maintained at 4 °C in order to fix the adhered cells. Membranes were then thoroughly washed five times with PBS.

The detection of the cells adsorbed onto the membrane surface was done with a confocal microscope (LSCM, A1R, Nikon, Japan). Images were taken at  $\lambda_{ex} = 488 \text{ nm}/\lambda_{em} = 520 \text{ nm}$ , in z-steps of 1  $\mu\text{m}$ , at three different places on the same chip and at a magnification of 200x. From the confocal microscope images obtained the blood cell count was done by ImageJ software, taking into account the size and shape of the cells (Table 2.3).

**Table 2.3:** Blood cells: types and dimensions.

Blood cell type	Description	Dimensions ( $\mu\text{m}$ )
Red blood cells	Biconcave disks, flattened in the center	<i>Diameter:</i> 6-8
		<i>Thickness:</i>
		Centre: 1 Sides: 2.5
White blood cells	Spherical, granulated on surface	<i>Diameter:</i> 10-15
Platelets	Lens-shaped when unactivated	<i>Diameter:</i> 2-3

### 2.2.8 Filtration protocol

Dead-end filtration experiments with Amicon® stirred cells (Series 8050, Merck Millipore) were carried out at a stirring speed of 200 rpm, temperature of 20 °C and pressure of 0.2 bar to assess the efficiency of the coating for different coating times.

Coated membranes with a copolymer concentration in coating solution of 5 mg/mL were left with PBS 1x solution overnight, and the initial PBS flux was recorded ( $J_{PBS_i}$ ). Then 1 g/L BSA was filtered until 400 mL of permeate was collected, and afterwards the rinsing step was performed with 20 mL of PBS 1x for 20 min. The final PBS flux ( $J_{PBS_f}$ ) was recorded (Figure 2.4). Experiments were

repeated twice, the average experimental error was of 15 %.

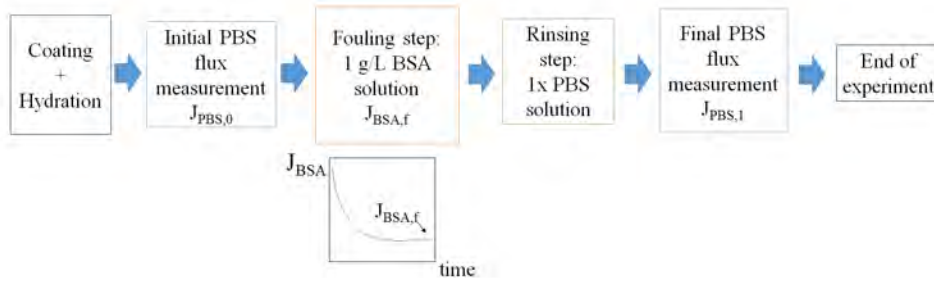


**Figure 2.4:** Diagram of the protocol for the filtration.

### Calculations

From the filtration data it is possible to calculate some indexes that aim to describe how well the membranes performed in terms of the final BSA and PBS fluxes. The first one is the Reversibility index (RI):

$$RI = \frac{J_{PBS_f} - J_{BSA_f}}{J_{PBS_i} - J_{BSA_f}} \quad (2.4)$$

where  $J_{BSA_f}$  refers to the final registered BSA flux - before starting the rinsing process.

It is a measurement of the reversibility of the fouling of the membrane. The following figure (Figure 2.5) depicts the relationship between the different parameters taken into account to calculate this index. Since the filtration flux will be lower than the initial PBS flux, the denominator in Eq. 2.4 depicts the maximum flux potential that could be recovered after the rinsing was performed. Therefore, the numerator would indicate the recovered filtration potential. In other words, the closer these terms are between each other, the more reversible the process will be. A *RI* of 0 would imply that the fouling is 100 % irreversible, while the fouling was 100 % reversible for an index of 1.

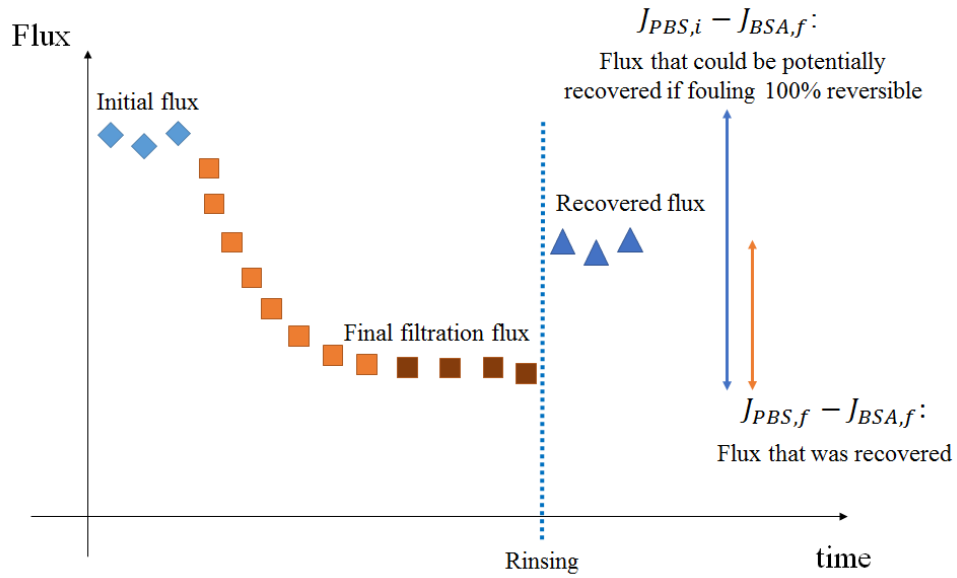


**Figure 2.5:** Illustration of the parameters taken into account to calculate the reversibility index.

Other indexes to take into account are the Fouling reversibility ratio (FRR) and Flux decline ratio (FDR). Their expressions are shown in the following equations.

$$FRR = \frac{J_{PBS_f}}{J_{PBS_i}} \quad (2.5)$$

$$FDR = \frac{J_{BSA_f}}{J_{PBS_i}} \quad (2.6)$$

### 2.2.9 Analysis of fouling - Resistances in series

Another way of analysing the data includes the calculation of the resistances in the filtration system. A general equation to express this matter is given below.

$$J = \frac{\Delta P}{\mu * R} \quad (2.7)$$

Where  $J$  (in  $\text{m}^3 \text{cm}^{-2} \text{s}^{-1}$ ) refers to the flux,  $\Delta P$  (in Pa) to the transmembrane pressure,  $\mu$  (in Pa s) to the viscosity of the fluid, and  $R$  (in  $\text{m}^{-1}$ ) to the resistance of the membrane system.

Assuming that we can model the total resistance as a series of resistances caused by the different components affecting the filtration efficiency,  $R$  will have different expressions depending which part of the filtration cycle we are taking into account. For the first PBS filtration the only resistance against the flow of liquid through the membrane concerns the membrane, hence, it is possible to calculate the resistance of the membrane as follows:

$$R_M = \frac{\Delta P}{\mu * J_0} \quad (2.8)$$

where  $J_0$  refers to the initial PBS flux, and  $R_M$  to the resistance of the membrane.

This resistance is the one of the membrane alone when filtration with the unmodified membrane are concerned. For the modified membranes this term can be considered as the sum of the resistance of the unmodified membrane ( $R_{M^*}$ ) and the one of the coating layer ( $R_C$ ) (2.9).

$$R_M = R_{M^*} + R_C \quad (2.9)$$

When the BSA filtration step is involved, the total resistance ( $R_{total}$ ) can be calculated from the BSA fluxes ( $J_{BSA}$ ) as shown by equation 2.10.

$$R_{total} = \frac{\Delta P}{\mu * J_{BSA}} \quad (2.10)$$

This total resistance is composed by the resistance of the membrane, coating, and fouling layer ( $R_{fouling}$ , equation 2.11).

$$R_{total} = R_{M^*} + R_C + R_{fouling} \quad (2.11)$$

Finally, after we proceed with the rinsing protocol - which is intended to remove the reversible fouling layer - only the irreversible fouling would be present in the system. Therefore, from the calculation of the total resistance after cleaning ( $R_{total}^*$ ) in a similar way that  $R_{total}$  was calculated (see equation 2.10), the contribution of the fouling can be calculated from equation 2.11 assuming  $R_{fouling} = R_{ir}$ , where  $R_{ir}$  corresponds to the resistance due to the irreversible fouling layer. Once we have this number, the resistance due to reversible fouling ( $R_{rev}$ ) can be calculated from the  $R_{fouling}$  value obtained previously as follows.

$$R_{rev} = R_{fouling} - R_{ir} \quad (2.12)$$

### 3 Results and Discussion

In the following chapters we will be showing the results obtained on the characterisation of the modification of the membranes and their anti-fouling properties (see Figure 2.6). First, we will present results concerning physical and chemical properties of the modified membranes. Then, general biofouling tests will be carried out as static adsorption of proteins - BSA and LYZ -, as well as the adsorption of blood cells. Finally, single filtration tests will be carried out to better assess the performance of the membranes.

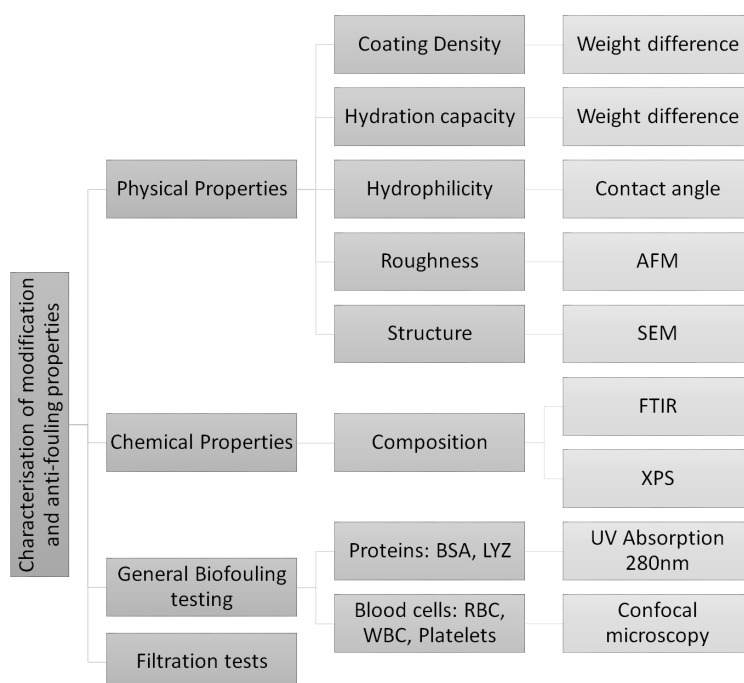


**Figure 2.6:** General chart on the results for this chapter.

#### 3.1 Physical and chemical properties of the modified membranes

In this section we are going to present some of the most used techniques applied for the characterization of the membranes when modified with the random, diblock, and triblock copolymers - PS-r-PEGMA, PS-b-PEGMA, and PEGMA-b-PS-b-PEGMA, respectively - with the methods described in the section 2 at the page 44. The results obtained for the SEM and AFM techniques are shown in Appendix A (section 1, page 187).

### 3.1.1 Coating density

The results obtained for the determination of the coating density are shown in Figure 2.7 in which two graphs with the evolution of the coated amounts of copolymer against copolymer concentration in the copolymer solution are depicted.

For increasing solution concentration, the amount of adsorbed copolymer increased up to a maximum value or plateau. For the three types of copolymer this maximum coating was the same when we take into account mass quantities. When calculating the molar densities, the triblock copolymer showed the lower molar adsorptions, caused by its larger structure (almost double the MW of the others). The PS-r-PEGMA copolymer reached the plateau at lower concentrations of copolymer than the other two copolymers.

It is interesting to note that the main difference between the random and diblock copolymers is the distribution of the PS and PEGMA units. While the first one has a random distribution of lengths between these chains, the diblock copolymer has a long PEGMA chain attached to the end of the PS. The random nature of the copolymer structure seemed to yield better adsorption properties.

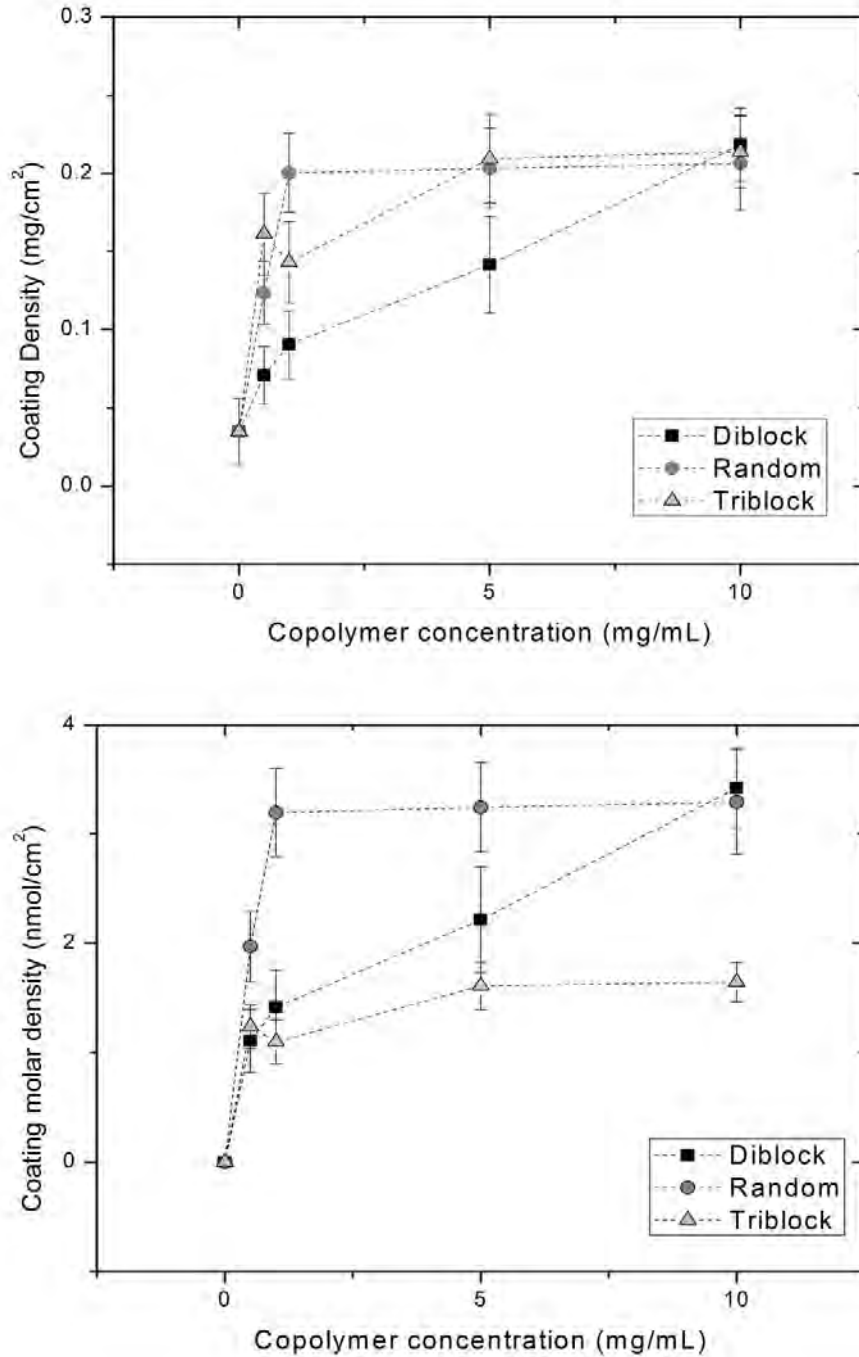


**Figure 2.7:** Calculated coating density for the diblock, random and triblock copolymers as a function of copolymer concentration in the coating solution. Top: coating density in mg/cm<sup>2</sup>, bottom: molar coating density in nmol/cm<sup>2</sup>.

The presence of an adsorption plateau has been seen before [2, 5]. In Chiag et al. [2] the authors compare random and diblock copolymers with different chain lengths when coating UF membranes, while for [5] diblock copolymers are studied in MF membranes, the same commercial ones used in this chapter. A comparative table with some selected results from these two papers, and the results obtained in our case, is presented below (Table 2.4). The copolymers shown in this table have similar PS chain lengths.

**Table 2.4:** Maximum coating density for PS-PEGMA copolymers obtained in this work and others.

Membrane	Copolymer	Molecular weight	Max. coating density		Ref.
			g/mol	mg/cm <sup>2</sup> nmol/cm <sup>2</sup>	
PVDF MF	$PS_{53} - b - PEGMA_{124}$	63,850	0.22	3.4	-
	$PS_{61} - r - PEGMA_{121}$	66,950	0.21	3.3	-
	$PEGMA_{124} - b - PS_{54} - b - PEGMA_{124}$	125,930	0.21	1.6	-
PVDF UF	$PS_{52} - b - PEGMA_{25}$	17,423	0.08	4.6	[2]
	$PS_{20} - r - PEGMA_{12}$	8,124	0.16	19.7	
PVDF MF	$PS_{55} - b - PEGMA_{30}$	19,900	0.15	7.5	[5]
	$PS_{55} - b - PEGMA_{111}$	58,500	0.12	2.1	

Similar mass coating densities were obtained for the different works when coating MF membranes, even when the coating conditions, i.e., coating time and copolymer structures, were not exactly the same. In our work we used a coating time of 2 h while for Lin et al. [5] the membranes were coated for 24 h. Concerning the coating of UF membranes, comparisons with other works have to be made quite carefully since the modification time used by this other work was of 30 min. The comparison of the coating densities between different types of membranes (MF and UF) could not lead to reasonable conclusions, because the area used as the reference coated area in MF membranes is highly underestimated; typically only the superficial area is taken into account for the calculations.

Further results will be expressed in relation to the molar coating density.

### 3.1.2 Water contact angle and hydration capacity

The determination of Water contact angle (WCA) is one of the most widely used when trying to assess the modification success in terms of increased hydrophilicity of the materials. Lower contact angles indicate an increase of hydrophilicity while higher one an increase in hydrophobicity. According to many researchers, the increase in hydrophilicity could mean better anti-fouling properties, however, conclusions based solely on this measurement should not be drawn. The measurement can lack sensitivity and varies with rugosity, porosity, and pore size distribution among others. Therefore, it is also difficult to use it as a comparison reference between studies.

As for the hydration capacity of the membranes, as long as we are adsorbing higher amounts of copolymers, more water will be hydrating the copolymer structure, hence potentially increasing the hydrophilicity of the membrane and lowering the water contact angle.

The following figure illustrates the variation of water contact angle and hydration capacity with the molar coating density of the coating layer, for the different copolymers used in this work (Figure 2.8).

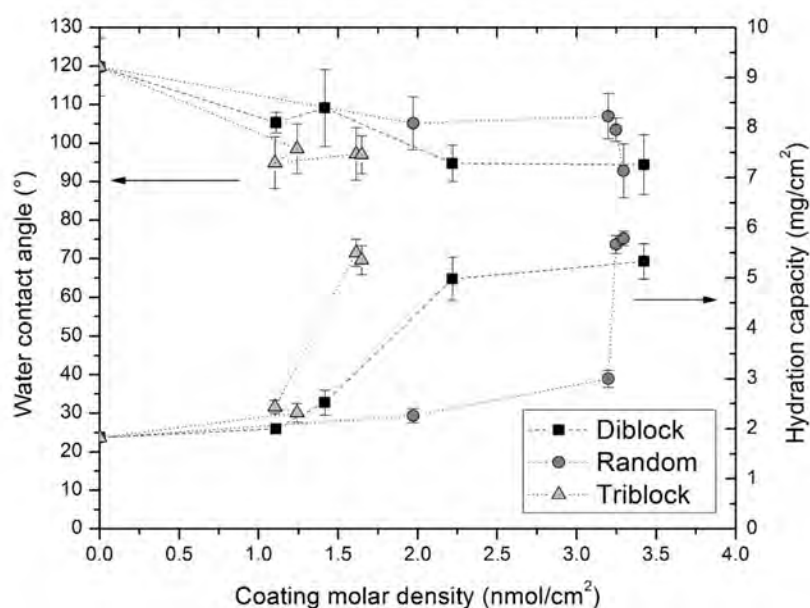


**Figure 2.8:** Water contact angle and Hydration capacity for the diblock, random and triblock copolymers as a function of molar coating density.

It is possible to appreciate an increase in hydrophilicity when comparing the modified and unmodified membranes. The contact angle decreased from  $120^\circ$  to a minimum of approximately  $95^\circ$ . For the triblock copolymer this minimum value was reached with a lower molar density than for the other two copolymers. This final WCA angle was found to be relatively high, particularly when we are trying to produce hydrophilic membranes. First, the type of modification performed was not intensive enough to yield very low WCA angles. Another factor to take into account is that these copolymers were designed to be used as biocompatible materials, for which the wettability of the surface needs to be high enough for biocompatibility reasons, yet low enough to prevent cell-cell interaction. Thus, depending on the application, a balance between hydrophilicity and hydrophobicity has to be reached to take into account this, and extremely low WCA could be counterproductive [8].

It was not possible to fully appreciate whether the different molar densities of copolymer reached affect any further on the properties of the membranes. However, these changes were more visible if we take a look on the hydration capacity chart

(Figure 2.8).

The hydration capacity of the membranes increased with the increase of copolymer adsorbed. For the different copolymers, the maximum hydration capacity reached a similar value of  $5.5 \text{ mg/cm}^2$ . However, for the membranes modified with the triblock copolymer this value is reached at a lower molar density. The membranes modified with the diblock copolymer reached their maximum hydration capacity at a lower molar coating density than for the random ones. The extra PEGMA chain in the triblock copolymer seemed to improve the hydration capacity of the membranes, when compared with the other copolymers for a given coating molar density. The different configurations of the chains - long brushed vs. loops - also seemed to affect the point where the maximum hydration capacity was reached. For the random copolymer it was possible to appreciate that for very small changes in molar density the hydration capacity rapidly reached its maximum.

The relationship between WCA and hydration capacity is depicted in Figure 2.9. For all of the copolymers and conditions used, a higher hydration capacity was associated with lower WCA. For the membranes modified with the triblock copolymer, the lowest WCA was reached at a value of hydration capacity of around  $2.5 \text{ mg/cm}^2$  which was lower than the values registered for the modifications performed with the diblock and random copolymers ( $5 \text{ mg/cm}^2$  and  $6 \text{ mg/cm}^2$ , respectively).

### 3.1.3 X-ray photoelectron spectroscopy (XPS)

XPS is a technique widely used to analyse the surface chemistry of a material. Only the electrons emitted from the top 1 nm to 10 nm are analysed by the spectrometer. For our system it is possible to detect the difference in the composition of the surface with the peaks that are detected at the different binding energies (B.E.) and the change in peak size and shape.

A summary of the variation of the atom percentages on the survey scan, and specific C1s and O1s scans is presented in the table below (Table 2.5).

With higher concentrations of copolymer present in the sample, the atom percentages of the C1s and O1s increase, while the percentages of F1s decrease. There was no oxygen detected on the virgin membrane, while for the modified

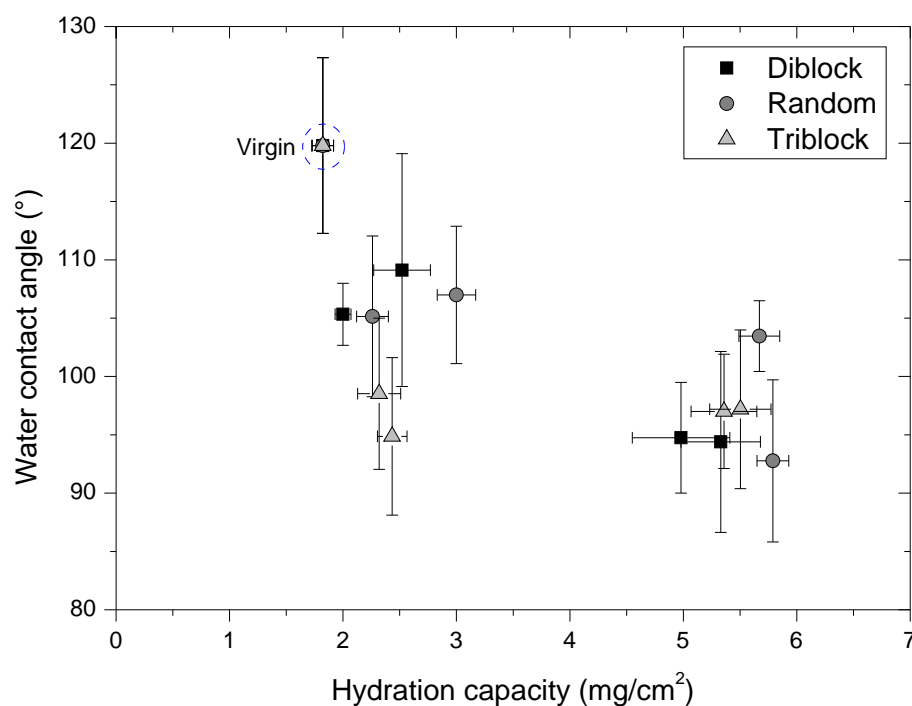


**Figure 2.9:** Water contact angle as a function of Hydration capacity for the diblock, random and triblock copolymers.

membranes it increased with molar density. The atom percentage scans of O1s confirmed these trends.

The C1s presence of the survey scan were the lowest for the unmodified membrane, while for the modified ones, they increased with increasing coating density. The percentage of the F1s peak showed opposite trends: it was the highest for the virgin membrane, while the more copolymer was present, the lower signals of this peak were detected. This implies that a coating layer was deposited on the membrane surface, and this layer was denser - and maybe thicker - the more copolymer was present on the surface.

The detection of the peak C in the C1s scan for the membranes modified with the random and triblock copolymers could be showing that the general copolymer backbone is more exposed towards the surface, which could ultimately affect the anti-fouling properties of the membranes. For the peak B, which gives an indication on the detected PVDF, the virgin membrane had the highest peak percentage value.

**Table 2.5:** XPS results. Survey scan, C1s and O1s scans.

Membrane	Coating density nmol/cm <sup>2</sup>	At% Survey scan			At% Scan O1s	At% C1s scan		
		F1s	C1s	O1s	532 eV	A	B	C
Virgin	0	48.68	51.32	0.00	0.00	53.06	46.94	0.00
Diblock	1.11	43.53	53.38	3.10	32.52	57.24	42.76	0.00
	3.42	41.78	53.64	4.59	51.15	61.21	38.79	0.00
Random	1.97	39.24	55.42	5.34	53.27	56.79	36.87	6.34
	3.29	35.89	57.06	7.05	76.97	58.58	33.00	8.43
Triblock	1.24	43.47	53.29	3.24	35.30	55.97	41.41	2.62
	1.65	33.74	59.41	6.85	66.65	52.67	29.19	18.14

The modified membranes presented lower percentages of this peak, and when the coating density was higher the presence of this peak was lower. As the coating layer covered the surface and probably increased its thickness, this peak decreased. It was especially noticeable for the triblock copolymer, in which the B peak decreased by almost 56 %.

From the C1s scans, the CSCI ratio was calculated according to section 2.2.5 on page 48. The following graph follows the evolution of calculated CSCI ratio as a function of coating density (Figure 2.10).

For the diblock copolymer this value remains almost unchanged after a certain coating density value while for the random and (especially) for the triblock copolymers it rapidly increases at a specific density. This behaviour could be attributed to the chain conformation; after reaching a “saturation” density the hydrophobic part of the copolymers are fully rearranged into brush-like structures protruding outside the membrane. The increase in thickness of the coating layer could also be influencing the obtained results.

### 3.2 General biofouling tests

Other set of tests to evaluate the anti-fouling properties of the modified membranes is the adsorption of bioagents, such as proteins and blood cell components. The results

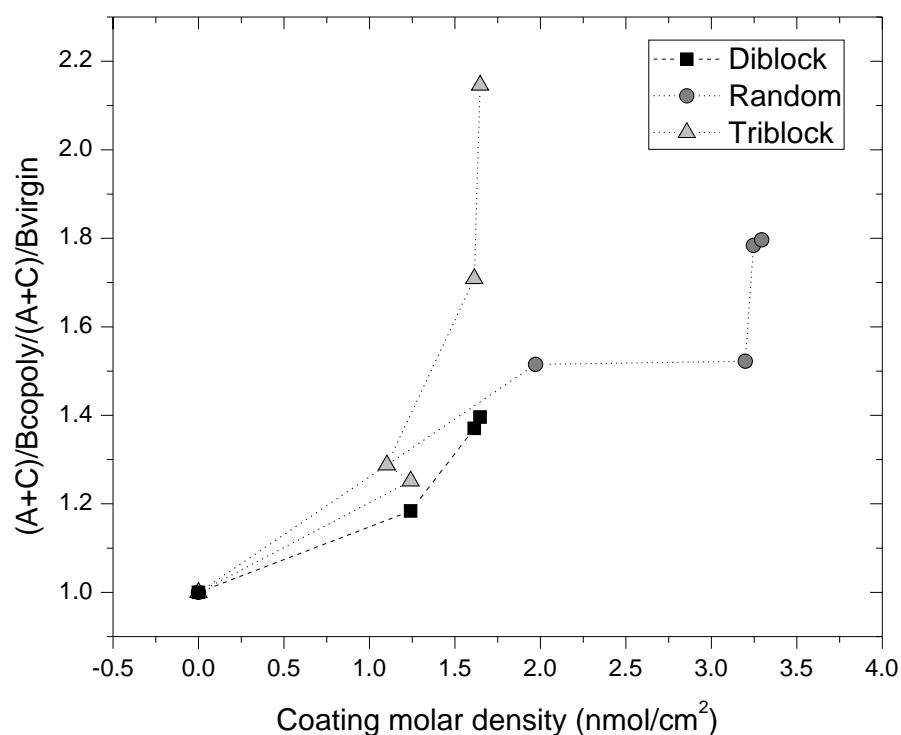


**Figure 2.10:** Evolution of copolymer present on the membrane surface for the different copolymers as a function of molar coating density, calculated from XPS data.

obtained for these tests are shown in the following sections.

### 3.2.1 Adsorption of proteins

The adsorption of Bovine serum albumin (BSA) and Lysozyme (LYZ) as a function of coating molar density and for the different copolymers is shown in the figure below (Figure 2.11).

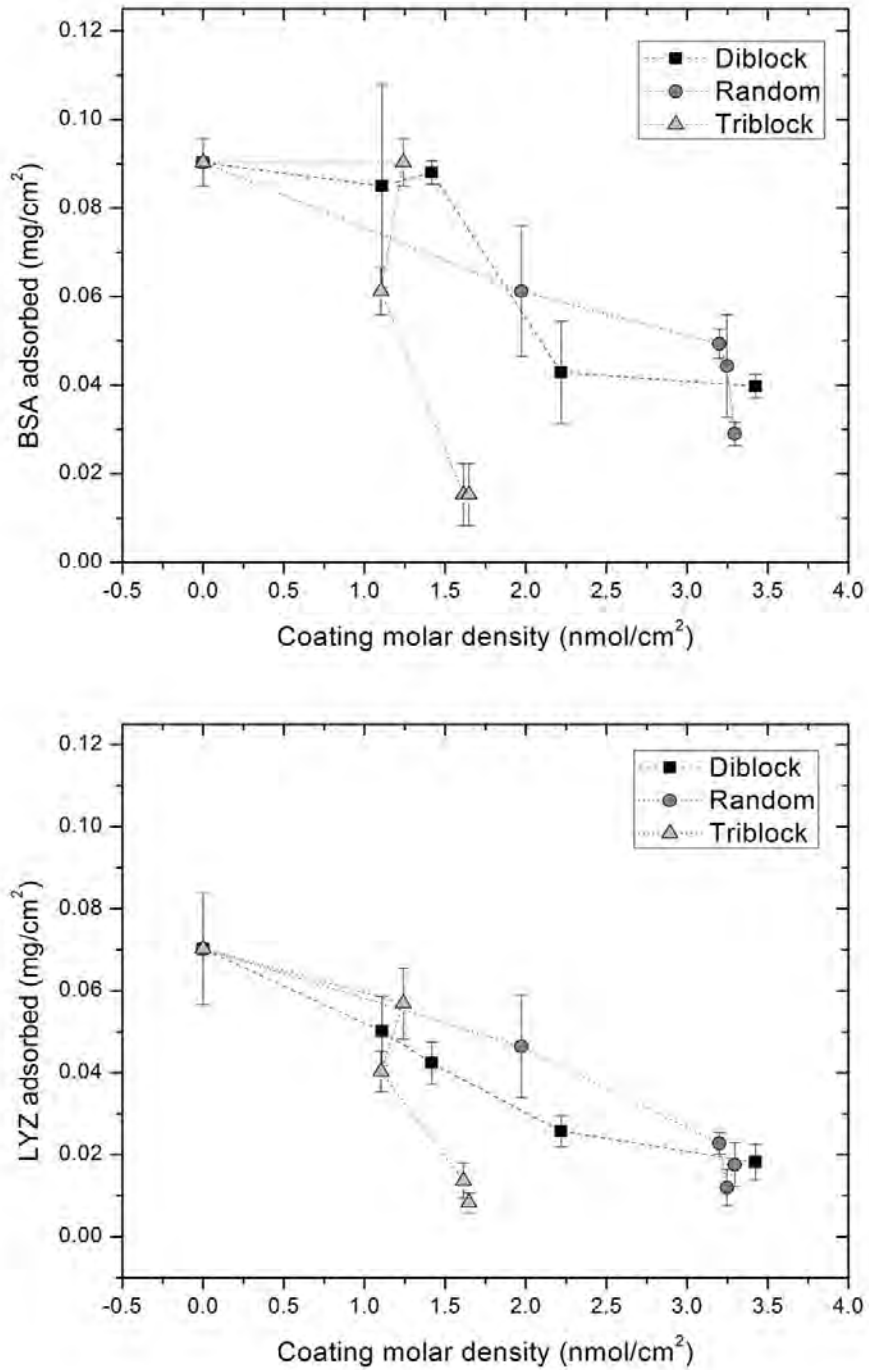


**Figure 2.11:** Protein adsorption as a function of the molar coating density for the diblock, random, and triblock copolymers. Top: Adsorption of BSA; bottom: adsorption of LYZ.

For all of the copolymers and proteins, the more copolymer present on the membrane, the lower the protein adsorption. Hence, protein adsorption was hindered by the modification process.

For BSA, the triblock, random, diblock copolymers reduced the adsorption of this protein by 83 %, 67 %, and 55 %, respectively, when compared to the adsorptions obtained for the virgin membrane. The final LYZ adsorption reduction was of about 85 % for the three copolymers. In the tested conditions, a zero protein adsorption was never reached, however, a saturation coverage of the surface was achieved. This could be due to an heterogeneous coverage of the surface.

For both proteins, the triblock copolymer seem to be more efficient in molar terms to decrease their adsorption. Both the random and diblock copolymers showed no great difference in BSA or LYZ adsorptions suggesting that the PEGMA chain conformation is not an important factor, for the adsorption of these proteins under the conditions of this study. If we take now into account the triblock copolymer, only how much PEGMA is present in relationship with the PS would have a greater impact.

It is also important to note that BSA and LYZ are different, mainly in size and isoelectric points (pI). BSA has a MW of approximately 66 000 g/mol and a pI of 4.8, while for LYZ these values are of 14 000 g/mol and 10.3, respectively. At the working pH of 7.4, BSA will have a global negative charge, while LYZ a positive one. In any case, the modified membranes - especially the ones with triblock copolymer - showed good anti-adsorption properties against these two proteins.

### 3.2.2 Adsorption of blood cells

When membranes systems are intended to be used in biomedical devices, it is also important to have an indicator on the adsorption of physiological components. In our work, we studied the adsorption of blood cell components: Red blood cells, erythrocytes (RBC), White blood cells, leukocytes (WBC), and Platelet-rich plasma, thrombocytes (PRP). An example of the confocal microscope images obtained from these sets of experiments are shown below for the case of RBC (Figure 2.12). The images corresponding to the adsorption of WBC and PRP can be consulted on Appendix A (section 2, page 191).

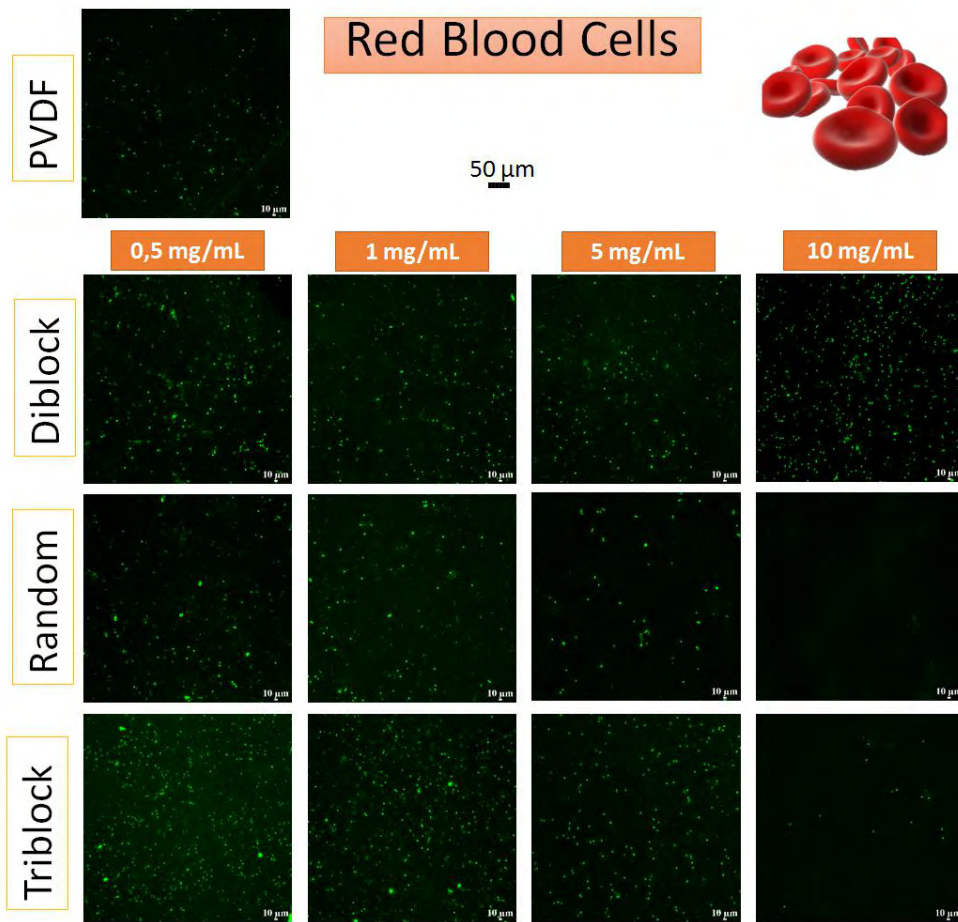


**Figure 2.12:** Example of confocal microscopy images of RBC for the membranes coated with different concentrations of copolymers.

From these images, the blood cell count was done with the ImageJ software taking into account the dimensions of the type of cell. Three images per experimental condition were counted and averaged. The results are shown in the following figure as a function of the molar density for the different copolymers (Figure 2.13).

In general it was possible to appreciate a reduction of the adsorption of the blood cells. The smaller and more irregular blood cell components (platelets followed by RBC) were more adsorbed in general, while the bigger and more spherical WBC were the least adsorbed. In the human body, PRP are specialised to adhere to walls to help close or cure wounds, so their higher adsorption levels can also be explained by this fact.

The results are different when comparing the different copolymers. For the diblock case, the reached adsorptions were generally higher or in the range of the counts obtained for the virgin membrane. Hence, the modification process would not change the final outcome of the adsorption or it would worsen it.

The best results were obtained for the triblock and random copolymers, with the triblock showing more efficiency per mole of adsorbed copolymer. The membranes modified with these two copolymers showed a reduction in cell adsorption of almost 100 % for RBC and WBC, and of 65 % for platelets, while the diblock copolymer reduced the adsorption of RBC in around 30 %, increased the adsorption of WBC by 75 %, and did not have any differential effect on the platelet adsorption, when compared to the performance of the virgin membrane.

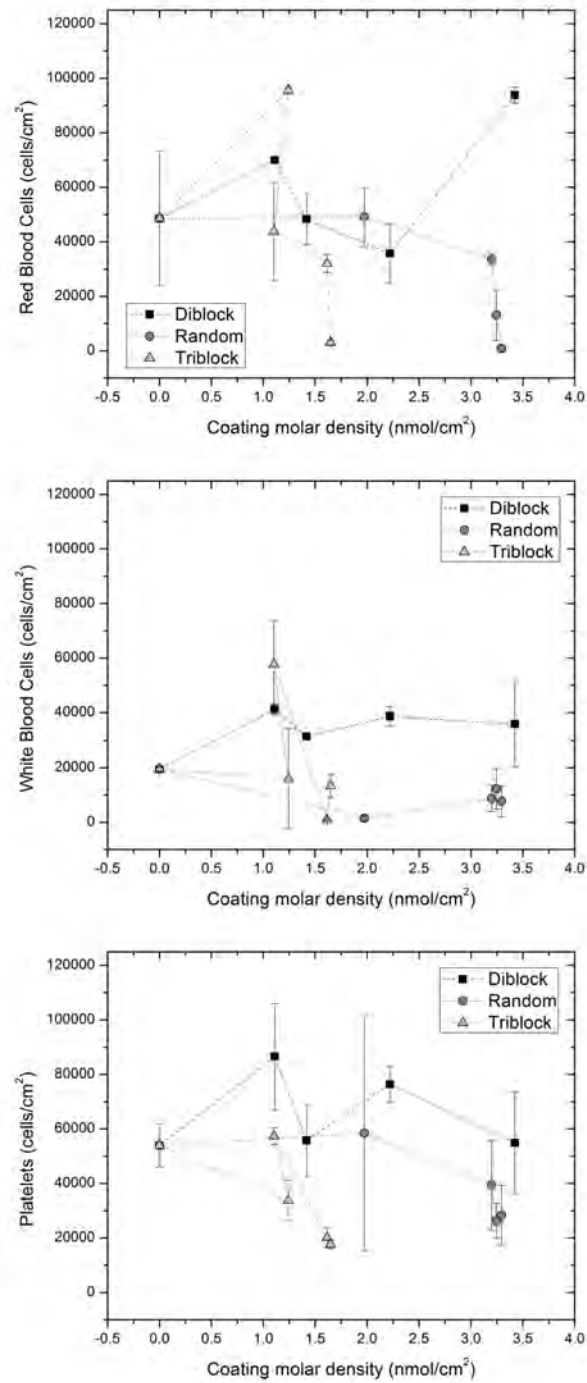


**Figure 2.13:** Blood cell count of RBC, WBC, and PRP for the membranes coated with different concentrations of copolymers as a function of molar density. Top: RBC; middle: WBC, and bottom: PRP.

The distribution of the PEGMA polymer on the surface could be a key factor to be able to explain these results. For the triblock copolymer, the two PEGMA chains are separated from each other at a similar distance set by the PS that connects them. The random copolymer could be creating also a good spacing and coverage of the PEGMA polymers on the surface of the membrane.

It is also important to point out that these differences were not so marked for the smaller proteins, for which only the amount of PEGMA present on the surface seemed to affect the anti-adsorption properties of the membranes. A smaller protein is more prone to diffuse through a network of polymer chains (size exclusion).

Cell-surface interactions can vary due to many factors and can be very difficult to explain, however, one important point to avoid the adherence of cells on the surfaces would be to avoid the adsorption of proteins, since they can cause further cell adsorption [9].

### 3.3 Filtration tests

Simple filtration tests were performed according to the Materials and Methods, section 2.2.8, page 49. In them the initial PBS fluxes were registered. Afterwards, the BSA filtrations were carried out until approximately 400 mL of permeate was collected. Then, the membranes were rinsed with PBS, and the final PBS fluxes were registered. The results of this process are depicted in Figure 2.14 with the evolution of permeability with time, and the evolution of the relative fluxes with time.

The initial PBS permeability of the virgin membrane was slightly higher than for the modified ones; the random and diblock membranes had similar initial permeability and the membrane modified with the triblock copolymer showed the lowest initial PBS permeability. Final BSA fluxes for the random and diblock modified membranes were the highest, followed by the permeability of the triblock, and the lowest being the one for the virgin membrane. The final PBS permeabilities - after rinsing cycle - showed similar tendencies.

Since the initial PBS fluxes were not the same for the different membranes, the relative fluxes were calculated taking the average initial PBS flux as the reference (bottom graph of Figure 2.14). There, it is possible to appreciate that the membranes

modified with the different copolymers performed similarly when BSA was filtered through the system, and in their final PBS relative fluxes. The performance of the virgin membrane was the worst of the tested ones.

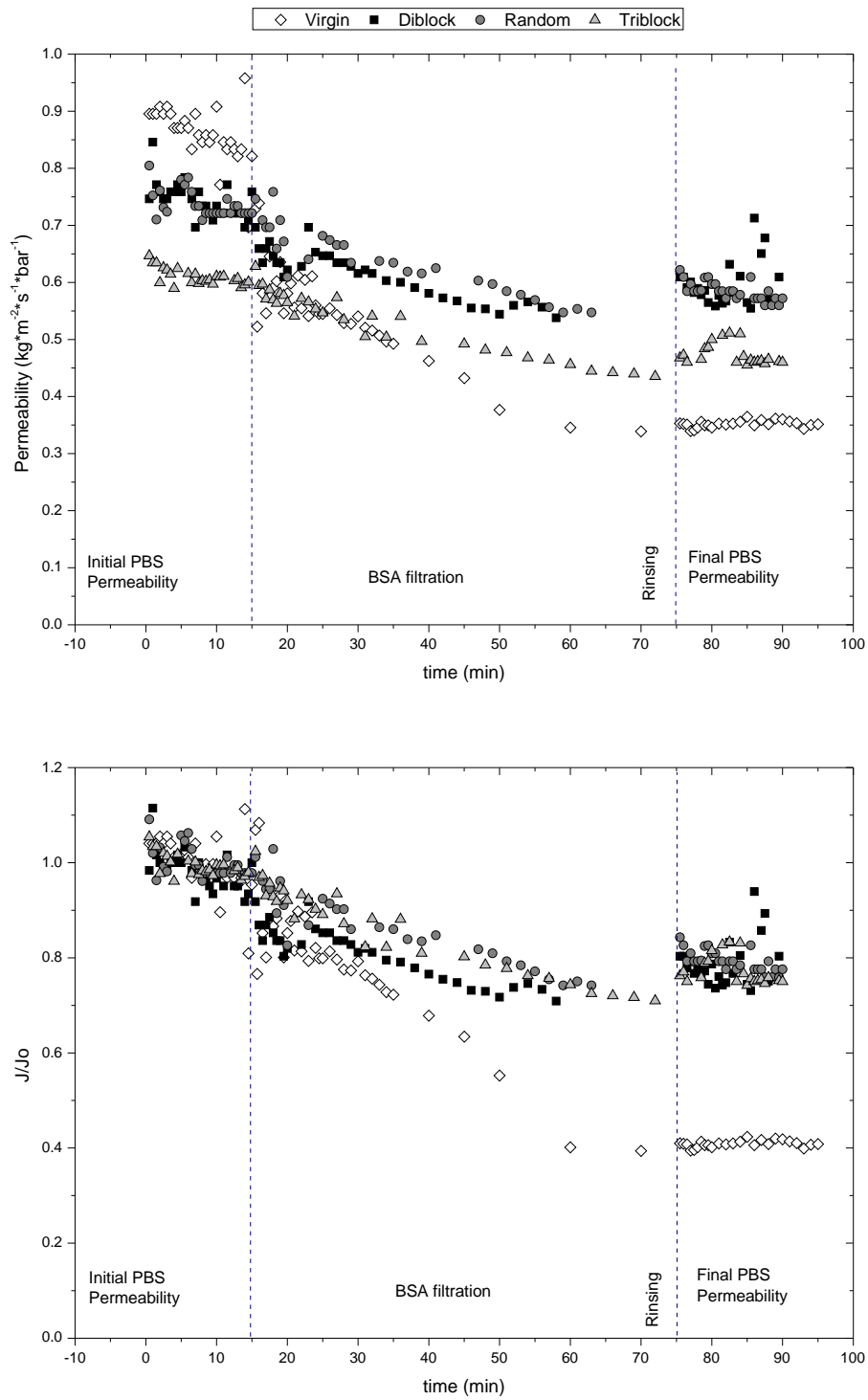


**Figure 2.14:** Filtration tests for the unmodified and modified membranes. Top: Permeabilities vs. time; bottom: relative fluxes vs. time.

A better look on this values is given in the table below (Table 2.6), where a summary of fluxes and indexes can be found.

**Table 2.6:** Summary of registered fluxes and calculated indexes for the modified membranes.

Copolymer	Initial PBS flux $kg * m^{-2} * s^{-1}$	Final BSA flux $kg * m^{-2} * s^{-1}$	Final PBS flux $kg * m^{-2} * s^{-1}$	RI	FRR	FDR
Virgin	$0.17 \pm 0.03$	$0.07 \pm 0.01$	$0.07 \pm 0.01$	0.02	0.41	0.39
Diblock	$0.15 \pm 0.02$	$0.12 \pm 0.02$	$0.12 \pm 0.02$	0.12	0.80	0.77
Random	$0.15 \pm 0.02$	$0.11 \pm 0.02$	$0.12 \pm 0.02$	0.19	0.79	0.74
Triblock	$0.12 \pm 0.02$	$0.09 \pm 0.01$	$0.09 \pm 0.01$	0.18	0.76	0.71

The reversibility index was generally low, but slightly higher for the modified membranes than the unmodified one. This is expectable since we are filtering BSA molecules with a diameter of around 7 nm through a membrane of a pore size of 0.1  $\mu\text{m}$ , therefore fouling will occur not only on the top layer of the surface of the membranes, but it will also affect the inner structure, which is more difficult to remove by simple rinsing.

The loss of PBS flux after fouling is less evident for the modified membranes. They also present higher FDR; filtration fluxes for BSA were higher in relationship with the initial PBS flux.

### 3.4 Analysis of fouling - resistances in series

The analysis of the resistances in series was performed for the filtration data registered previously. The following table sums up the values for the resistances of the system obtained for our system (Table 2.7).

For the modified membranes, the additional resistance of the coating layer was around one order lower than the resistance of the bare membrane. In percentages, this additional resistance for the membranes modified with diblock, random, and triblock copolymers with respect to the non-modified one was of 13 %, 17 %, and 40 %, respectively. The resistance of the coating layer for the triblock copolymer was the highest among the copolymers used.

**Table 2.7:** Summary of calculated resistances for the modified membranes.

Copolymer	$R_{M^*}$ $m^{-1}$	$R_C$ $m^{-1}$	$R_{fouling}$ $m^{-1}$	$R_{rev}$ $m^{-1}$	$R_{ir}$ $m^{-1}$	$R_{rev}/R_{fouling}$ %	$R_{ir}/R_{fouling}$ %
Virgin	$12 \times 10^{11}$	-	$18 \times 10^{11}$	$1.1 \times 10^{11}$	$17 \times 10^{11}$	6	94
Diblock		$1.6 \times 10^{11}$	$3.9 \times 10^{11}$	$0.61 \times 10^{11}$	$3.3 \times 10^{11}$	15	85
Random		$1.9 \times 10^{11}$	$4.7 \times 10^{11}$	$1.1 \times 10^{11}$	$3.6 \times 10^{11}$	24	76
Triblock		$4.7 \times 10^{11}$	$6.7 \times 10^{11}$	$1.6 \times 10^{11}$	$5.1 \times 10^{11}$	24	76

The total resistance of the fouling layer was higher for the virgin membrane, while the modified ones showed similar values, with the triblock having a slightly higher fouling resistance than the other two. Taking the virgin membranes as a reference, the resistance of the fouling layer was reduced by 78 %, 74 %, and 63 % for the membranes modified with diblock, random, and triblock copolymers, respectively. The modification did reduce general fouling deposition on the membrane, and affected the percentage distribution of the reversible or irreversible fouling in a certain degree, in that a higher proportion of it is more reversible.

### 3.5 General discussion

Each of the different characterisation techniques presented in this chapter gave different insights on how the presence of these copolymers are affecting the properties of the membranes. In general, the modification process improved the anti-fouling properties of the membranes, for example by reducing the adsorption of the proteins down to 80 % when they were modified with the triblock copolymer. However, the relationship between the changes in physicochemical properties and anti-fouling properties is not quite clear.

When coating the membranes with different copolymer concentrations, a kind of saturation of the surface - quantified by the mass of coating copolymer adsorbed in the membrane - was reached (Figure 2.7, page 45), whereas Figure 2.11 (page 64) showed that the resistance to adsorption of the proteins was not complete. The measurement of WCA proved not to be sensitive enough, confirming what can be found in the literature. The higher rugosity measured by AFM for the triblock membranes did not affect the good results obtained for this copolymer, while, for a certain copolymer concentration - the random, diblock and virgin membranes

showed similar rugosities and very different anti-fouling properties. The increase in the rugosity for the membranes modified with the diblock and triblock copolymer with the copolymer concentration - hence coating density - did not imply worse properties.

There seemed to be a good correlation between the hydration capacity and the adsorption of proteins (Figure 2.15). The increase in hydration capacity seemed to be associated with a decrease in protein adsorption. For LYZ there are no evident differences between the different copolymers. For the diblock and triblock copolymers, BSA was less adsorbed at equal hydration capacity for the membranes modified with the triblock copolymer. The modification with this last copolymer seemed to be more efficient in repelling the BSA molecules than for the diblock. The random copolymer seemed to be as efficient as the triblock copolymer up to a certain value of hydration capacity, after this value was reached, the behaviour mirrored the one of the diblock copolymer.

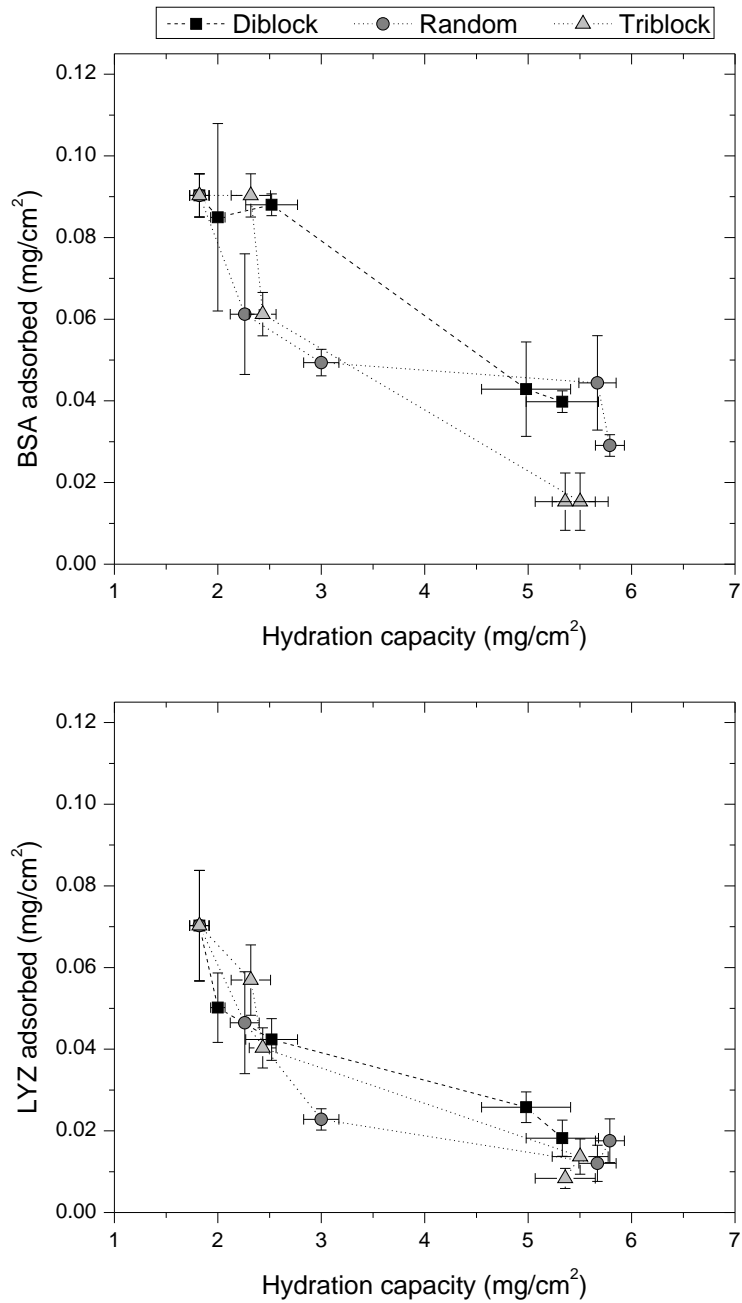


**Figure 2.15:** Relationship between protein adsorption and hydration capacity. Top: BSA adsorption; bottom: LYZ adsorption.

Theoretically, by adsorbing polymers with a MW higher than 2000 g/mol the resistance against the adsorption of proteins is increased [10] and high grafting densities should be reached to prevent adsorption [11, 12]. There is no clear agreement among researchers whether long brushes are a necessary condition for a good anti-fouling material. Some consider that long chains are not essential [13], others that longer brushes would hamper the access of the proteins to the surface of the membrane [11], and others did not find any significant effect on polymer length [14]. In our case and for most of the tested conditions, the fact of adsorbing the copolymers on the membrane surface hindered fouling. The brush conformation of the triblock or diblock copolymers did not necessarily mean that they performed better than the random one, which would have a loop-like conformation of the PEGMA chains in solution. The distance between the PEGMA brushes, the grafting density, and the general distribution of the PEGMA seemed to be causing different effects on how the proteins are being adsorbed onto the surface of the membranes.

All of the previous tests were performed under "static" conditions, and, since the membranes are supposed to be used in filtration equipments, special attention should be drawn to this item. Modified membranes performed better in comparison to the unmodified ones. Reversibility indexes were better, and the analysis of fouling resistances also reflected this fact. There was a small compromise in the initial fluxes, particularly for the triblock copolymer, which could also be affecting the overall fouling parameters. The filtration results generally agreed with the information that was obtained from the static experiments, however, detecting differences among the performance of the different copolymers were harder to assess in the filtration tests.

## 4 Conclusions

The copolymers were present on the membrane surface at comparable values than the ones found in the bibliography. As shown on Table 2.4, page 57, the coating density for the diblock copolymer was of  $0.22 \text{ mg/cm}^2$  and  $3.4 \text{ nmol/cm}^2$ , whereas in [5] these values for a similar PS-PEGMA molecules and same MF membrane were of  $0.12 \text{ mg/cm}^2$  and  $2.1 \text{ nmol/cm}^2$ .

In general, the presence of more copolymer on the surface provided an anti-fouling effect against proteins and cells when static adsorption conditions were applied. However, the adsorption of the foulants never reached a value of zero, no matter how much copolymer was adsorbed on the membrane, or the type of copolymer used.

The filtration tests also showed the improved properties of the modified membranes without modifying the initial flux with respect to the unmodified membrane - the lowest initial fluxes were registered for the membranes modified with the triblock copolymer at  $0.12 \pm 0.02 \text{ kg m}^{-2} \text{ s}^{-1}$  versus  $0.17 \pm 0.03 \text{ kg m}^{-2} \text{ s}^{-1}$  for the virgin membrane, at a working TMP of 0.2 bar. The filtration working fluxes were better for the membranes modified with the diblock and random copolymers, at around  $0.12 \text{ kg m}^{-2} \text{ s}^{-1}$ , when the respective fluxes for the virgin and triblock cases were of approximately  $0.08 \text{ kg m}^{-2} \text{ s}^{-1}$ . From the static adsorption tests it was evident that some foulant was still left on the membranes, which agreed with the fact that the fluxes were not quite recovered after the filtration cycle was performed, and with the fact that less amount of foulant was present in the modified membranes than for the unmodified ones.

Differences in the filtration behaviour between the membranes modified with the different copolymers were difficult to assess. From static adsorption tests it seemed that the most important parameter to improve the anti-fouling properties of the membranes was more related to the coverage of the copolymer; more specifically the spatial distribution of the PEGMA chains and the distance between them.

The techniques presented on this chapter have been widely used among researchers, and the question always remains whether it is possible to find new and more direct ways of "seeing" this fouling, or of analysing the superficial distributions of the modification and the foulant layers. Even though the membrane

surface seems to be saturated with the grafted polymer (one cannot add more even if times goes on or if the concentration in solution is increased) the amount of adsorbed proteins is not zero. The next two chapters of this thesis try to tackle these points by using microfluidic devices coupled with fluorescent microscopy, and the use of FTIR mapping, respectively.

## 5 References

- [1] Séverine Carretier, Li-An Chen, Antoine Venault, Zhong-Ru Yang, Pierre Aimar, and Yung Chang. Design of PVDF/PEGMA-b-PS-b-PEGMA membranes by VIPS for improved biofouling mitigation. *Journal of Membrane Science*, 510:355–369, 2016.
- [2] Yen-Che Chiag, Yung Chang, Wen-Yih Chen, and Ruoh-Chyu Ruaan. Biofouling resistance of ultrafiltration membranes controlled by surface self-assembled coating with PEGylated copolymers. *Langmuir*, 28(2):1399–1407, 2011.
- [3] Yung Chang, Chao-Yin Ko, Yu-Ju Shih, Damien Quémener, André Deratani, Ta-Chin Wei, Da-Ming Wang, and Juin-Yih Lai. Surface grafting control of PEGylated poly (vinylidene fluoride) antifouling membrane via surface-initiated radical graft copolymerization. *Journal of Membrane Science*, 345(1):160–169, 2009.
- [4] Antoine Venault, Yi-Hung Liu, Jia-Ru Wu, Hui-Shan Yang, Yung Chang, Juin-Yih Lai, and Pierre Aimar. Low-biofouling membranes prepared by liquid-induced phase separation of the PVDF/polystyrene-b-poly (ethylene glycol) methacrylate blend. *Journal of Membrane Science*, 450:340 – 350, 2014.
- [5] Nien-Jung Lin, Hui-Shan Yang, Yung Chang, Kuo-Lun Tung, Wei-Hao Chen, Hui-Wen Cheng, Sheng-Wen Hsiao, Pierre Aimar, Kazuo Yamamoto, and Juin-Yih Lai. Surface self-assembled PEGylation of fluoro-based PVDF membranes via hydrophobic-driven copolymer anchoring for ultra-stable biofouling resistance. *Langmuir*, 29(32):10183–10193, 2013.
- [6] Jing Jin, Wei Jiang, Jie Zhao, Jinghua Yin, Paola Stagnaro, et al. Fabrication of PP-g-PEGMA-g-heparin and its hemocompatibility: From protein adsorption to anticoagulant tendency. *Applied Surface Science*, 258(15):5841–5849, 2012.
- [7] Yung Chang, Yu-Ju Shih, Chao-Yin Ko, Jheng-Fong Jhong, Ying-Ling Liu, and Ta-Chin Wei. Hemocompatibility of poly (vinylidene fluoride) membrane grafted with network-like and brush-like antifouling layer controlled via plasma-induced surface PEGylation. *Langmuir*, 27(9):5445–5455, 2011.

- 
- [8] Kara L Menzies and Lyndon Jones. The impact of contact angle on the biocompatibility of biomaterials. *Optometry & Vision Science*, 87(6):387–399, 2010.
- [9] Shudong Sun, Yilun Yue, Xiaohua Huang, and Deying Meng. Protein adsorption on blood-contact membranes. *Journal of Membrane Science*, 222(1):3–18, 2003.
- [10] Angus Hucknall, Srinath Rangarajan, and Ashutosh Chilkoti. In pursuit of zero: polymer brushes that resist the adsorption of proteins. *Advanced Materials*, 21(23):2441–2446, 2009.
- [11] Avraham Halperin, G Fragneto, Audrey Schollier, and Michele Sferrazza. Primary versus ternary adsorption of proteins onto PEG brushes. *Langmuir*, 23(21):10603–10617, 2007.
- [12] John Pieracci, David W Wood, James V Crivello, and Georges Belfort. UV-assisted graft polymerization of N-vinyl-2-pyrrolidinone onto poly (ether sulfone) ultrafiltration membranes: comparison of dip versus immersion modification techniques. *Chemistry of materials*, 12(8):2123–2133, 2000.
- [13] Emanuele Ostuni, Robert G Chapman, R Erik Holmlin, Shuichi Takayama, and George M Whitesides. A survey of structure-property relationships of surfaces that resist the adsorption of protein. *Langmuir*, 17(18):5605–5620, 2001.
- [14] Xiangrong Chen, Yi Su, Fei Shen, and Yinhua Wan. Antifouling ultrafiltration membranes made from PAN-b-PEG copolymers: Effect of copolymer composition and PEG chain length. *Journal of Membrane Science*, 384(1):44–51, 2011.

Coupling of microfluidic chips  
with fluorescence microscopy for  
the study of fouling



## 1 Introduction

Microfluidic devices have been in continuous development over the past few decades. With microfluidics, the study of the system of interest is performed with small amounts of fluids ( $10^{-9}$  to  $10^{-18}$  litres) at a scale of tens to hundreds of micrometres [1]. The following figure (Figure 3.1) illustrates the difference in sizes between a widely used dead-end filtration system - Amicon filtration cell - and a microfluidics chip.

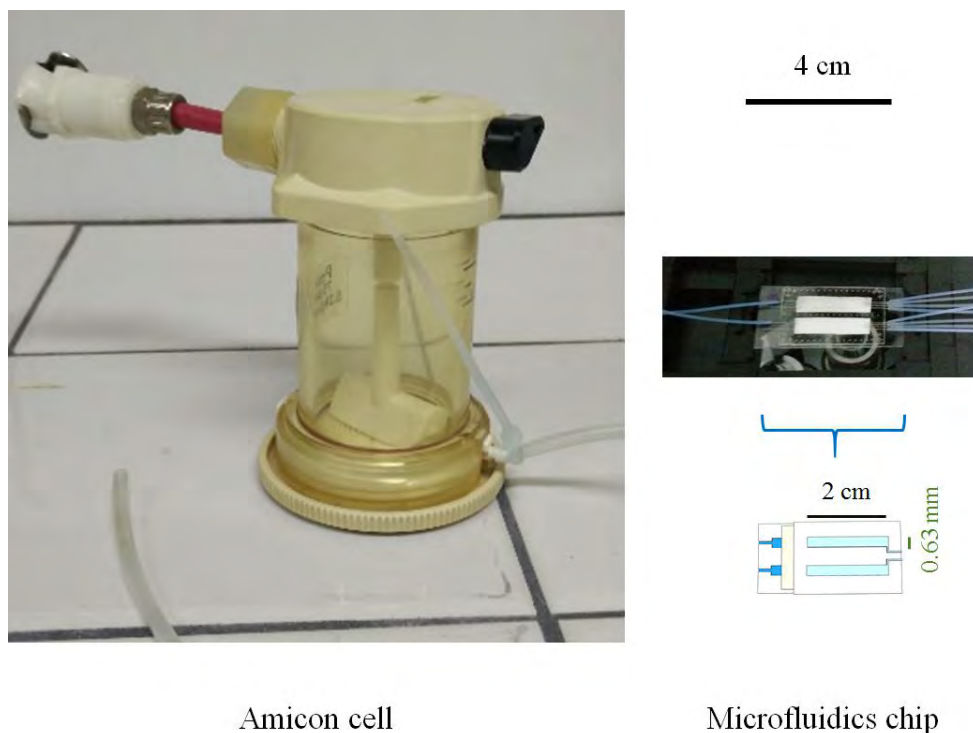


**Figure 3.1:** Comparison of an Amicon filtration cell with a microfluidics chip.

Microfluidics are applied in a diverse range of subjects, such as DNA analysis, cell handling, optical sensing elements, and electronics [2].

The advantages of using microfluidic devices are numerous. Due to their reduced size, the consumption of chemical reagents is decreased - which also implies reduced waste to dispose -, they are portable devices, and can be designed for single-use since fabrication costs are also minimised. Flexibility in design options is also to be considered.

Challenges in the microfluidics world include the need of costly equipment for the proper control of the flows, fabrication of the chip, leakage, and the selection of the appropriate material for the intended application and manufacturing method.

Polydimethylsiloxane (PDMS) has been one of the primary materials used for the fabrication of microfluidic devices, due to its optical transparency. However, depending on the application, its high permeability for different gases - including water vapour - can make it a non-ideal material to work with [3]. Other polymers used for chip fabrication can include epoxy resins [4], and preparations based on mercapto-esters.

When the chip is fabricated out of a polymer, one of the most used methods for the fabrication of these microfluidic devices, is soft lithography with rapid prototyping and replica molding [5]. Basically, the channels are created by designing them with the aid of computer software, then this pattern is printed at high-resolution. This film will have a transparent part and a dark one - usually the channel. This pattern will be transferred to a resist by exposing it to UV light, which will polymerise the regions that are exposed. These treated regions will be dissolved, and a positive relief of the channel is produced. This will be used as the master to cast on the polymeric material of choice. Multiple layers can be produced and aligned by using the same procedure. A diagram of this process can be observed in the Materials and Methods section (section 2.2, page 87). The final chip is usually cured at 40 °C to 80 °C for a couple of hours.

Integrating membranes inside the chips can be achieved by different means [3]. Fouling can be studied by producing transversal channels during the fabrication of the chip [4, 6], or membranes can be introduced inside the chip, better known as the "sandwich" method. This last method poses quite a few challenges to avoid leakage between the different materials [7, 8].

The use of optically transparent materials allow the integration of microfluidic devices with microscopy techniques. Operational parameters of the filtration can be controlled while the clogging or fouling of the species is directly observed [9]. When the particles used are fluorescent, fluorescence microscopy can be used.

Therefore, the understanding of the behaviour of fouling could be improved by developing microfluidic devices that include modified and unmodified membranes, and place them under a fluorescent microscope to directly detect the accumulation

of the foulant on the retentate side of the membrane. Direct ways to observe (bio)fouling while performing filtration with the actual membrane have been reported before. On a work by Kang et. al [10], researchers mounted a glass on a filtration cell to observe the accumulation of cells on the membrane. Other works also use direct microscopy observation methods for the observation of particle deposition at  $\mu\text{m}$  scale [11]. However, there is little work done in the study of fouling using microfluidic devices that include the membrane inside [12, 13], and normally it is limited to "bigger" particles - in the order of the tenths of  $\mu\text{m}$ . It is also important to note that by designing channels in the chip that mimic hollow fibers in terms of geometry, and, ideally, of hydrodynamics, a direct observation of what happens in these small channels, which are so widely used over the world now, could be done.

This chapter will be dedicated to apply the developed microfluidic devices that contain the PVDF membranes modified with the PS-PEGMA copolymers, and observe the fouling phenomena with fluorescence microscopy when proteins are being used as the foulant.

## 1.1 Objectives

The objective of this chapter is to observe the deposition of the foulant layer on the surface of the membrane while performing cross-flow filtrations.

This involves the coupling of fluorescence microscopy to specifically-designed microchips - with retentate, membrane, and permeate sides - and the control of flow and pressure parameters while registering the flow passing through the membrane. This will allow the direct observation of the behaviour of fouling on the surface of the membrane - with the microscope - and the filtration behaviour, at the same time.

## 2 Methodology

### 2.1 Materials

The ethanol ( $\text{EtOH}_{abs}$ ) used to dissolve the copolymers was provided by VWR Prolabo Chemicals (AnalaR NORMAPUR). Phosphate buffered saline solutions (PBS 1x, pH=7.4) were prepared from concentrated PBS 10x bulk solution from Fisher BioReagents (BP399). Ultrapure water used in the experiments was purified from the osmotic water obtained from an ELGA PURELAB Prima purification system with an ELGA PURELAB Classic water purification system (final minimum resistivity of  $18 \text{ M}\Omega \text{ cm}$ ).

BSA with fluorescein isothiocyanate conjugate (BSA-FITC, A9771), which has a MW of 66 000 Da, was purchased from Sigma®. 0.1 g/L BSA-FITC in PBS solutions were prepared and used in the filtration experiments. This fluorescently-labelled BSA molecule was chosen so as to have a good contrast between the macromolecule and other components of the filtration system, particularly against the PVDF membrane.

For the fabrication of the chips the following materials were used: Dry film photoresist (WBR2100, DuPont, USA), Novec™(3M, USA), NOA 68 (Norland Optical Adhesive 68, Norland Products, USA), Polydimethylsiloxane (PDMS, Sylgard®184 silicone elastomer, Dow Corning, USA).

The PS-r-PEGMA, PS-b-PEGMA, and PEGMA-b-PS-b-PEGMA copolymers used were the same as the ones presented in Chapter 2, section 2 (page 44, Table 2.1 and Figure 2.2). 5 mg/mL solutions of the copolymers were prepared in ethanol.

The PVDF membranes used for this chapter and the rest of the manuscript were changed to ultrafiltration PVDF membranes (UF PVDF). This was done due mainly due to the better adhesion of these membranes to the components of the chip, and due to their smoother surface it was able to perform the FTIR mapping of their surface (see Chapter 4, page 113), which was not possible for the rougher commercial MF membranes. The PVDF membranes used inside the chips were prepared according to [14]. Briefly, 25 wt% of PVDF was dissolved in 75 wt% NMP at  $40^\circ\text{C}$  and stirred for at least 24 h until homogeneous blend was obtained. After solutions were well rested and stopped bubbling, membranes were prepared using the liquid-induced phase separation process. Casting was done on a glass plate with a metal casting knife

with a height of 300  $\mu\text{m}$ . Glass plates were immersed in ultrapure water to induce phase separation and membranes were kept in water for 24 h. Afterwards, membranes were dried at room temperature for 24 h before use. The obtained membranes have a pore size of 43 nm, measured by capillary flow porometry. The membranes were coated according to section 2.2.1, page 45, with 5 mg/mL copolymer solutions for two hours. Membranes were dried at 40 °C before inserting inside the membrane cavity of the microchip.

## 2.2 Chip fabrication

The chip fabrication procedure was developed and optimised by Dmytro Snisarenko [15]. Each chip consisted of a permeate and a retentate side with a membrane in the middle, imitating a real cross-flow membrane filtration system. The fabrication of such chips involved several parallel steps, and used the standard soft lithography method. Thus, the resulting microchip had a multilayer structure, where a membrane was sandwiched between two monoliths with embedded channels prepared from the novel UV-curable adhesive NOA 68. A schematic representation of the manufacturing process of the chips can be seen in Figure 3.2.

The fabrication started with the lamination of the dry film photoresist at a temperature of 85 °C on the top of a glass slide with size of 80  $\times$  50 mm (A), which was used as a substrate. The structure of the microchannel system was patterned through the high-resolution printed mask under a continuous UV treatment for 30 s (B). The laminated and treated substrate was heated for 1 min at 100 °C on the hotplate to achieve better fixation between the glass and the laminate. Then, the structure was cooled down and the untreated part of the dry film was removed by the development process in 1 % wt  $K_2CO_3$  at 28 °C for 10 min and used as a mold (C). In the case of the fabrication of the retentate side, the cooled down system, instead of being developed, was used as new substrate, and was subjected to the second lamination-treatment-fixation process aiming to the formation of a hierarchical structure. Only after this multilayer system was formed, the developer was used to clear the uncured sections.

Then, a 10:1 weight mixture of Polydimethylsiloxane (PDMS) prepolymer and curing agent was used to get a replica of the mold. Prior to the pouring of prepolymer,

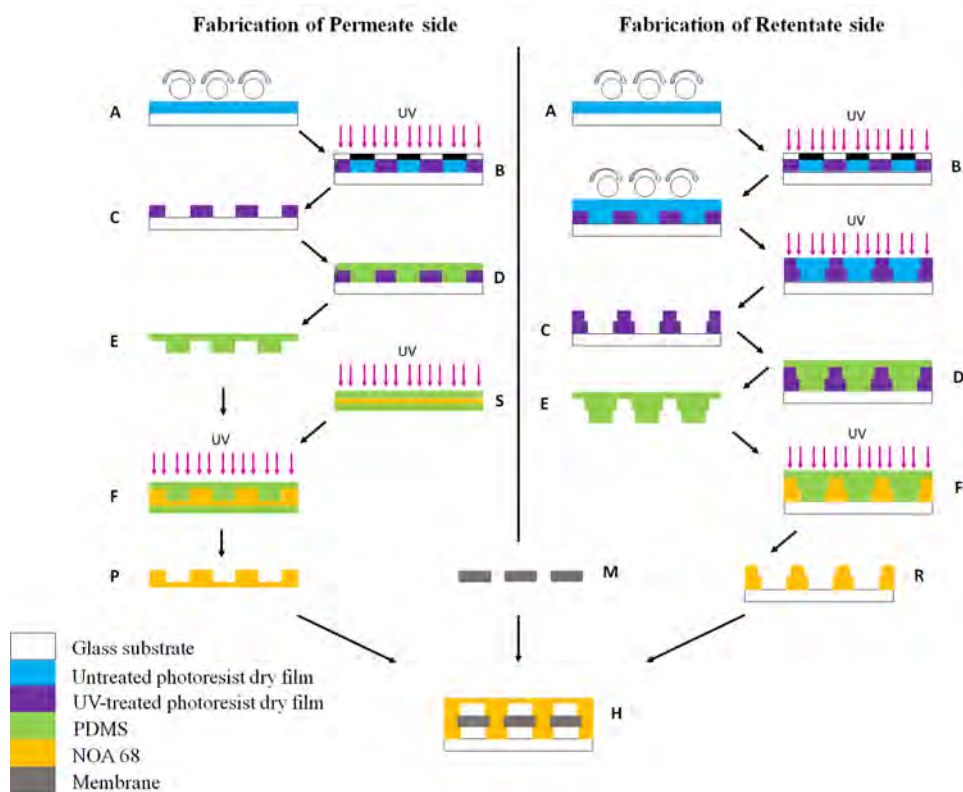


**Figure 3.2:** Schematic representation of the fabrication process of the microfluidic device.

the mold was silanized by immersion in Novec<sup>TM</sup> for 20 min and dried overnight in order to ensure an easier PDMS detachment. The prepolymer-agent mixture was poured on the dry film master mold and degassed under vacuum for 45 min, and then it was heat-cured for 4 h at 80 °C (D). When the PDMS replica (E) was ready, it was peeled off from the mold, and was placed under vacuum for degassing before further use.

In order to ensure a good adhesion between layers on the step of the final assembling of the device, different supports were used for fabrication of retentate and permeate side layers. The retentate layer was prepared on the glass slide, while for the fabrication of the permeate layer a flat layer of Norland optical adhesive 68 (NOA 68) (S) was used. For this, approximately 2 g of NOA 68 were placed between two flat PDMS forms and cured for 3 min under the UV light. Then, the respective supports were used for the fabrication of the permeate and retentate sides.

At this step, liquid NOA 68 was poured on top of the support, covered by the degassed PDMS replica and kept for 30 min at room temperature, so that the trapped air bubbles would be absorbed by PDMS. The degassed system was exposed to UV light for 14 s to achieve partial solidification of NOA 68, after which the PDMS replica could be safely peeled off (**F**). Then, the unmodified or modified membrane was placed in the designed cavity in the retentate side of the microchannel system. Finally, the retentate (**R**) and permeate (**P**) sides were brought into contact and manually aligned under the optical microscope. The assembled chip (**H**) was finally cured by a two-step procedure: 3 min treatment under UV light, followed by 12 h baking at 45 °C. The 3D structure and final microchip is shown in Figure 3.3.

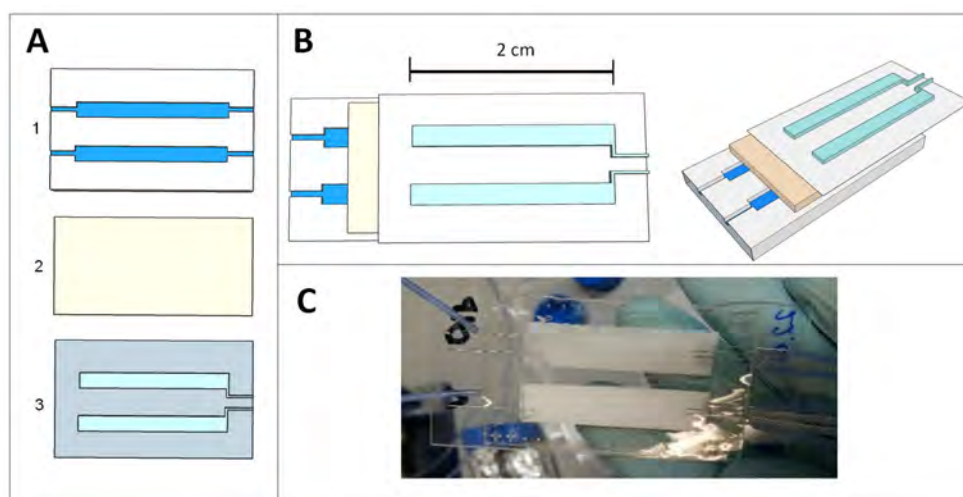


**Figure 3.3:** Microfluidic chip. (A) Design of the different layers: 1-retentate, 2-membrane and 3-permeate; (B) 3D diagrams of the layers and chip assembly; and (C) real chip. Each chip has two membranes with two channel per membrane. One channel (blue) has a length, height, and width of 2 cm, 300  $\mu\text{m}$ , and 630  $\mu\text{m}$ , respectively.

### 2.3 Filtration protocol

The filtration experiments were followed with two systems: a Zeiss Axio Observer.Z1m inverted microscope equipped with a HXP 120C power supply, a filter set 38 - to be able to detect the fluorescence of the BSA-FITC protein used -, and an automated stage. The magnification used to observe the channels was of

50 x. The microscope is controlled by the Zeiss AxioVision Software. The other equipment used was the Fluigent MFCS-Flex pressure controller, combined with a FLOWELL flow-controller. There are a total of 3 pressure and flow controllers. Out of the three pressure controllers, two can work up to 1 bar of pressure, while the other one goes up to 350 mbar. As for the flow controllers, one can operate at a maximum flow of  $7 \mu\text{L}/\text{min}$ , the other one at maximum flow of  $55 \mu\text{L}/\text{min}$ , and the last one at a maximum flow of  $1000 \mu\text{L}/\text{min}$ . The pressure-flow system is controlled by the MAESFLO software. The microfluidic chips are connected to the tubes of the pressure-flow controller and placed on the microscope stage to start the experimental protocol (Figure 3.4).

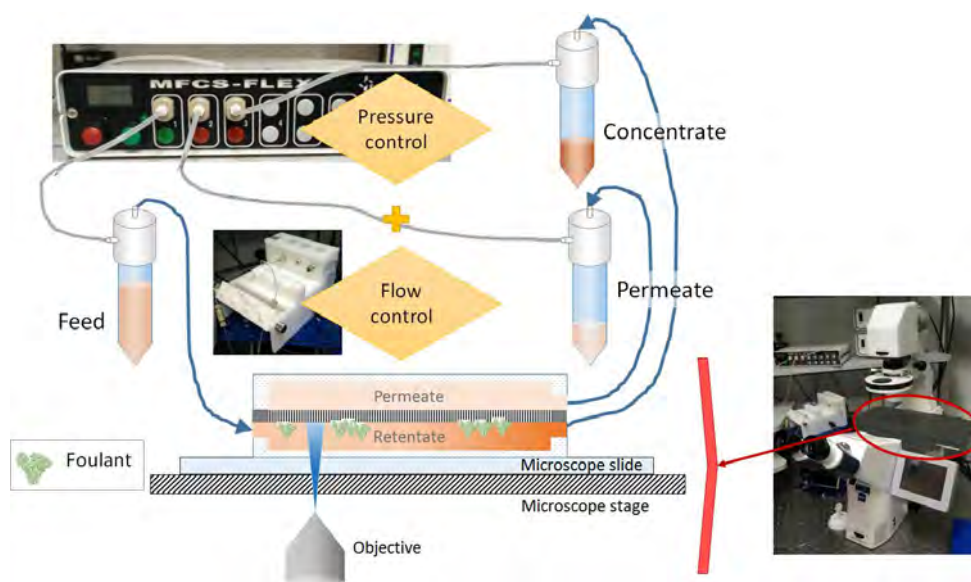


**Figure 3.4:** Diagram of the equipment used in combination with the microfluidic chip.

Before starting with the filtration protocol, the modified membranes were wetted with PBS the night before. For the virgin membrane, 50% *EtOH* was used to wet the membrane 30 min before the beginning of the experiments. The day of the experiment, PBS was passed through the retentate chamber at a low pressure  $< 50\text{mbar}$  and pressure was gradually increased for 3 h to 5 h until permeate side was filled.

For the determination of the filtration and PBS fluxes, the Trans membrane pressure (TMP) was set between 100 mbar and 120 mbar by controlling the inlet

and outlet pressures on the retentate side - the pressure at the permeate side was set to zero -, so as to register an initial inlet flow of 63  $\mu\text{L}/\text{min}$  to 66  $\mu\text{L}/\text{min}$ . Under these conditions, the calculated Reynolds number was of about 0.5. The obtained permeate flowrate was registered with the MAESFLO software. The TMP was lowered to 50 mbar for the rinsing steps. The fluorescence on the retentate side of the channel was also followed; images of the whole channel were acquired every 1 or 2 min with the GFP filter - filter 38 - at an exposure time of 50 ms by the microscope software, then the Grey value (GV) was measured by the ImageJ software.

The following figure illustrates the filtration protocol (Figure 3.5). First, the initial PBS flux was determined. Then, the fouling or filtration step was performed with the BSA solution for 30 min, always keeping the set TMP and inlet flow conditions. Afterwards, the retentate side was rinsed with PBS at the lower inlet pressure of 50 mbar for 15 min. The final PBS flux was registered. These steps constitute the first cycle. Two more cycles were performed in a similar way to follow the reversibility of the process.

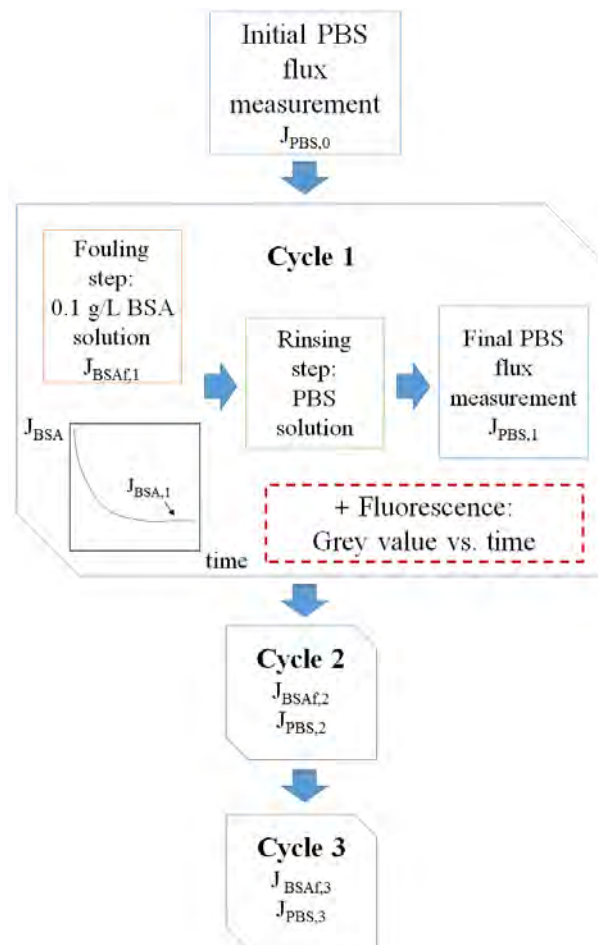


**Figure 3.5:** Protocol of the filtration performed with the microfluidic chips.

## 2.4 Image analysis protocol

The images obtained from the microscope were exported as .tiff files and analysed using ImageJ software [16]. The fluorescence was measured as GV and the more fluorescent - the whiter the pixel - the higher the GV will be. This is depicted in the following image (Figure 3.6). There were also two strategies used for the measurement of the grey value: one taking into account different positions in the channel (A on the figure below), and another taking into account the whole length and width of the channel (B on the figure). This was done to see if there were detectable differences on the deposition of the foulant along the channel, and to try to relate what is happening on the retentate channel with the fluxes that are being registered in parallel, respectively.

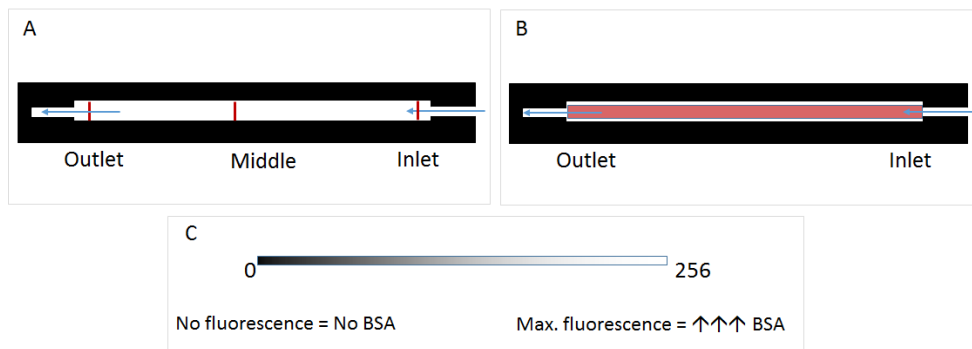


**Figure 3.6:** Image analysis. **A:** Diagram of the measurement of the GV at different positions of the channel; **B:** Diagram of the measurement of the GV for the whole channel; and **C:** Grey value scale for an 8-bit image.

The average grey values are computed by the ImageJ software by taking the sum of the grey values of all the selected pixels divided by the number of pixels. The standard deviation is calculated accordingly.

## 2.5 Calculations

With respect to the data of fluxes, similar indexes can be calculated as in the previous chapter: Fouling reversibility ratio (FRR) and Flux decline ratio (FDR).

Their expressions are shown in the following equations.

$$FRR_{C_i} = \frac{J_{PBS_{f,C_i}}}{J_{PBS_0}} \quad (3.1)$$

$$FDR_{C_i} = \frac{J_{BSA_{f,C_i}}}{J_{PBS_0}} \quad (3.2)$$

where  $J_{PBS_0}$  is the initial PBS flux,  $J_{PBS_{f,C_i}}$  the final PBS flux at the Cycle  $i$ , and  $J_{BSA_{f,C_i}}$  the final BSA flux at cycle  $i$ .

For the measurement of the grey values similar indexes can be defined:

$$FRR_{GV,C_i} = \frac{GV_{PBS_0}}{GV_{PBS_{f,C_i}}} \quad (3.3)$$

$$FDR_{GV,C_i} = \frac{GV_{PBS_0}}{GV_{BSA_{f,C_i}}} \quad (3.4)$$

where  $GV_{PBS_0}$  is the initial grey value for the PBS filtration,  $GV_{PBS_{f,C_i}}$  the final PBS grey value at the Cycle  $i$ , and  $GV_{BSA_{f,C_i}}$  the final BSA grey value at cycle  $i$ .

This definition of the indexes still complies with the following:

$$Index = \begin{cases} 0 & \text{Irreversible fouling} \\ 0 < x < 1 & \text{Reversible and irreversible fouling} \\ 1 & \text{Reversible fouling} \end{cases}$$

The relationship between the calculated indexes for the BSA fluxes and grey values was also calculated (eq. 3.2 divided by eq. 3.4):

$$\text{Fouling ratio index} = \frac{FDR_{C_i}}{FDR_{GV,C_i}} \quad (3.5)$$

From this ratio, two main situations can occur:

$$Index = \begin{cases} x \leq 1 & \text{Non-consolidated cake - concentration polarisation} \\ x > 1 & \text{Accumulation of foulant on membrane surface - Consolidated cake} \end{cases}$$

When the ratio is higher than the unity, there would be a more intense accumulation of the foulant on the surface of the membrane - detected by the ratios in grey values -, that would be not detectable by the change in flux ratios.

### 3 Results and Discussion

In the present section, results from the experiments performed with the above-mentioned chips are presented for the unmodified and modified membranes. First, the general flux graphs will be depicted and the initial fluxes registered with the chips will be compared with the ones obtained for dead-end filtrations. Then, the results concerning the grey values will be shown for the different sites of the membrane - inlet, middle, and outlet -, and for the whole channel. Finally, the comparison of the results of fluxes and grey values will be made and the different filtration indexes will be calculated. Most of the results for the diblock copolymer will not be shown in this section, since problems with the leakage of the chip after the first filtration cycle compromised the data obtained.

#### 3.1 Comparison of fluxes in the microchip with dead-end filtration

One of the first indicators to assess the success of the microfluidic device is the permeabilities obtained, and how they compare with other systems. In our case, they were compared with experiments performed in dead-end filtration systems (Amicon cells, TMP of 2 bars, stirred at 200 rpm, and area of filtration of  $1.34 \times 10^{-3} \text{ m}^2$ ). These filtrations will be better discussed in a following chapter (see Chapter 5, page 147). The filtrations performed with the microchip were operated in cross-flow conditions. In the following figure (Figure 3.7) it is possible to see both types of filtrations, for two different types of membranes (virgin and modified with triblock copolymer).

## 3.1 Comparison of fluxes in the microchip with dead-end filtration

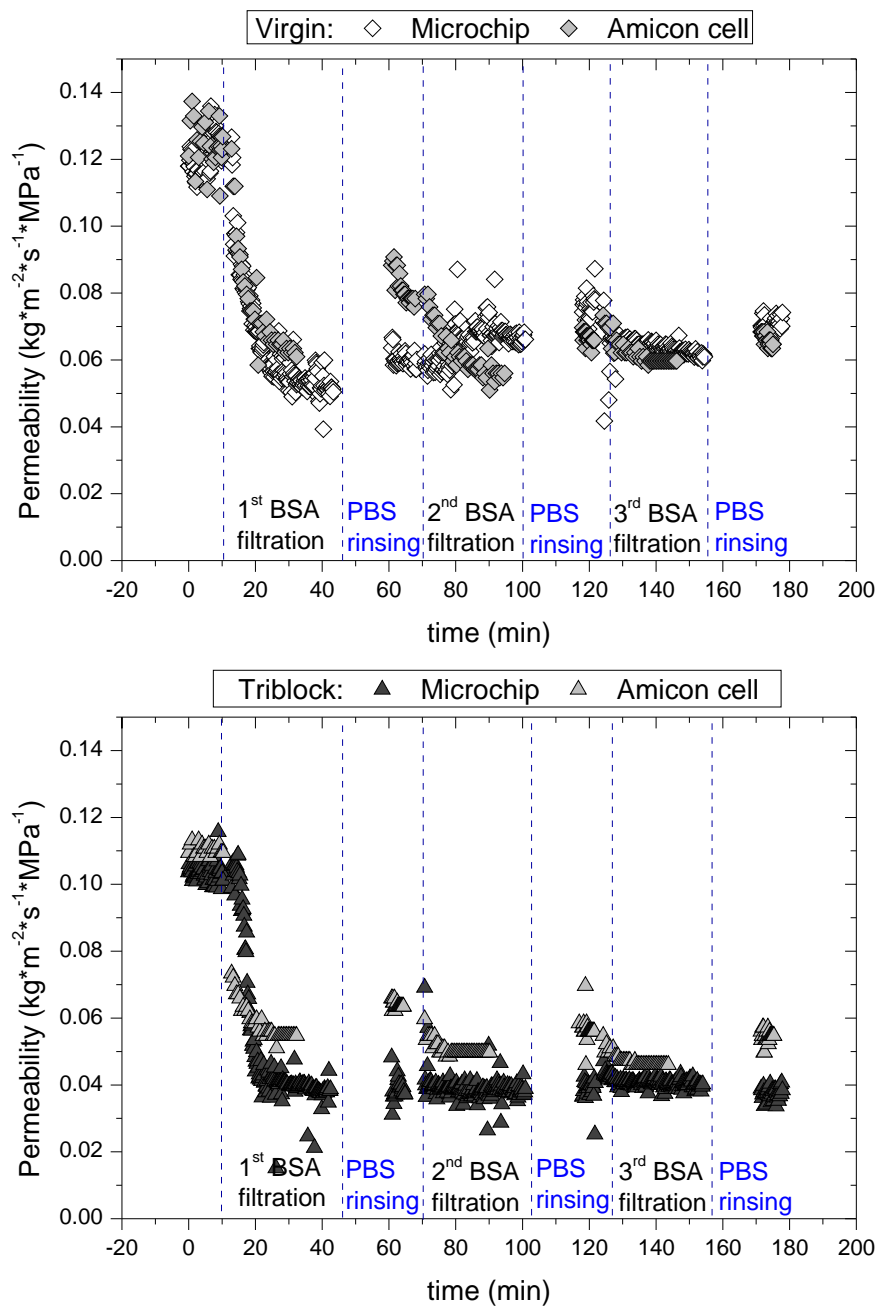


**Figure 3.7:** Permeabilities obtained for the microchip vs Amicon cell for the unmodified membrane (virgin - upper graph) and membranes modified with 5 mg/mL triblock copolymer for two hours (lower graph).

For the unmodified membrane, the PBS permeabilities and filtration behaviour seemed to follow a similar pattern, even though the TMP conditions: 0.1 bar and 2 bar, operation mode: cross-flow vs. dead-end, and geometry, are different between the microfluidic chips and the Amicon cells, respectively. Similar observations could be made for the case of the membrane modified with the triblock copolymer. However, for this last case, it seemed that there was a higher loss in BSA fluxes and reversibility of the fouling for the experiments performed in the microchip than in the larger set-up. Data for the first filtration cycle is shown in the following table (Table 3.1).

**Table 3.1:** Comparison of initial permeabilities between filtrations performed with the microchip (TMP=0.1 bar) and Amicon cells (TMP=2 bar).

Copolymer type	Permeability		
	PBS, initial ( $\text{kg m}^{-2} \text{s}^{-1} \text{MPa}^{-1}$ )	BSA, final 1 <sup>st</sup> Cycle ( $\text{kg m}^{-2} \text{s}^{-1} \text{MPa}^{-1}$ )	PBS, final
Amicon cell			
Virgin	$0.124 \pm 0.007$	$0.063 \pm 0.001$	$0.081 \pm 0.005$
Random	$0.081 \pm 0.009$	$0.045 \pm 0.002$	$0.057 \pm 0.007$
Triblock	$0.110 \pm 0.002$	$0.055 \pm 0.001$	$0.064 \pm 0.001$
Microchip			
Virgin	$0.121 \pm 0.006$	$0.051 \pm 0.001$	$0.060 \pm 0.002$
Random	$0.138 \pm 0.007$	$0.056 \pm 0.009$	$0.061 \pm 0.008$
Diblock	$0.140 \pm 0.013$	$0.093 \pm 0.007$	$0.092 \pm 0.009$
Triblock	$0.103 \pm 0.006$	$0.038 \pm 0.001$	$0.039 \pm 0.003$
*Filtration area:	Amicon cell $1.34 \times 10^{-3} \text{ m}^2$ ; Microchip $1.26 \times 10^{-5} \text{ m}^2$		

Even though the same tendencies could be seen regarding the initial PBS permeabilities and final BSA permeabilities, the membranes inserted inside the microchip did not present good reversibility capacities as the ones tested under dead-end filtration conditions, even when the TMP was lower and the cross-flow conditions should reduce fouling when compared to dead-end. This could be due to different factors, such as rinsing conditions, drying of the membrane to insert inside

the microchip, and, especially, the re-hydration of the copolymer chains prior to the beginning of the experiments. This last item proved to be difficult since there were no efficient ways of keeping the inlets and outlets of the channel sealed once liquid is introduced to start the hydration procedure. The needles also started to get loose after some operational time, making the system prone to leakage. A future solution to this issue could be to use more permeable membranes, and to soak the membranes in glycerol and dry them prior to being inserted in the microchip to protect the copolymer and pore structure.

Despite these issues, the data collected showed that it was possible to perform filtrations with these chips, and the values of permeabilities fell in expectable ranges.

### 3.2 Coupling of filtration and fluorescence data

The data of fluxes presented in the previous section was only one part of the data obtained for each microchip experiment. The adsorption of BSA-FITC was detected with a fluorescence microscope on the retentate side of the membrane due to the fluorescent nature of the foulant used, and images were taken every minute or two. Fluorescence values are measured as grey values, where a value of zero indicated no fluorescence, hence no BSA, and a value of 256 would indicate the maximum fluorescence value (very high amounts of BSA present at the surface). The following figure (Figure 3.8) shows some images taken by the microscope of the filtration channels.

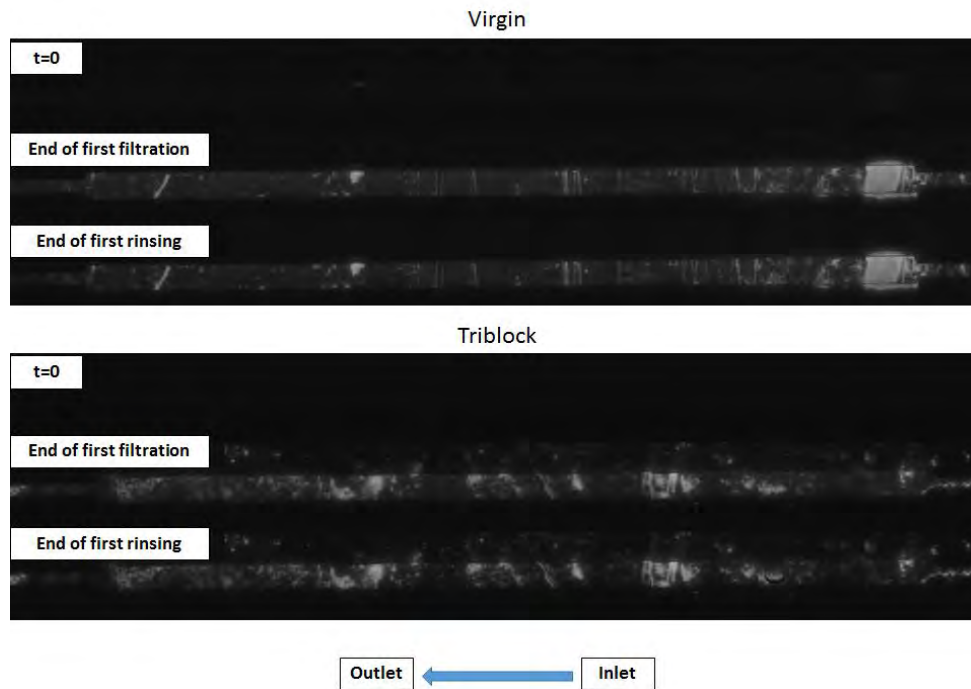


**Figure 3.8:** Images of the channels taken at different points of the filtration experiments of the unmodified membrane (virgin - upper images) and membranes modified with 5 mg/mL triblock copolymer for two hours (lower images).

At the beginning there was almost no signal coming from the membrane surface or its surroundings, and, as the foulant started being pumped inside the system, the fluorescent signal started to become more evident, especially in areas where the membrane seemed to be damaged on its surface. The measurement of the grey values at different positions for the unmodified membrane and the modified ones - with the random and triblock copolymers - was performed and the results are shown in the following figure (Figure 3.9).

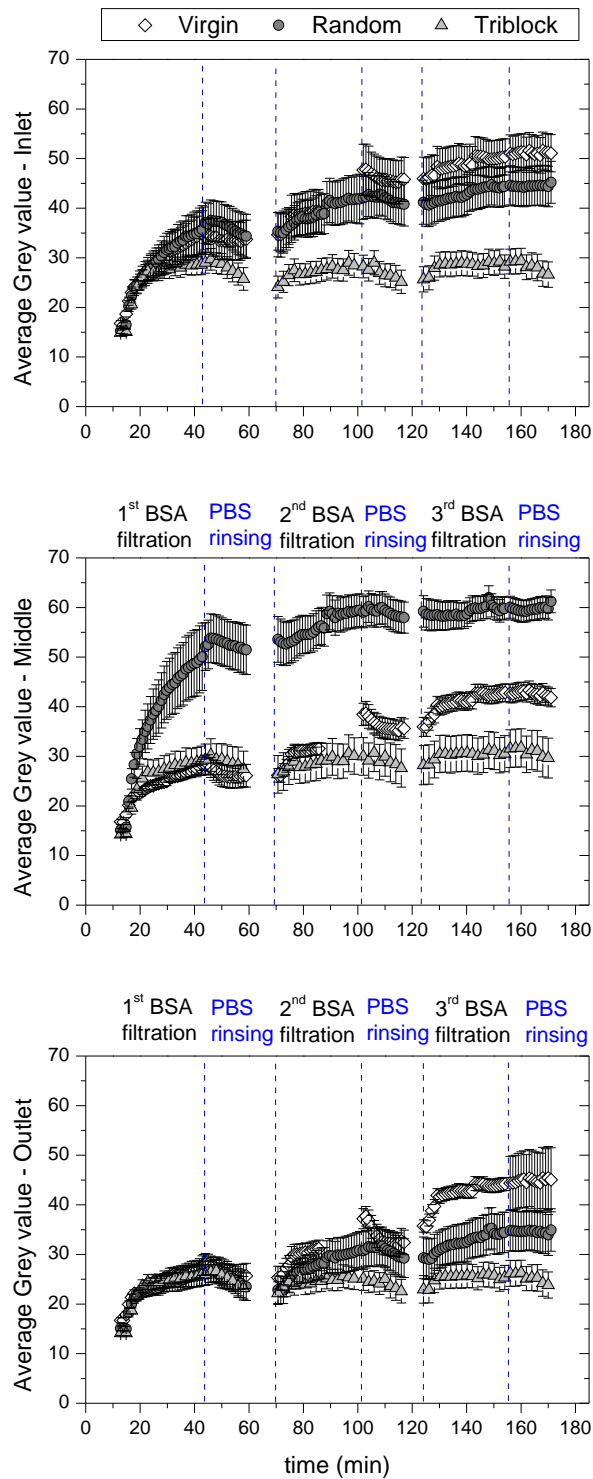


**Figure 3.9:** Measured average grey values at different sites of the channel for the unmodified membrane (virgin) and membranes modified with random and triblock copolymer.

In most of the cases, the longer BSA was inside the channel, the more fluorescence was detected. After the rinsing cycles, the grey value was slightly decreased. The higher BSA signals came from the inlet and middle parts of the channel, whereas at the outlet lower grey values were detected. For the virgin membrane, the grey values constantly increased for all of the measurement regions, and presented the highest signals at the outlet for the final filtration cycle. The triblock copolymer appeared to be the least influenced by the adsorption of BSA, yielding the lowest grey values at any measurement point. The membranes modified with the random copolymer had an intermediate behaviour, except for the signals at the middle part of the channel, where the membrane was highly damaged (Figure 3.10). This damage could come from the fabrication process of the membrane itself and/or after the modification process is performed. Membranes tended to bend when they were dried and the subsequent repositioning inside the chip - their flattening - could have produced such damage.

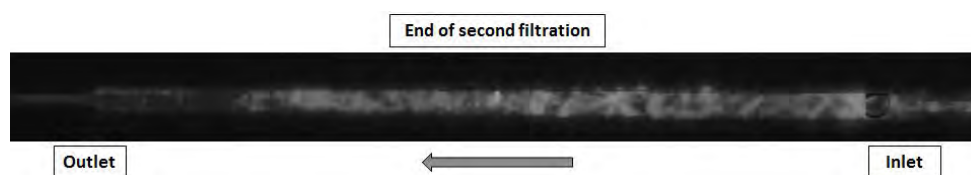


**Figure 3.10:** Image of the channel at the end of the second BSA filtration for the membrane modified with the random copolymer.

In order to be able to compare and couple the results obtained with the measurement of the fluxes, the average grey value was also measured for the whole channel (see Figure 3.6 on page 93 in section 2.4). The combined graphs of the evolution of permeability and average grey value for the different membranes with time can be seen on Figure 3.11. The standard deviation of the averaged grey value is also shown. This value can represent up to 13 %, 29 %, and 20 % of the average grey value measurement for the membranes modified with the virgin, random, and triblock copolymers, respectively, and depicts the variability of the measurement along the membrane channel.

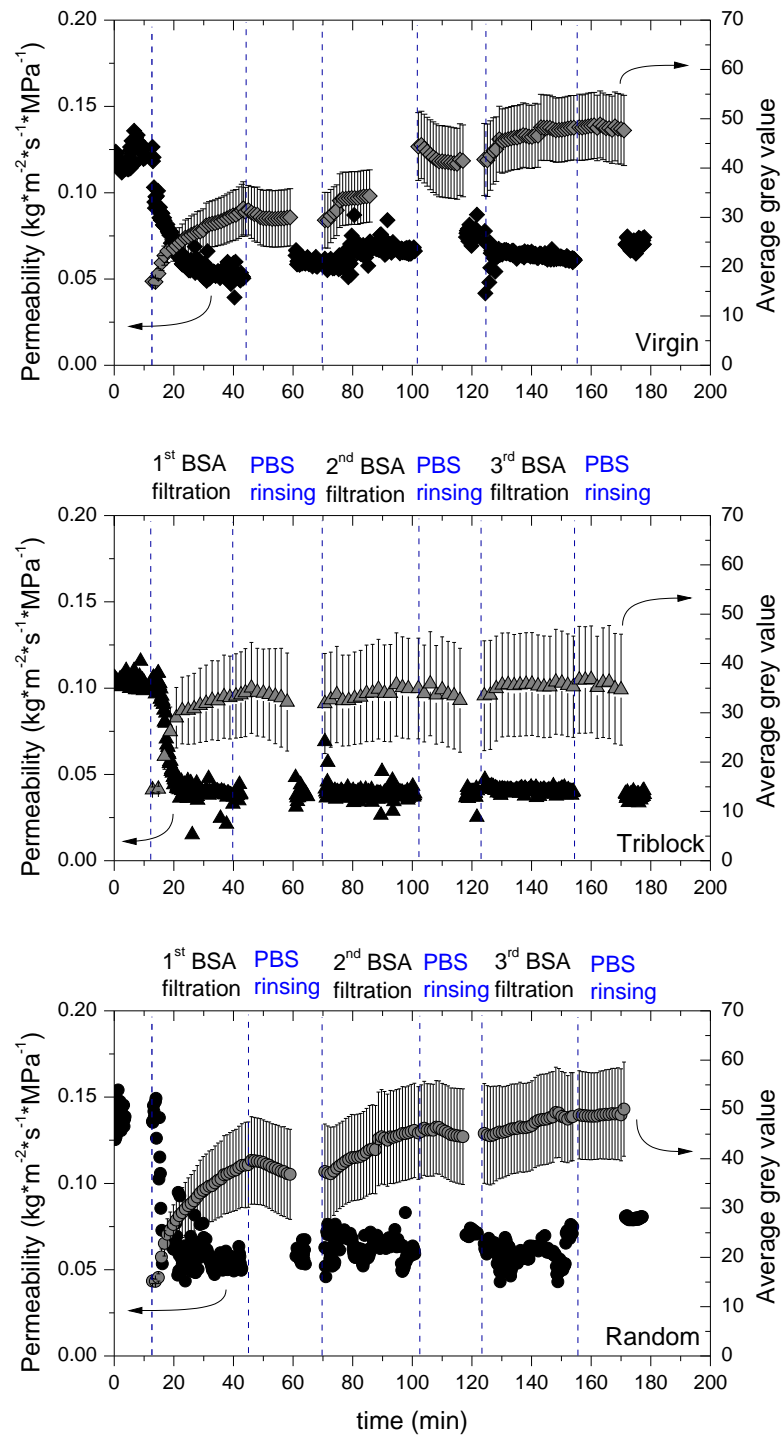


**Figure 3.11:** Evolution of the measured average grey values for the whole channel and the permeability of the membranes for the unmodified membrane (virgin) and membranes modified with the random and triblock copolymer.

In the previous figure it was evident that for an increase in grey value, i.e. fluorescence or presence of BSA, the flux decreased. However, even when the flux reached a steady-state variations in grey value could still be seen. These tendencies are more visible when the permeabilities - and relative permeabilities - are plotted against the average grey value (Figure 3.12). As discussed before, the permeability decreased for increasing grey values (Zone I in Figure 3.12), down to a point where it was almost stable but the grey value continued increasing (Zone II of the same figure). This unexpected behaviour was independent of the membrane system studied, what is more, for Zone I the correlation between relative fluxes and grey values seemed to be the same for all systems studied. By the end of the first filtration, a steady flux was reached, and for the subsequent BSA filtrations all of the experimental points remained in the second zone. These two zones could in fact be related to concentration-polarisation and cake-formation phenomena. The behaviour of the permeability curve depends on the interactions of the particles with the membrane and operational conditions - mainly TMP and flux -. When the filtration starts there is a concentration polarisation phenomenon established near the membrane surface - plus a convective diffusion phenomena -, thus the flux decreases in time due to the accumulation of solutes that are rejected/retained by the membrane. As filtration time - or cycles - increases, this accumulation will cause the formation of a cake layer. This layer will still affect the permeate flux up to a point - a cake-layer thickness - in which its permeation properties remain almost unchanged, therefore, a steady-flux can be achieved even if the layer keeps accumulating on the retentate side. As long as a limiting molecule concentration near the membrane is not reached, the fluorescence detected by the microscope will be dependent on the permeate flux: the accumulation of the fluorescent particles mainly depend on the flux conditions. Once a threshold is reached, a thick fluorescent cake will increase fluorescence on the retentate side, while there will be no significant changes in flux, hence the detection of Zone II. This behaviour was not expected, and could be due to a rearrangement of the cake that would not affect the values of the flux. Further experiments would be necessary to improve the understanding of this process. Regarding this last zone, the membranes modified with the triblock copolymer did not adsorb as much BSA on the surface as the other two.

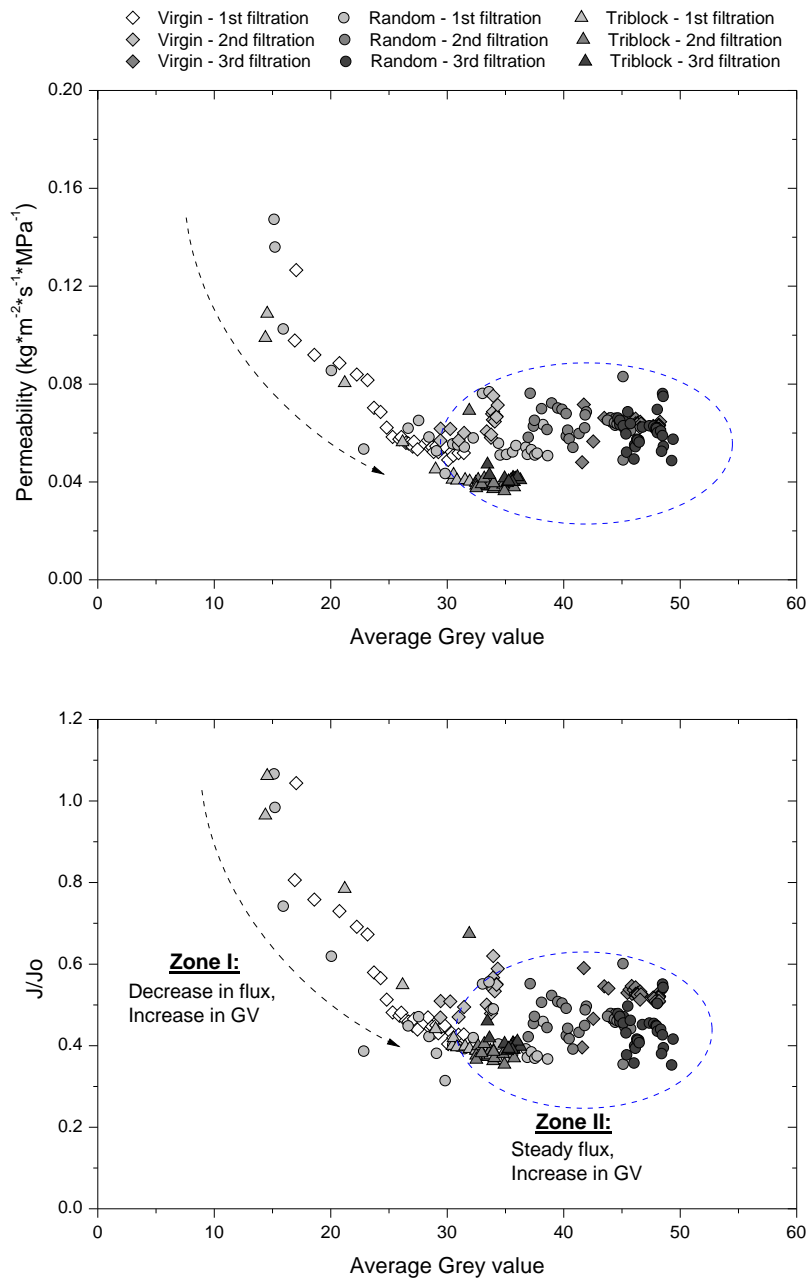


**Figure 3.12:** Permeability and Relative permeability versus average grey value during the filtration of BSA for the unmodified membrane (virgin) and membranes modified with the random and triblock copolymer.

The FRR and FDR were also calculated for these sets of experiments (see 2, page 94). Figure 3.13 shows the results of the indexes calculated from the data of fluxes and from the data or the average grey value of the retentate side (whole channel).

When looking at the indexes extracted from fluxes, the FRR did not change dramatically after each rinsing cycle. The membranes modified with the triblock copolymer seemed to be the more affected by fouling since they presented lower FRR than the ones calculated for the membranes with no modification or modified with the random copolymer. The rinsing procedure of the membranes did not seem to be enough to reverse the observed fouling and the copolymers did not seem to provide better anti-fouling properties than the unmodified membrane. With Amicon cells differences could be seen at least between the behaviours of the unmodified and the unmodified membranes in that the virgin membrane was more prone towards irreversible fouling. Similar tendencies can be seen with the flux decline ratio index.

Regarding the indexes extracted from the average grey values, their values were similar to their flux-calculated counterpart for the first cycle of filtration, however for the subsequent cycles they started to decrease. This decrease could be related to the accumulation of fluorescent particles at the surface of the membrane on the retentate side. For the triblock copolymer this variation was not detected, indexes remained practically unchanged and close to the ones calculated from fluxes.

Thus, the ratio between the FDR for the fluxes and the GV was calculated according to equation 3.5. When this value is higher than 1, there is a more consolidated cake with an accumulation of foulants on the surface of the membrane without affecting the flux properties, while if this number is closer to one, this accumulation is not evident and the GV is inversely related to the flux passing through the membrane. For all of the tested membranes, this ratio was close to the unity for the first cycle of filtrations. For subsequent cycles only the membrane modified with the triblock copolymer did not show a significant increase of the relative FDR value and it also remained lower than one. The index for the unmodified membrane and the one modified with the random copolymer, however, increased after each cycle and surpassed the unity. The triblock copolymer seemed to give a better protection against further accumulation of the foulant on the surface.

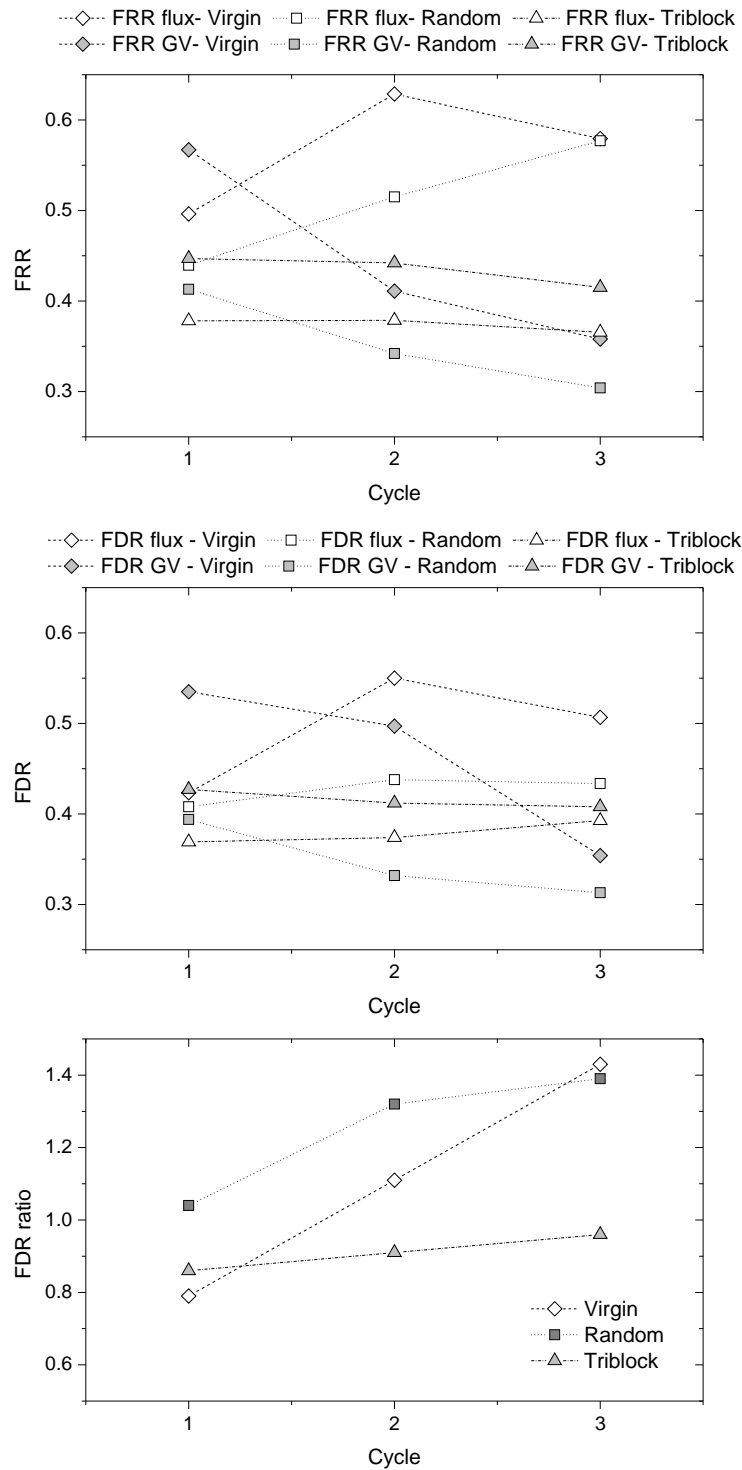


**Figure 3.13:** Evolution of the flux and grey value indexes after each filtration/rinsing cycle for the experiments performed in the microfluidic chips. FDR ratio was calculated by dividing the  $FDR_{flux}$  by the  $FDR_{GV}$ .

The measurement of the grey values during filtration had a clear advantage over the determination of fluxes. GV are directly correlated with the accumulation of the foulant on the retentate side of the membrane. During our experiments we showed that the accumulation of the foulant could occur even after the steady fluxes were reached, or even when these fluxes were found to be similar after each filtration cycle was performed. The long-term impact on the membrane viability could also be followed up and explained with the measurement of the accumulation behaviour of the foulants on the retentate side rather than - or in addition to - the determination of fluxes.

## 4 Conclusions

It was possible to insert a membrane in a microchip and design it as to have "real" retentate and permeate compartments. The coupling of this microchip with the observation of the fouling by means of fluorescence microscopy was also possible, and data of fluxes and GV gave an interesting view on the behaviour of fouling.

The permeabilities measured on the microchip with the pressure-flow controller were in similar ranges with the ones determined during larger-scale filtrations, even though the filtration conditions were not of similar nature. This validated the use of microchips that include the membrane for the study of our system, at least when considering the integrity of the membrane. Nevertheless, at this scale and with the current set-up, it was quite difficult - and a long process - to fill the channels and wait until the permeate side was full, and the system was stable to start with the experiments.

This system also allowed us to explore the relationship between the measured grey values - accumulation of foulant - and the flux behaviour during filtration. Two zones were detected, one in which there was a direct correlation between the flux and grey value - less flux meant more accumulation - and another one in which a steady flux was reached but the grey value would continue to increase. Although we still can't completely explain why this happened, it was a phenomena that was detected in all of the experiments performed in this work - same base membrane, foulant, and operative conditions, but different copolymers -, and as well as in the work of Dmytro Snisarenko [15], in which different membranes and operative conditions were used.

There are still some issues to overcome and improve. The way to hydrate the modified membranes needs to be solved. Perhaps more permeable membranes should be used and/or the modified membranes should be protected with glycerol prior to their insertion into the microchip - provided this glycerol can be fully removed during the set-up of the experiments. The membranes should also be kept as flat as possible during drying to avoid possible damage, or an uneven distribution of the coating layer. More work should also be performed in varying the operative conditions of the micro filtrations: variation of fluxes, concentration of BSA, and concentration of copolymer used. The observation of fouling with other type of membranes, other foulants, and other type of modifications (chemical grafting, blending) could be performed.



---

## 5 References

- [1] George M Whitesides. The origins and the future of microfluidics. *Nature*, 442(7101):368–373, 2006.
- [2] David Erickson and Dongqing Li. Integrated microfluidic devices. *Analytica Chimica Acta*, 507(1):11–26, 2004.
- [3] J De Jong, RGH Lammertink, and M Wessling. Membranes and microfluidics: a review. *Lab on a Chip*, 6(9):1125–1139, 2006.
- [4] Zenamarkos B Sendekie and Patrice Bacchin. Colloidal Jamming Dynamics in Microchannel Bottlenecks. *Langmuir*, 32(6):1478–1488, 2016.
- [5] Abraham D Stroock and George M Whitesides. Components for integrated poly (dimethylsiloxane) microfluidic systems. *Electrophoresis*, 23(20):3461–3473, 2002.
- [6] Patrice Bacchin, Aurélie Marty, Paul Duru, Martine Meireles, and Pierre Aimar. Colloidal surface interactions and membrane fouling: investigations at pore scale. *Advances in colloid and interface science*, 164(1):2–11, 2011.
- [7] Bor-han Chueh, Dongeun Huh, Christina R Kyrtos, Timothée Houssin, Nobuyuki Futai, and Shuichi Takayama. Leakage-free bonding of porous membranes into layered microfluidic array systems. *Analytical chemistry*, 79(9):3504–3508, 2007.
- [8] ZF Wang, YP Seah, and ZP Wang. Seamless joining of porous membrane with thermoplastic microfluidic devices. *Microelectronic Engineering*, 110:386–391, 2013.
- [9] Aurélie Marty, Christine Roques, Christel Causserand, and Patrice Bacchin. Formation of bacterial streamers during filtration in microfluidic systems. *Biofouling*, 28(6):551–562, 2012.
- [10] Seok-Tae Kang, Arun Subramani, Eric MV Hoek, Marc A Deshusses, and Mark R Matsumoto. Direct observation of biofouling in cross-flow microfiltration: mechanisms of deposition and release. *Journal of Membrane Science*, 244(1):151–165, 2004.

- 
- [11] H Li, AG Fane, HGL Coster, and S Vigneswaran. Direct observation of particle deposition on the membrane surface during crossflow microfiltration. *Journal of Membrane Science*, 149(1):83–97, 1998.
- [12] Ikenna S Ngene, Rob GH Lammertink, Matthias Wessling, and Walter van der Meer. A microfluidic membrane chip for in situ fouling characterization. *Journal of Membrane Science*, 346(1):202–207, 2010.
- [13] PZ Culfaz, M Haddad, M Wessling, and RGH Lammertink. Fouling behavior of microstructured hollow fibers in cross-flow filtrations: Critical flux determination and direct visual observation of particle deposition. *Journal of Membrane Science*, 372(1):210–218, 2011.
- [14] Antoine Venault, Yi-Hung Liu, Jia-Ru Wu, Hui-Shan Yang, Yung Chang, Juin-Yih Lai, and Pierre Aimar. Low-biofouling membranes prepared by liquid-induced phase separation of the PVDF/polystyrene-b-poly (ethylene glycol) methacrylate blend. *Journal of Membrane Science*, 450:340 – 350, 2014.
- [15] Dmytro Snisarenko. *Middle molecules clearance through artificial kidneys*. PhD thesis, 2016. Unpublished manuscript.
- [16] Caroline A Schneider, Wayne S Rasband, Kevin W Eliceiri, et al. NIH Image to ImageJ: 25 years of image analysis. *Nat methods*, 9(7):671–675, 2012.

# FTIR mapping for the study of coating and fouling

4



## 1 Introduction

Membrane technologies as separation processes have proved to be a go-to solution for the treatment of water and wastewater. Easy scale-up, low temperature operation, and space-efficiency of plants are among some of the advantages of the use of membranes for the filtration of fluids.

However, the fouling of the membrane structure – surface and pores – is one of the key problems membrane researchers have to overcome to render more efficient and attractive processes.

Fouling can be classified as reversible or irreversible; when the permeate flux can be restored by means of a gentle cleaning protocol then the fouling is mostly reversible. On the other hand, when we need to apply harsher chemical cleaning, we are in the presence of irreversible fouling. Some parameters of the membrane surface that affect fouling are: hydrophilicity, roughness, charge and steric hindrance/repulsion.

One of the approaches to manage fouling is the modification of the structure of the membranes to produce materials that will repel foulants from their structure and/or make fouling more reversible. The modification of polymeric membranes can be carried out in different ways. Physical methods include the adsorption of a hydrophilic-hydrophobic component on a hydrophobic membrane – also known as coating – or its addition in the polymer dope before casting – blending. Chemical modification of the membranes involve the grafting of a chemical group onto their structure [1].

A large part of these modification techniques focuses on the increase of the hydrophilicity of the membranes [2–5] since most of the foulants – proteins, bacteria – are of a more hydrophobic nature, although it is possible to find literature where more hydrophobic surfaces could be less fouled than hydrophilic ones [6]. The addition of a negative charge or of zwitterionic charged materials on the membrane structure has also been reported to improve the anti-fouling properties of membranes [7, 8]. Fouling can also be decreased when long polymer chains are added onto the membrane structure, since there will be an increase in the repulsive steric interactions among others [9].

No matter how we approach the membrane modification issue, we need to be able

to properly characterize, first, the modification that has been carried out, and then the anti-fouling properties of these membranes.

Several techniques are widely used to assess the presence of the modifying agent, hydrophilicity of the membrane, and adsorption of the foulant. The most direct method to determine the hydrophilicity of the membrane is the water contact angle analysis. It is a quite simple method, with an easy sample preparation and results do not require a big expertise for their processing. However, results can be affected by changes in pore size, roughness, porosity and pore size distribution. Fourier-transform infrared spectroscopy FTIR has been used to qualitatively assess the modification process and sometimes of the foulants. The peaks that can be measured on these spectra correspond to a particular bond stretching, allowing the identification of the chemical species on the sample [10, 11]. Sample preparation and data analysis is quite simple, although the technique is limited to the analysis of the surface of the membrane. Atomic force microscopy AFM can be used to measure surface roughness. When used in force spectroscopy mode specific particles are attached to the probe, and it is possible to measure surface-particle interaction forces [9]. These particles can be very varied depending on which kind of system researchers want to study and their experience the team has with attaching them to the probe. A drawback of AFM is that it is a very local measurement. If the surface of membrane is not perfectly homogeneous, as it is generally assumed when membranes are produced, it might not be possible to get a realistic view of the coating homogeneity. The adsorption of foulant species can be determined by UV spectrophotometry (proteins) [2], confocal microscopy (blood cells and bacteria), X-ray photoelectron spectroscopy (XPS) [12] or sometimes with Scanning electron microscopy (SEM) [13]. The determination of fouling by most of these techniques can be regarded as static, foulants reach the surface by diffusion and adsorb, and then its presence and concentration is determined. It is an indication of the behaviour and properties of the system but they have not to be regarded as the absolute truth. These membranes are supposed to be used for filtration set-ups or in systems that there will be a flow, thus final fouling behaviour can be different.

One interesting extension of the FTIR technique is FTIR microspectrometry. Here, the infrared interferometer is coupled with a microscope that has specialized detectors, giving the possibility to scan a surface and get chemical maps of the

sample. In this way, it is possible to detect polymers and other compounds – like proteins – and their distribution on the surface [14, 15]. FTIR imaging has been extensively used in biomedical, biomaterials, and tissue studies [16, 17]. Using this technique for the scanning of the surface of modified membranes that have been modified and fouled could yield interesting results concerning the modification itself and the adsorption – or fouling depending on the method used – of the foulant. There is little bibliography on this subject concerning filtration membranes. On one conference paper the authors used FTIR microscopy so see the distribution of the fouling of a membrane used in a desalination plant [18]. In it, they quickly show the distribution of different foulants – proteins, polysaccharides and inorganic species – with the proteins being the major component found on that fouling layer. Other authors use Attenuated total reflectance-Fourier Transform infrared microspectroscopy (ATR-FTIR microspectrometry) combined with a multivariate analysis to study the effect of fouling agents on membranes and to evaluate cleaning protocols [19]. The data collected on this work did not seem to have been treated as a surface map, but more as averaged or independent values. Another group studied the fouling on Polyethersulfone (PES) membranes used in the milk industry [20]. In this case, the resolution of the equipment was adjusted so a large area of the membrane could be analysed. Thygesen et al. [21] also used ATR-FTIR imaging to assess different cleaning techniques on the composition of the foulant layer of Polypropylene (PP) and Polytetrafluoroethylene (PTFE) membranes.

FTIR maps yield very interesting pieces of information, yet the question remains on how we could obtain more data out of them. By having the chemical distribution maps of the modification agent and the foulant for the same surface it should be possible to improve the critical analysis and, hopefully, get a better understanding of the relationships between the modification of the membrane and its fouling behaviour.

## 1.1 Objectives

The main goal of this chapter is to apply FTIR mapping and develop the data analysis protocol necessary for the assessment of the modification of PVDF membranes by coating PS-PEGMA copolymers, and its adsorption/fouling behaviour. To reach this goal, we use two different types of copolymers – diblock,

and random – and vary some of the coating parameters: copolymer solution concentration and coating time. We use image analysis software to measure the coating and fouling presence on the maps, either by taking averages or by defining coverage/adsorption levels. When necessary we carry out other more classic experiments to complement the data obtained from the FTIR mapping analysis.

Most of the data in this chapter were prepared and accepted for publication [22].

## 2 Materials and Methods

### 2.1 Materials

Polyvinylidene fluoride (PVDF) (Kynar®), MW of  $150.000 \text{ g mol}^{-1}$ ) was washed with methanol and deionized water before use. N-methylpyrrolidone (NMP) was used as solvent without any further purification (Tedia). The ethanol ( $\text{EtOH}_{abs}$ ) used for solubilising the copolymers was provided by VWR Prolabo Chemicals (AnalaR NORMAPUR). Bovine Serum Albumin labelled with fluorescein isothiocyanate conjugate (BSA-FITC, A9771) was acquired from Sigma Aldrich. This labelled BSA had an orange colour, which helped into visually identifying its degree of adsorption on the surface of the membrane. Phosphate buffered saline solutions (PBS, pH = 7.4) were prepared from concentrated PBS bulk solution from Fisher BioReagents (BP399). Ultrapure water used in the experiments was purified from the osmotic water obtained from an ELGA PURELAB Prima purification system with an ELGA PURELAB Classic water purification system (final minimum resistivity of  $18 \text{ M}\Omega \text{ cm}$ ).

Polystyrene (PS) and poly(ethylene glycol) methacrylate (PEGMA) copolymers were synthesized by the R&D Center for Membrane Technology and Department of Chemical Engineering of the Chung Yuan Christian University in Chung-Li, Taiwan. Random (PS-r-PEGMA or RND) and diblock (PS-b-PEGMA or DB) copolymers were used with the repeated units of PS and PEGMA shown in the table below (Table 4.1). More detailed information on how these copolymers were synthesized can be found in [23].

**Table 4.1:** Copolymers used for the modification of the membrane.

Copolymer type	Formula	MW ( $\text{g mol}^{-1}$ )	PI
Random	$PS_{61} - r - PEGMA_{121}$	66,950	1.83
Diblock	$PS_{53} - b - PEGMA_{124}$	63,850	2.10

PI: Polydispersity index

## 2.2 Methods

### 2.2.1 Membrane casting

PVDF membranes were prepared according to [24]. Briefly, 25 wt% of PVDF was dissolved in 75 wt% NMP at 40 °C and stirred for at least 24 h until an homogeneous blend was obtained. After solutions were well rested and stopped bubbling, membranes were prepared using the liquid-induced phase separation process. Casting was done on a glass plate with a metal casting knife with a height of 300 μm. Glass plates were immersed in ultrapure water to induce phase separation and membranes were kept in water for 24 h. Afterwards, membranes were dried at room temperature for 24 h before use. The obtained membranes have a pore size of 43 nm, measured by capillary flow porometry. Other membrane properties can be consulted on a previous work by Venault et al. [25].

### 2.2.2 Coating

Copolymer solutions were prepared adding  $EtOH_{abs}$  to weighed amounts of copolymer and stirring overnight to ensure complete dissolution. The concentrations ranged from 1 mg to 10 mg of copolymer per mL of ethanol. The procedure to modify the virgin membranes was as follows. The PVDF membranes were left in contact with the corresponding copolymer solution at 25 °C. For the experiments done at constant coating time, this value was set to 2 h and the coating solution concentrations used were of 1 mg, 5 mg and 10 mg of copolymer per mL of ethanol. The virgin membranes were treated the same way as the coated ones but using pure absolute ethanol solution instead of the copolymer one. For the experiments carried out at constant copolymer concentration, a 5 mg/mL copolymer solution was used and the coating times varied between 0 h and 8 h. The membranes were rinsed three times with PBS solution after the coating was performed to remove non-adsorbed or loosely adsorbed copolymer.

### 2.2.3 BSA adsorption

For the preparation of 1 g/L BSA-FITC, the albumin was weighed, dissolved in PBS and stirred for 1 h. The mother solution was divided in 1 mL aliquots and stored at

−18 °C. For all the preparation and storage steps the containers were wrapped in aluminium foil to avoid contact with light. After membranes were modified BSA adsorption was carried out. First, PBS was poured onto the membranes and left in contact for 12 h at 25 °C to hydrate the copolymer structure. Afterwards, the PBS was removed and 1 g/L BSA-FITC solution was added to the hydrated membranes for 2 h at 25 °C. The foulant was rinsed three times with PBS and membranes were dried at 35 °C for two hours.

#### 2.2.4 Contact Angle

Contact angle measurements were carried out by dropping 4 μL water droplets on a dry membrane at 10 different sites and measuring the contact angle in air at 25 °C until reaching thermodynamic equilibrium at the three-phase interface (constant value) with an angle-meter (Automatic Contact Angle Meter, Model CA-VP, Kyowa Interface Science Co., Ltd., Japan). These experiments were carried out by out partners in Taiwan.

#### 2.2.5 Coating density

Coating density was determined by performing a mass balance between the unmodified and modified membranes. First, the membranes were dried overnight at 37 °C and their dry weights were registered ( $W_D$ ). The coating was performed as specified by the experimental parameters and the membranes were dried at 37 °C overnight. Modified membranes weights were then registered ( $W_M$ ). Coating density with respect of membrane area ( $A_{membrane}$ ) was calculated as follows:

$$Coating\ density = \frac{W_M - W_D}{A_{membrane}} \quad (4.1)$$

For each experimental condition, the final coating density is an average of five dry weight measurements. The average experimental uncertainty was of  $\pm 0.02\ mg/cm^2$ . These experiments were carried out by out partners in Taiwan.

### 2.2.6 FTIR mapping

The membrane surfaces were scanned with an infrared spectrometer (IN10MX Thermo Scientific) under reflection mode with an analysed surface of  $50 \times 50 \mu\text{m}$  for each point (one point was measured every  $50 \mu\text{m}$ ). The spectral resolution is  $8 \text{ cm}^{-1}$ , and 16 scans are acquired on each measurement point. The spectrometer is equipped with MCT-A detector cooled with liquid nitrogen, and a KBr beamsplitter. The measurements were made using a gold mirror as a reference, and external reflection was used as the acquisition mode. The obtained spectra were no further processed, except for the atmospheric correction. External reflection was chosen instead of attenuated total reflection (ATR) because the penetration depth is smaller, thus thin depositions of compounds are easier to detect and peaks are more defined. External reflection allows to detect superficial modifications, while with ATR the signal coming from deeper layers of the material is more predominant, since the evanescent wave created by the internal reflection inside the crystal penetrates the sample. A comparison on the spectra obtained for ATR and external reflection can be found in Appendix B, page 193.

Dry membranes were attached onto microscope slides and analysed under the FTIR equipment.

The obtained chemical maps can have a size of around 2 by 2 mm and are colour coded with respect of peak height intensity. Low intensities are coded as blue and highest as red; intermediate colours are light blue, green, yellow and orange (ordered on increasing intensity on a rainbow colour scale). Higher peaks are related to more presence of that compound on the sample.

A sample spectra with information regarding the peaks of interest is shown in the figure below (Figure 4.1). The sample corresponds to a modified membrane with BSA adsorbed on its surface. For each experiment, peak heights were measured by taking the baseline limits at similar wavenumbers. More information on the reflection technique used and the peaks of interest can be found in the Appendix B, page 193.

Several authors already established the correspondence between these peaks and the compounds present in our system [10, 13, 24]. The peak corresponding to the C=O stretching present on the PEGMA structure is found at a wavenumber of approximately  $1737 \text{ cm}^{-1}$ . Since this is the hydrophilic polymer on our modifying

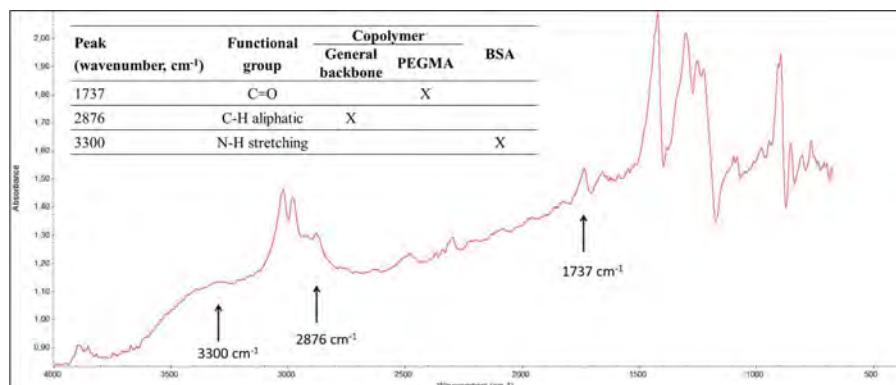


**Figure 4.1:** Sample spectra of a coated and fouled membrane with additional information on the peaks of interest, functional groups related to them and to the compounds present in our study.

copolymer, maps created based on this signal are related to “hydrophilicity maps”, whereas the peak at a wavenumber of  $2876\text{ cm}^{-1}$  corresponds to the aliphatic C-H bonds present in the general copolymer backbone, therefore general copolymer presence and distribution on the membrane surface can be related to this signal. In the same way, the foulant can be detected by measuring peak heights at a wavenumber of  $3300\text{ cm}^{-1}$ , hence rendering “fouling maps”.

### 3 Methodology for the analysis of FTIR maps

Files obtained from the FTIR analysis were first processed with the OMNIC Software Suite (OMNIC Atl $\mu$ s v.9.2, Thermo Fisher Scientific) which allowed to open the scanned maps, select the peak of interest and create the corresponding map. The maps were extracted either with a colour scale - rainbow type - or a grey scale, for the measuring of the grey values. The scale of the maps obtained in our work was adjusted from a peak height of 0 to 0.5 to be able to perform further image analysis (Figure 4.2).

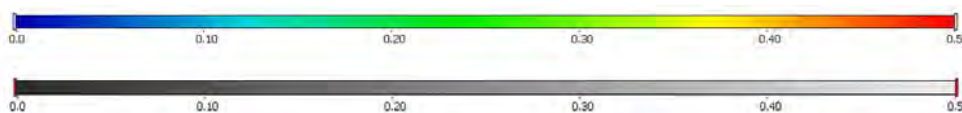


**Figure 4.2:** Colour (up) and grey (down) scale bars for peak heights between 0.0 and 0.5.

We also performed a calibration curve of the peak height with respect to the grey value measured on the scale bar above by measuring the grey value with the ImageJ software at the specific peak height of that grey scale bar. This allowed us to transform the grey values measured during the image analysis to their corresponding peak heights. The fitting curve obtained ( $r^2 = 0.99998$ ) was the following:

$$\text{Peak height} = 0.00258 * \text{Grey value} - 0.1106 \quad (4.2)$$

Maps created with the OMNIC software were exported as image files (.tiff extension) and further image analysis was carried out with ImageJ software [26].

#### 3.1 Measurement of the average grey value

As a first image analysis approach, we proceeded to calculate the average peak height of the whole areas for the peaks of interest. For this, the grey-scale maps were converted to 8-bit images, the area of interest was selected, and the grey value of that area was measured with the image analysis software. The software measured the grey value of each pixel and calculated the average and standard deviation. Afterwards, this values were converted to peak height with Equation 4.2.

### 3.2 Analysis of heterogeneity - Methodology for the definition of coating and adsorption levels

The analysis of the distribution of the coating and foulant layer required of a more particular approach. It is important to note that it can still be greatly improved.

To define different coating and fouling levels, it was important to determine the lower and upper limits of the scale (the zero and 100%). In order to achieve this, we scanned the surface of four membranes; one virgin PVDF, another one being the PVDF with 1 g/L BSA and the other two in which 10 mg/mL of copolymer solution – either diblock or random – was added to the membranes. The main difference with the experiments done before is that we did not rinse the solutions, we just left them dry at room temperature. This would give us a maximum peak signals that could be detected for our systems. The values obtained are shown in the table below (Table 4.2).

**Table 4.2:** Maximum grey values and calculated peak heights for the different experimental set-ups.

<b>Condition</b>	<b>GV at 1737 cm<sup>-1</sup></b> <b>(Peak height - AU)</b>	<b>GV at 3300 cm<sup>-1</sup></b> <b>(Peak height - AU)</b>
PVDF	80.68 (0.099)	62.07 (0.051)
PVDF + BSA	-	152.04 (0.285)
Random	118.66 (0.198)	-
Diblock	122.66 (0.208)	-

\*GV: Grey value, as measured by the image analysis software

With these values we proceeded to define different levels (Table 4.3) graded as low, medium, high and maximum. The “no coverage/adsorption” level was defined between the grey values/peak heights of zero and the value obtained for the

unmodified PVDF membrane. The “maximum” value was also set from the highest values obtained, and from then the three levels in between were equally divided.

**Table 4.3:** Definition of coating and adsorption levels. The numbers represent the limiting grey values.

Type	No coverage /adsorption	Low	Medium	High	Max.
Coating coverage (1737 cm <sup>-1</sup> )	0-80	81-95	96-110	111-125	126-256
Foulant adsorption (3300 cm <sup>-1</sup> )	0-62	63-82	83-102	103-122	123-256

With these levels defined it was possible to establish areas on the maps in which the grey values fell between the specified ones, rendering black areas (the areas of interest) against a white background – for a B/W threshold procedure. Then we measured the percentage of each of those regions on the total membrane area that was analysed.

## 4 Results and Discussion

In this section we will be showing the results we obtained when modifying our PVDF membranes with the two different copolymer types – random and diblock – first by varying the copolymer concentration in the coating solution and using the same coating time, and then by varying the coating time and leaving the copolymer concentration constant. All of these experiments were also carried out by adding our foulant solution – 1 g/L of BSA, and the FTIR maps were acquired for the membrane-copolymer-foulant system.

### 4.1 Variation of copolymer concentration in coating solution

Classically, coated amounts as a function of the copolymer concentration of the coating solution have been determined by calculating coating densities from mass balances [2, 23]. Authors have found that there was an increase in the adsorbed mass with increasing concentrations of copolymer in the solution until a plateau was found beyond a concentration of 3 mg to 5 mg of copolymer per mL of solution. FTIR analysis – taking the average value of spectra taken at 3 to 5 different membrane locations – confirmed this tendency. FTIR in these cases was used to identify the presence of the copolymer on the membrane surface and qualitatively assess the amounts by looking at the peak heights from the raw spectra.

When we performed similar experiments by coating our membranes with different concentrations of coating solutions and analysed the surface under FTIR mapping the results were the following (Figure 4.3 and Figure 4.4).

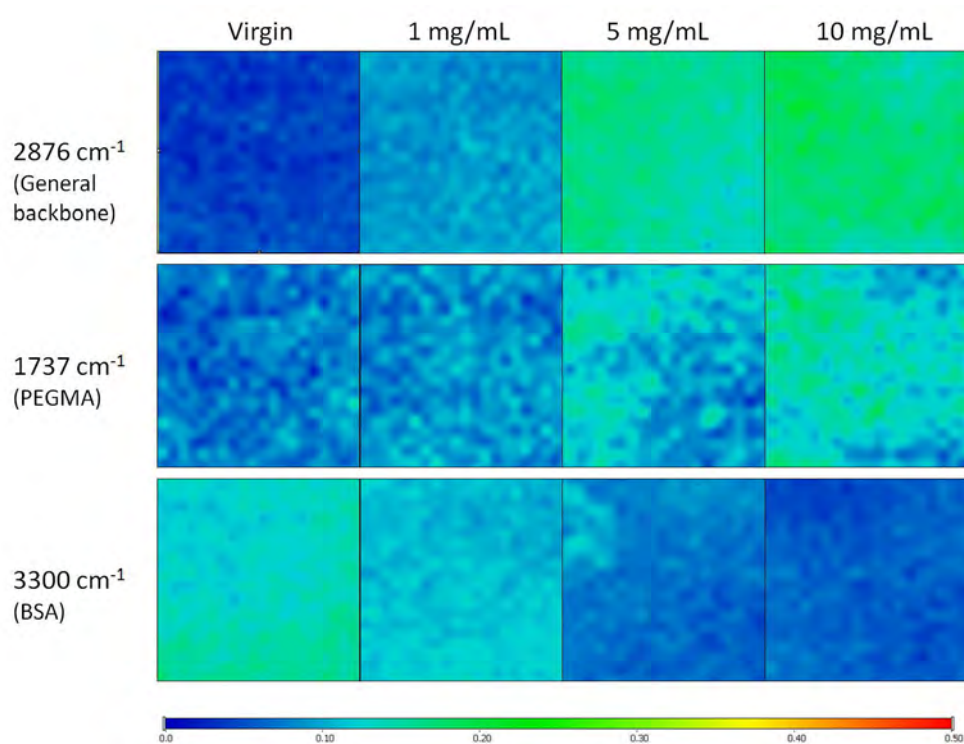


**Figure 4.3:** Example of FTIR maps obtained for membranes modified with the random copolymer at different concentrations. Each map has an area of 1 mm<sup>2</sup>.

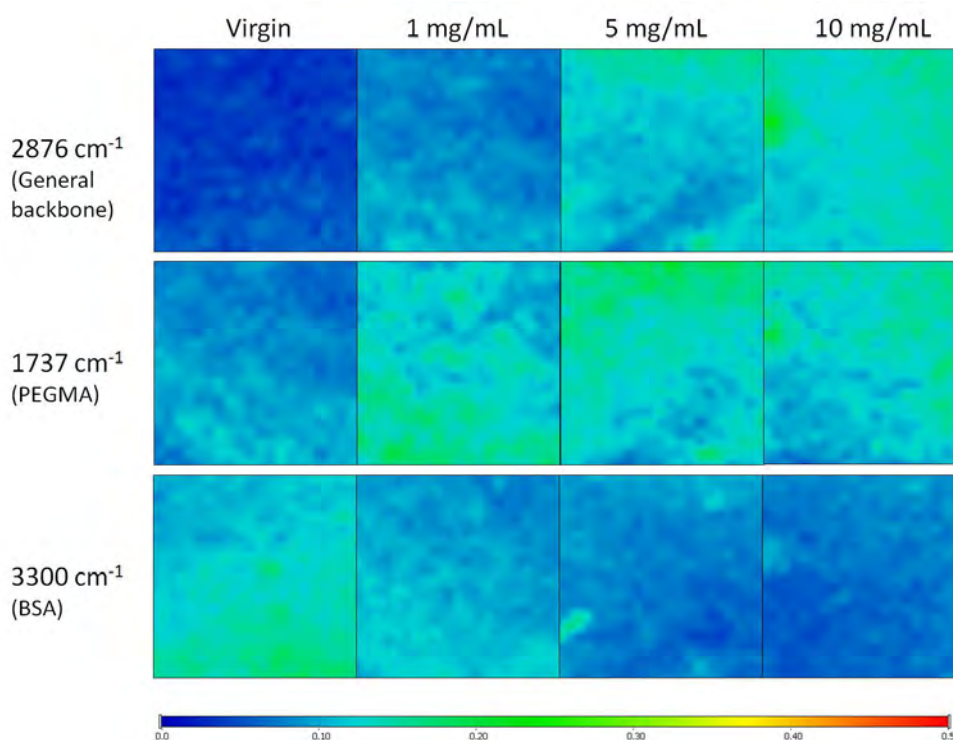


**Figure 4.4:** Example of FTIR maps obtained for membranes modified with the diblock copolymer at different concentrations. Each map has an area of  $1 \text{ mm}^2$ .

For the  $2876 \text{ cm}^{-1}$  and  $1737 \text{ cm}^{-1}$  peaks, with increasing copolymer concentration the peak intensities were higher which suggests that there was more copolymer adsorbed and the surface could be more hydrophilic. It was still possible to observe differences between the  $5 \text{ mg/mL}$  and  $10 \text{ mg/mL}$  concentration levels, showing that this technique could be a little more sensitive than the coating densities calculated as mentioned above. It is important to mention that the problem with the measurement of the coating density by mass balance is that the surface area is not properly assessed: the contribution of the pores to the surface is overlooked, and we do not have clear information on how much polymer penetrated into the pores during coating. So the trend (coating density vs. copolymer concentration in the coating bath) should be considered rather than the actual value.

It was also possible to observe that the copolymer distribution on the surface was not homogeneous and it was noticeable at a millimetre level, which could affect the adherence of foulant on the surface.

If we take a look at the foulant contribution on the image (last row on Figure 4.3 and Figure 4.4), it is possible to appreciate that the foulant adsorption decreased with increasing coating concentration. This behaviour could also be seen on plain sight, since the BSA used was of an orange colour (Figure 4.5).

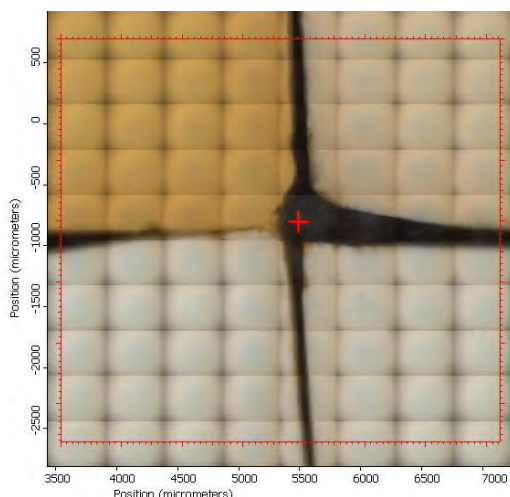


**Figure 4.5:** Image of the membrane surface modified with the random copolymer and incubated with 1 g/L BSA solution. Virgin membrane (upper left) and modified with copolymer solution concentration of 1 mg/mL (upper right), 5 mg/mL (lower right), and 10 mg/mL (lower left). The mesh is a consequence of the images taken by the microscope to determine the subsequent surface to be analysed by the FTIR microspectrometer.

As a first image analysis approach, we proceeded to calculate the average peak height of the whole 1x1 mm areas for the peaks corresponding to the C=O and the N-H functional groups ( $1737\text{ cm}^{-1}$  for PEGMA and  $3300\text{ cm}^{-1}$  for BSA contributions, respectively); those results are shown in Figure 4.6. In this figure it is possible to appreciate the evolution of the peak heights for the different concentrations of copolymer in the coating solution.

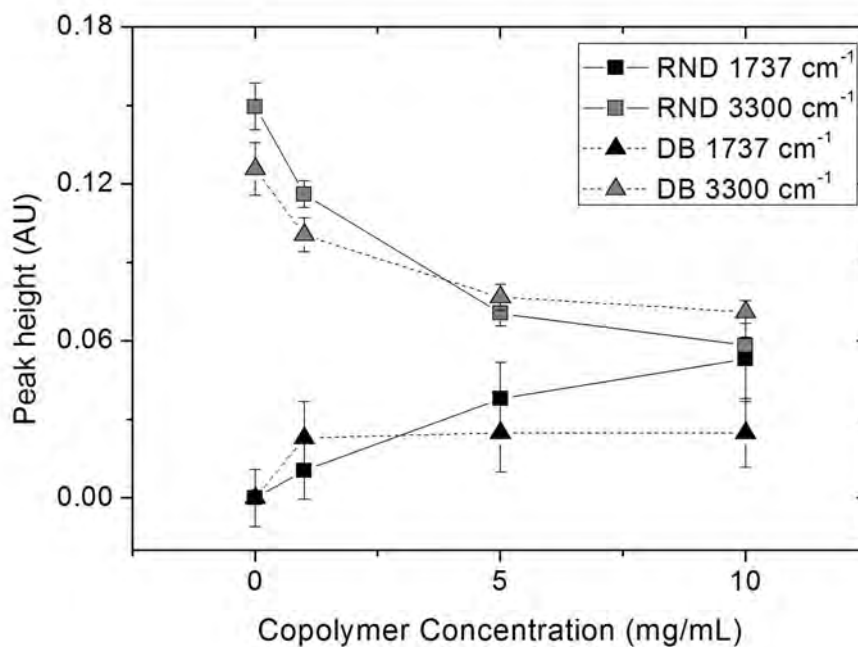


**Figure 4.6:** Average peak height of the 1737 cm<sup>-1</sup> and 3300 cm<sup>-1</sup> peaks as a function of random (RND) and diblock (DB) copolymer concentration.

For both copolymers, the C=O peak was higher with the increase of copolymer in the coating solution while the BSA adsorbed decreased with the increase of copolymer concentration. It was also possible to see the coating plateau mentioned before, especially for the diblock case and for the random case if we take into account the standard deviation.

On Figure 4.7 we represented the variation of the foulant signal in relation with the one of the copolymer. The diblock copolymer seemed to be a little more efficient than the random in its anti-adsorption properties, tendency that can be better appreciated in the following graph.

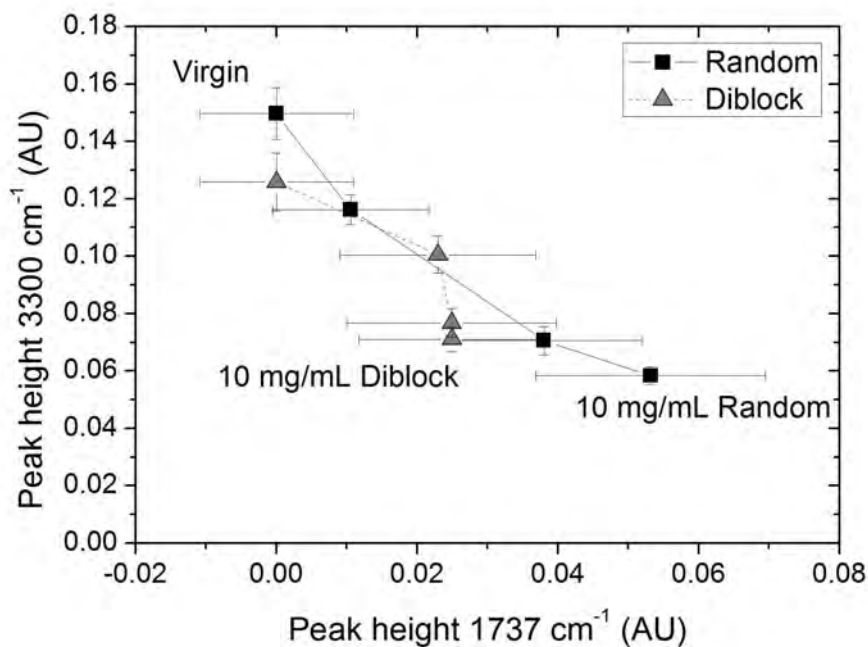


**Figure 4.7:** Evolution of the foulant adsorbed as a function of the copolymer presence for the different coating concentrations.

It was possible to see a trend in the previous graph despite the high standard deviation of the  $1737\text{ cm}^{-1}$  peak. The diblock copolymer reached the same foulant average peak value at a lower average peak height than for the random copolymer. This could imply that the long PEGMA brushes present in the diblock chain were somewhat more efficient to prevent protein adsorption than the loops on random case, for these experimental conditions.

We could also see that beyond a copolymer concentration of  $5\text{ mg/mL}$ , the adsorption detected did not significantly decrease.

It is important to mention that we were detecting coating and protein adsorption from the same sample at the same time on the same area. With other methods one part of the samples will be prepared and analysed for the detection of the coating layer while another set of samples will be dedicated to analyse foulant adsorption.

Previously, we rapidly commented on the heterogeneous distribution seen on the FTIR maps of the copolymer and foulant, and proceeded to analyse the data by

averaging all those values, therefore, losing the real potential of an heterogeneity analysis on a surface mapping technique such as FTIR microspectrometry.

One of the main problems we had to face was the definition of heterogeneity itself; whether it was possible to analyse it with standard deviations, or by defining different coating/fouling levels.

Analysing standard deviations would just give another “averaged” type of information from our system, since values are always compared against the mean. What is more, we can see from previous sections that it will not give us any further information.

Therefore, we proceeded to try to define different coating and adsorption levels to really see how they distributed on the membrane surface and their interrelationships.

The development of the methodology for the primary analysis of heterogeneity can be found previously (section 3.2, page 125).

The two figures below show the type of results that were obtained from this level-analysis (Figure 4.8 for the membranes modified with random copolymer and Figure 4.9 for the ones modified with the diblock one). The images on the left correspond to the copolymer maps (peak at a wavenumber of  $1737\text{ cm}^{-1}$ ), while the ones on the right to the foulant ones (peak at a wavenumber of  $3300\text{ cm}^{-1}$ ), for unmodified and modified membranes. The black areas correspond to the amount of copolymer - or foulant - that lie in each defined coverage or adsorption level.

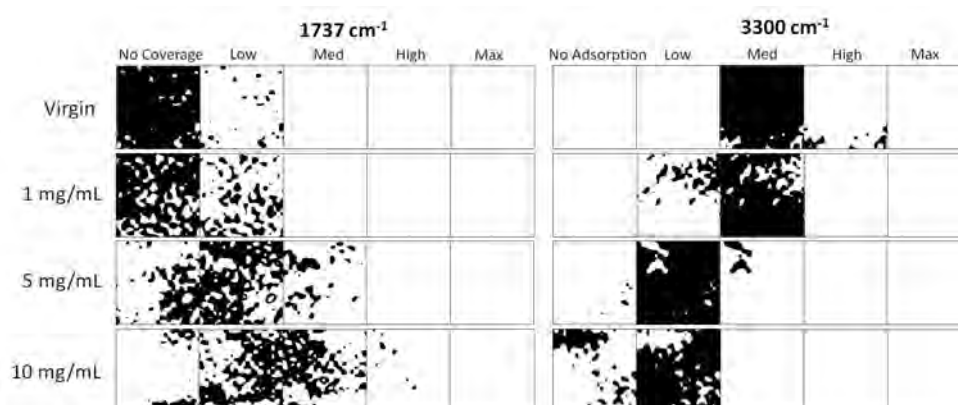


**Figure 4.8:** Coverage and adsorption levels for the membranes modified with different random copolymer concentrations and a coating time of 2 h.

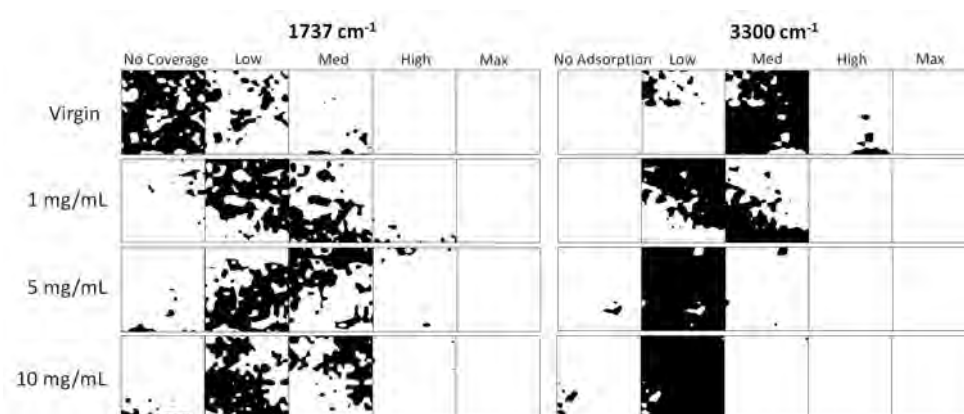


**Figure 4.9:** Coverage and adsorption levels for the membranes modified with different diblock copolymer concentrations and a coating time of 2 h.

As expected, the  $1737\text{ cm}^{-1}$  peak intensity was nil or low for the virgin membrane while there was a mainly medium level foulant adsorption. Coating levels migrated towards the low and medium values when membranes were modified with higher concentrations of copolymer, and adsorption levels decreased from medium to the low levels. The measured black area percentages are depicted in the following figure (Figure 4.10).

At coating concentrations of  $1\text{ mg/mL}$  and  $5\text{ mg/mL}$ , the diblock copolymer showed a better coverage level than the random one. At  $10\text{ mg/mL}$  the coating level percentages were similar. The adsorption levels were also affected by the different copolymer types. At a copolymer solution concentration of  $1\text{ mg/mL}$  there were lower adsorption percentages for the membranes modified with diblock copolymers than for the random. These values became similar for both copolymers at a concentration of  $5\text{ mg/mL}$  and beyond.

The anti-adsorption properties of the modified membranes – either with diblock or random copolymers – seemed to be effective once the surface reaches a "low" level of copolymer coverage of between 50 % and 60 %.

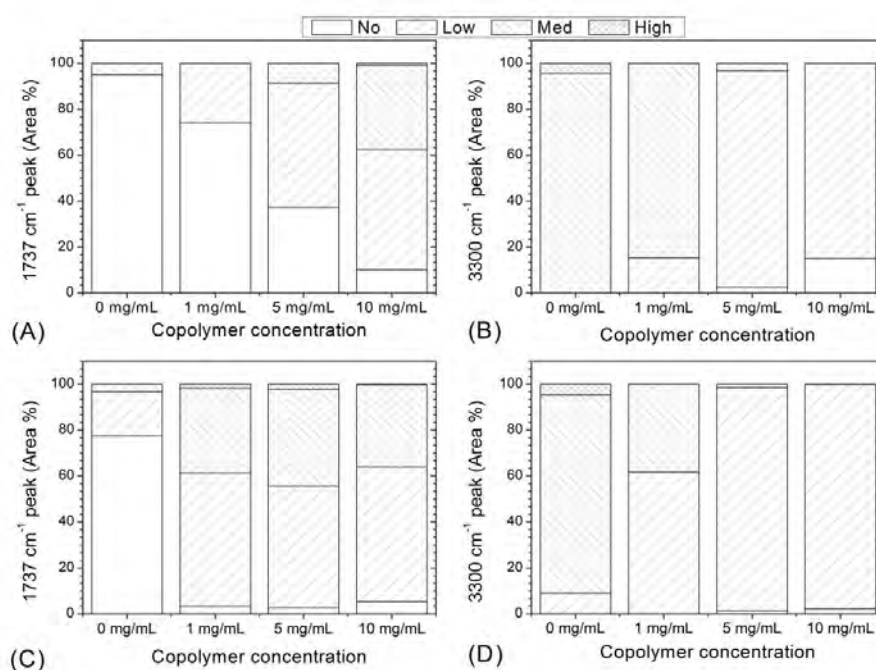


**Figure 4.10:** Measured area percentages for the different coverage and adsorption levels as a function of copolymer concentration. (A) and (B): Random copolymer; (C) and (D): Diblock copolymer.

The slight advantage of the diblock copolymer versus the random in its anti-adsorption characteristics could be due to higher "medium" and "low" levels coverages at lower copolymer concentration.

Nevertheless, there was not a significant anti-adsorption difference once a certain coating level was reached and neither brush nor loop configurations seem to matter for improving the properties of the membranes.

#### 4.2 Variation of coating time

Most of the bibliography related to membrane coating just focuses on the effect of copolymer concentration on the properties of modified membranes. Authors specify the coating time usually without further discussion on why that particular time was chosen. However, not so much attention has been drawn to the fact that the final coating layer may be heavily dependent on the time that the copolymer solution is in

contact with the membrane, i.e. coating time. Therefore, we are going to evaluate the effect of different coating times when 5 mg/mL copolymer solutions are left in contact with the membranes from 2 h to 8 h at 25 °C, and its subsequent fouling behaviour, with some traditional techniques and with FTIR mapping.

First, we determined the water contact angles and coating densities for a 5 mg/mL random copolymer solution with respect of coating time (Figure 4.11).

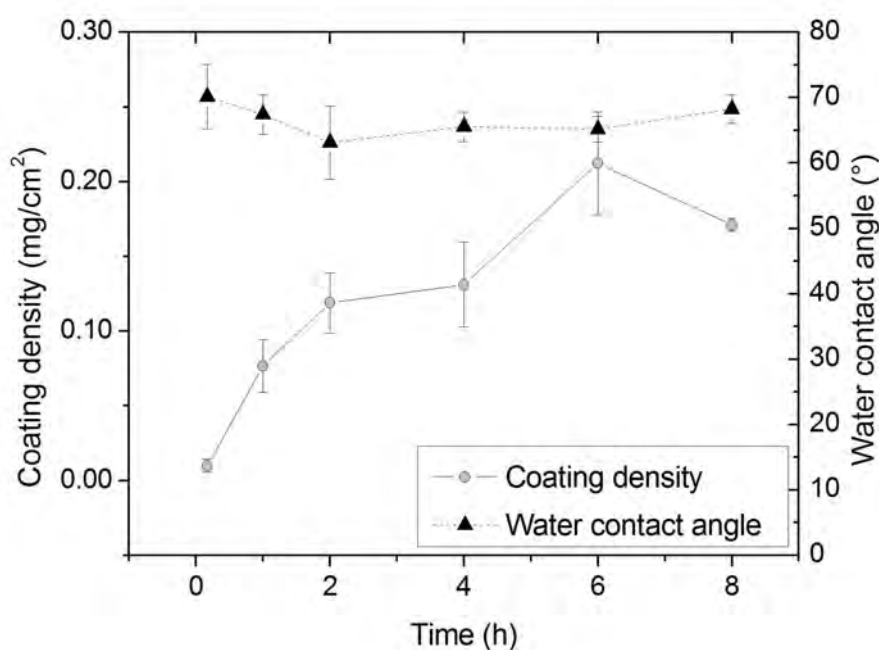


**Figure 4.11:** Water contact angle and average coating densities as a function of coating time. Coating solution: 5 mg of random copolymer per mL of ethanol.

For these experimental conditions, we can see that the coating density increased with the coating time, while the contact angle did not have a considerable change for any of the tested membranes. Water contact angle was not a very sensitive method to assess membrane hydrophilicity change, even though it is the most direct method to do it.

As seen on the previous section, we also registered the FTIR maps for the random and diblock copolymers at different coating times (Figure 4.12 – colour map shown for the random copolymer).

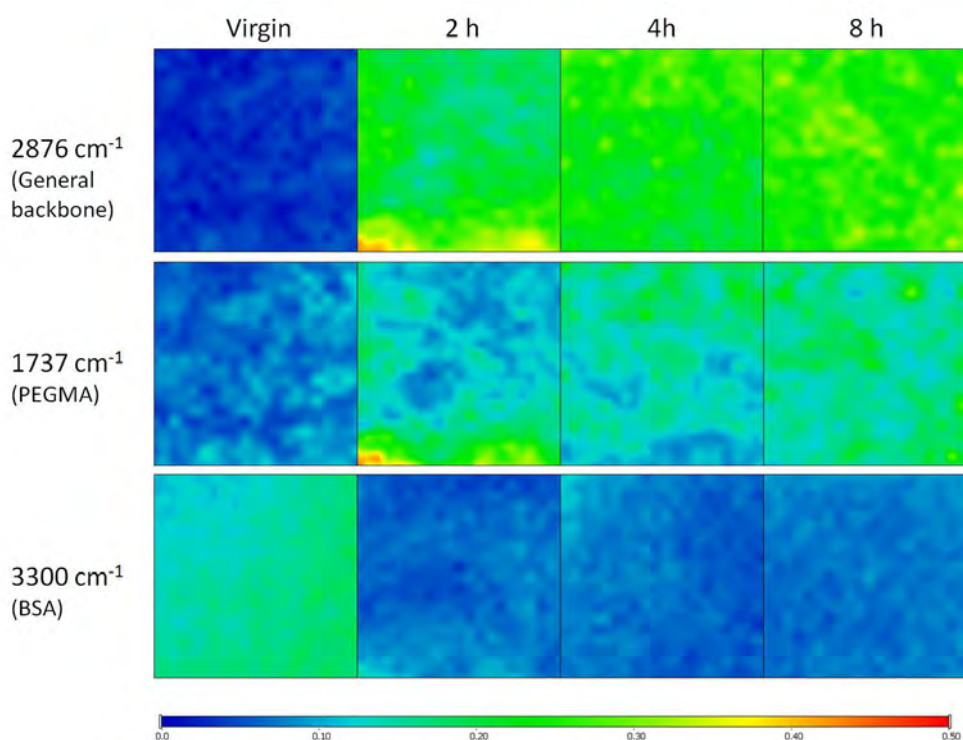


**Figure 4.12:** Example of FTIR maps obtained for membranes modified with the random copolymer at different coating times while keeping the copolymer concentration at 5 mg/mL. Each map has an area of 1 mm<sup>2</sup>.

When coating time increased copolymer presence increased as well. Heterogeneous distribution of the coating layer was again evident. It was also possible to appreciate an increase of the copolymer between the coating times of 2 h to 8 h.

Since a coating time of 2 h was taken as our reference coating time, it was important to know whether this difference is influencing the foulant adsorption levels or whether we should proceed for a longer coating time standard.

The measurement and analysis of the average peaks heights performed for this image confirmed the trends seen in Figure 4.12 (Figure 4.13). For both copolymers, we could see that the copolymer presence increased with coating time. For the random copolymer the detected BSA peak signals reached a plateau after a modification time of 2 h, while for the diblock copolymer it slightly decreased after 4 h. It also showed that after a coating time of 2 h there was no improvement in the

anti-adsorption properties of the modified surface, even when a higher coating signal was detected.

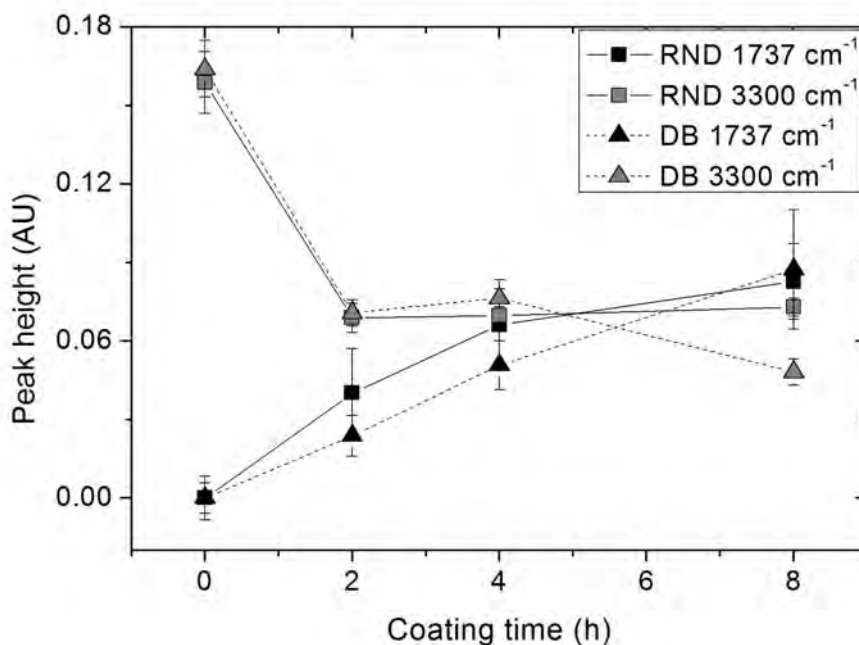


**Figure 4.13:** Average peak height of the 1737 cm<sup>-1</sup> and 3300 cm<sup>-1</sup> peaks as a function of coating time for the random and diblock copolymers.

As shown in Figure 4.14, the diblock copolymer still showed a slight anti-adsorption advantage over the random one, at same C=O density.

The increase of copolymer presence detected by the FTIR technique was also in accordance with the one registered in Figure 4.11. When copolymer was left in contact with the membrane for longer time periods, more copolymer was adsorbed onto the membrane structure.

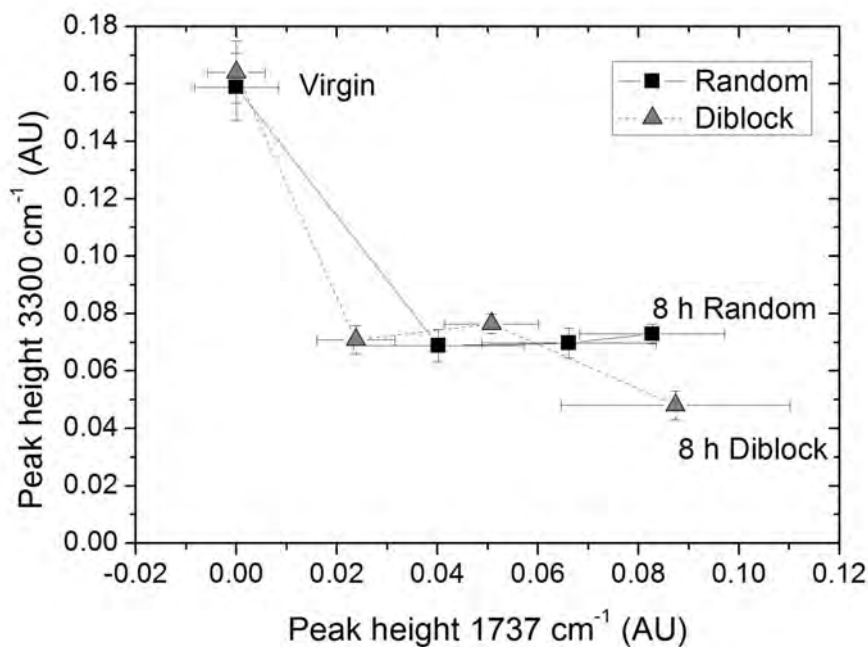


**Figure 4.14:** Evolution of the foulant adsorbed as a function of the copolymer presence for the different coating times and copolymers.

We proceeded to apply a similar heterogeneity analysis as the one previously shown for the membranes coated with a copolymer concentration of 5 mg/mL at different coating times (Figure 4.15).

As expected, the 1737 cm<sup>-1</sup> peak intensity was nil or low for the virgin membrane while having the highest BSA adsorption levels. When the coating time was increased, coating levels increased as well. The BSA adsorption levels drastically decreased from the virgin membrane to the modified ones.

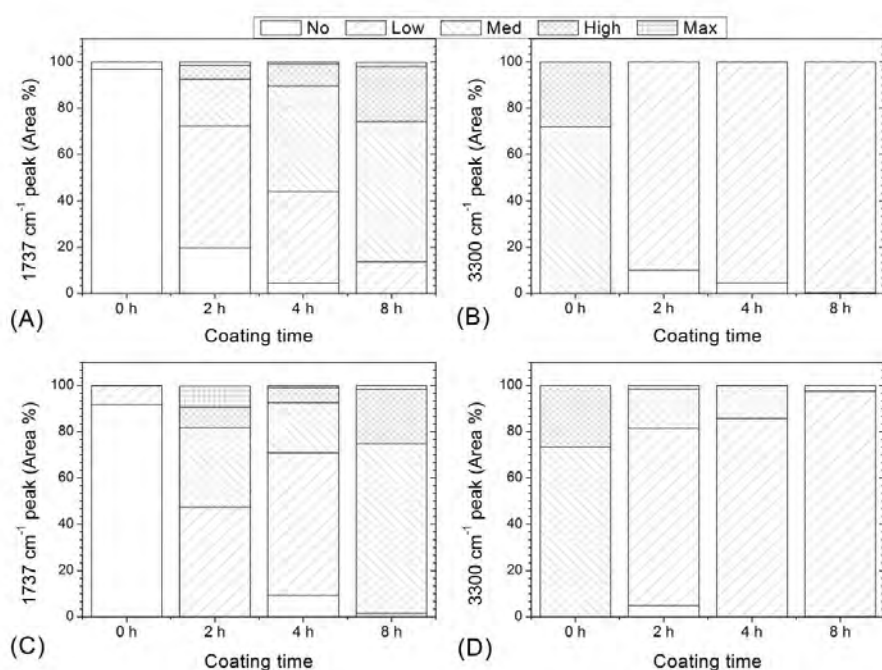


**Figure 4.15:** Measured area percentages for the different coverage and adsorption levels as a function of coating time. (A) and (B): Random copolymer; (C) and (D): Diblock copolymer.

Once the membranes have been coated for two hours and more, there was not much difference in the BSA adsorption levels for the different coating times, even though coating levels kept increasing. In Figure 4.10 (page 135) and Figure 4.15, one can see that a low level of BSA adsorption was achieved all over the membrane sample only when the level of coating reached at least a medium level over most part of the sample surface. Since we already started from “good” coating conditions (5 mg/mL and 2 h), a longer coating time did not have a measurable effect on BSA adsorption.

Coating time was clearly a factor that affected the anti-fouling properties of the membranes and discussions on whether the modification of membranes with coating techniques and their subsequent comparisons should be more efficient or not have to take this factor into consideration.

Coating density determination and FTIR mapping assessment techniques reached

similar conclusions on the matter of presence of the copolymer on the membrane surface, while water contact angle determination did not prove to be sensitive enough.

The results shown before involved the static adsorption of the foulant onto the surface, which gave a first overview of the system, however it is important to perform filtration experiments to have a better understanding of the influence of coating time with the anti-fouling properties of the membranes. These results will be shown in the next chapter (Chapter 5, page 147).

## 5 Conclusions

FTIR mapping is an important tool that can help us to complement our study of fouling phenomena by assessing chemical distribution of the different components of the system on the membrane surface at a millimetre scale.

We have shown that it is possible to apply this technique to assess coating and fouling of the membrane – at the same time – for the surface of the sample, and the data obtained can be analysed by image analysis software, either by calculating the average signal or by defining coating/fouling levels.

By using FTIR mapping, we confirmed that when there is more presence of the copolymer on the surface of the membrane the fouling is decreased, until a certain concentration or coating density of the copolymer is reached. Beyond this point, there is not an appreciable improvement of the anti-fouling properties of the membrane. From the results obtained it is also evident that the measurement of water contact angle has not proved to be very sensitive to assess the change in hydrophilicity of the modified membranes and its possible impact on their anti-fouling properties.

Hence, we recommend using FTIR mapping as a complementary technique for the study of the modification of membranes and assessment of their anti-fouling properties.

Future work should include the improvement of the image analysis protocol to have a better understanding and analysis of the obtained data, hence improving our understanding on the importance of the heterogeneous distribution of the coating and fouling layers and their interrelations.

The application of ATR-FTIR should also be addressed for the membranes used in filtration set-ups, or for membranes produced by LIPS or VIPS processes. In the case this acquisition method could be used for the analysis of the modification and fouling layers, a more quantitative approach could be reached with the analysis of the peaks, possibly yielding maps with concentration levels of the different species.

## 6 References

- [1] A Bhattacharya and BN Misra. Grafting: a versatile means to modify polymers: techniques, factors and applications. *Progress in polymer science*, 29(8):767–814, 2004.
- [2] Nien-Jung Lin, Hui-Shan Yang, Yung Chang, Kuo-Lun Tung, Wei-Hao Chen, Hui-Wen Cheng, Sheng-Wen Hsiao, Pierre Aimar, Kazuo Yamamoto, and Juin-Yih Lai. Surface self-assembled PEGylation of fluoro-based PVDF membranes via hydrophobic-driven copolymer anchoring for ultra-stable biofouling resistance. *Langmuir*, 29(32):10183–10193, 2013.
- [3] Ariya Akthakul, Richard F Salinaro, and Anne M Mayes. Antifouling polymer membranes with subnanometer size selectivity. *Macromolecules*, 37(20):7663–7668, 2004.
- [4] Ayse Asatekin, Adrienne Menniti, Seoktae Kang, Menachem Elimelech, Eberhard Morgenroth, and Anne M Mayes. Antifouling nanofiltration membranes for membrane bioreactors from self-assembling graft copolymers. *Journal of membrane science*, 285(1):81–89, 2006.
- [5] Somnuk Boributh, Ampai Chanachai, and Ratana Jiraratananon. Modification of PVDF membrane by chitosan solution for reducing protein fouling. *Journal of Membrane Science*, 342(1):97–104, 2009.
- [6] L Zhang, G Chowdhury, C Feng, T Matsuura, and R Narbaitz. Effect of surface-modifying macromolecules and membrane morphology on fouling of polyethersulfone ultrafiltration membranes. *Journal of applied polymer science*, 88(14):3132–3138, 2003.
- [7] Yong-Hong Zhao, Kin-Ho Wee, and Renbi Bai. Highly hydrophilic and low-protein-fouling polypropylene membrane prepared by surface modification with sulfobetaine-based zwitterionic polymer through a combined surface polymerization method. *Journal of Membrane Science*, 362(1):326–333, 2010.
- [8] Mingyan Zhou, Hongwei Liu, James E Kilduff, Robert Langer, Daniel G Anderson, and Georges Belfort. High-throughput membrane surface

- modification to control NOM fouling. *Environmental science & technology*, 43(10):3865–3871, 2009.
- [9] Seoktae Kang, Ayse Asatekin, Anne M Mayes, and Menachem Elimelech. Protein antifouling mechanisms of PAN UF membranes incorporating PAN-g-PEO additive. *Journal of Membrane Science*, 296(1):42–50, 2007.
- [10] Shuang Xue, Qing-Liang Zhao, Liang-Liang Wei, and Nan-Qi Ren. Behavior and characteristics of dissolved organic matter during column studies of soil aquifer treatment. *Water Research*, 43(2):499–507, 2009.
- [11] S Belfer, R Fainchtain, Y Purinson, and O Kedem. Surface characterization by FTIR-ATR spectroscopy of polyethersulfone membranes-unmodified, modified and protein fouled. *Journal of Membrane Science*, 172(1):113–124, 2000.
- [12] Peter Kingshott, Helmut Thissen, and Hans J Griesser. Effects of cloud-point grafting, chain length, and density of PEG layers on competitive adsorption of ocular proteins. *Biomaterials*, 23(9):2043–2056, 2002.
- [13] Jing Jin, Wei Jiang, Jie Zhao, Jinghua Yin, Paola Stagnaro, et al. Fabrication of PP-g-PEGMA-g-heparin and its hemocompatibility: From protein adsorption to anticoagulant tendency. *Applied Surface Science*, 258(15):5841–5849, 2012.
- [14] Rohit Bhargava, Shi-Qing Wang, and Jack L Koenig. FTIR microspectroscopy of polymeric systems. In *Liquid Chromatography/FTIR Microspectroscopy/Microwave Assisted Synthesis*, pages 137–191. Springer, 2003.
- [15] Marco van de Weert, Ron van't Hof, Jaap van der Weerd, Ron MA Heeren, George Posthuma, Wim E Hennink, and Daan JA Crommelin. Lysozyme distribution and conformation in a biodegradable polymer matrix as determined by FTIR techniques. *Journal of controlled release*, 68(1):31–40, 2000.
- [16] Matthew J Baker, Júlio Trevisan, Paul Bassan, Rohit Bhargava, Holly J Butler, Konrad M Dorling, Peter R Fielden, Simon W Fogarty, Nigel J Fullwood, Kelly A Heys, et al. Using fourier transform IR spectroscopy to analyze biological materials. *Nature protocols*, 9(8):1771–1791, 2014.

- 
- [17] Sergei G Kazarian and KL Andrew Chan. Micro-and macro-attenuated total reflection Fourier transform infrared spectroscopic imaging. *Applied spectroscopy*, 64(5):135A–152A, 2010.
- [18] Enrique Ferrero, Susana Navea, Carme Repolles, Jordi Bacardit, J Malfeito, and R&D Director-Acciona Agua-Spain. Analytical methods for the characterization of reverse osmosis membrane fouling. In *IDA World Congress Proceedings, Paper IDAWC/PER11-240*, pages 4–9, 2011.
- [19] Tilahun K Gelaw, Carme Güell, Montse Ferrando, and Sílvia De Lamo-Castellví. Use of attenuated total reflectance infrared microspectroscopy combined with multivariate analysis to study membrane fouling. *Journal of Food Engineering*, 143:69–73, 2014.
- [20] Murielle Rabiller-Baudry, Mylène Le Maux, Bernard Chaufer, and Lilian Begoin. Characterisation of cleaned and fouled membrane by ATR—FTIR and EDX analysis coupled with SEM: application to UF of skimmed milk with a PES membrane. *Desalination*, 146(1):123–128, 2002.
- [21] Ole Thygesen, Martin AB Hedegaard, Agata Zarebska, Claudia Beleites, and Christoph Krafft. Membrane fouling from ammonia recovery analyzed by ATR-FTIR imaging. *Vibrational Spectroscopy*, 72:119–123, 2014.
- [22] Lucia Benavente, Clémence Coetsier, Antoine Venault, Yung Chang, Christel Causserand, Patrice Bacchin, and Pierre Aimar. FTIR mapping as a simple and powerful approach to study membrane coating and fouling. *Journal of Membrane Science*, 2016.
- [23] Yen-Che Chiag, Yung Chang, Wen-Yih Chen, and Ruoh-chyu Ruaan. Biofouling resistance of ultrafiltration membranes controlled by surface self-assembled coating with PEGylated copolymers. *Langmuir*, 28(2):1399–1407, 2011.
- [24] Antoine Venault, Yi-Hung Liu, Jia-Ru Wu, Hui-Shan Yang, Yung Chang, Juin-Yih Lai, and Pierre Aimar. Low-biofouling membranes prepared by liquid-induced phase separation of the PVDF/polystyrene-b-poly (ethylene glycol) methacrylate blend. *Journal of Membrane Science*, 450:340–350, 2014.

- [25] Antoine Venault, Melibeth Rose B Ballard, Yi-Hung Liu, Pierre Aimar, and Yung Chang. Hemocompatibility of PVDF/PS-b-PEGMA membranes prepared by LIPS process. *Journal of Membrane Science*, 477:101–114, 2015.
- [26] Caroline A Schneider, Wayne S Rasband, Kevin W Eliceiri, et al. NIH image to ImageJ: 25 years of image analysis. *Nat methods*, 9(7):671–675, 2012.

Filtration-rinsing cycles for the  
assessment of fouling  
reversibility



## 1 Introduction

The effect of the modification process on PVDF membranes performed with the PS-PEGMA copolymers has been evaluated by different techniques in previous chapters: on MF membranes on Chapter 2, by the direct observation of the accumulation of the fouling layer and control of filtration parameters with microfluidic devices on Chapter 3, and by the adaptation of FTIR techniques on Chapter 4.

While most of the bibliography focuses on a general "static" characterisation of the modified membranes, with little to no-filtration tests, very few perform them, particularly multiple filtration-rinsing cycles or long-term tests [1, 2]. Single-cycle filtration tests involve the determination of the initial water filtration flux, and then the filtration with the foulant solution is carried out. Afterwards the system is cleaned and the final water flux is measured. Filtration-rinsing cycles involve single cycle filtration protocols carried out in series of at least two. The repetition of these cycles allows researchers to follow up the evolution of the flux after each cycle is completed, and determine if its decrease is significant and/or how protective the modification was against fouling. By performing rinsing - mild cleaning - cycles, only the reversible fouling would be removed, leading to calculate reversibility indices. Long-term filtrations are usually carried out at larger scale with real-life effluents.

Most of the techniques used in the manuscript involved static tests, or single cycle filtration protocols. A preliminary study of the behaviour of the modified membranes after the filtration-rinsing cycles were performed has been studied with microfluidic devices in Chapter 3, but only for the membranes modified for 2 h.

Further characterisation on the filtration properties of the membranes modified for longer periods of time is needed, since these membranes are ultimately intended to be used in filtration set-ups, and because we have determined that the coating time may be playing an important role on the anti-fouling properties of the membranes.

### 1.1 Objectives

The main objective of this chapter is to evaluate the efficiency of the coating on the UF PVDF membranes modified for different coating times by performing multiple filtration-rinsing cycles.

These results will also be related with other characterisation methods such as SEM, ATR-FTIR, WCA, and FTIR microspectrometry (mapping).

## 2 Materials and Methods

### 2.1 Materials

The ethanol ( $\text{EtOH}_{abs}$ ) used to make the copolymer solutions was provided by VWR Prolabo Chemicals (AnalaR NORMAPUR). Phosphate buffered saline solutions (PBS 1x, pH=7.4) were prepared from concentrated PBS 10x bulk solution from Fisher BioReagents (BP399). The ultrapure water used in the experiments was purified from the osmotic water obtained from an ELGA PURELAB Prima purification system with an ELGA PURELAB Classic water purification system (final minimum resistivity of 18 M $\Omega$  cm).

Bovine serum albumin (BSA) A4378, which has a MW of 66 000 Da, was purchased from Sigma®. 1 g/L BSA solutions in PBS were prepared and used in the filtration experiments.

The PS-r-PEGMA, PS-b-PEGMA, and PEGMA-b-PS-b-PEGMA copolymers used were the same as the ones presented in Chapter 2, Section 2 (page 44, Table 2.1 and Figure 2.2).

The UF PVDF membranes used for the filtrations were prepared according to [3], and were the same as those used in the previous chapter (Chapter 3, page 86). Briefly, 25 wt% of PVDF was dissolved in 75 wt% NMP at 40 °C and stirred for at least 24 h until homogeneous blend was obtained. After solutions were well rested and stopped bubbling, membranes were prepared using the liquid-induced phase separation process. Casting was done on a glass plate with a metal casting knife with a height of 300  $\mu\text{m}$ . Glass plates were immersed in ultrapure water to induce phase separation and membranes were kept in water for 24 h. Afterwards, membranes were dried at room temperature for 24 h before use. The obtained membranes have a pore size of 43 nm, measured by capillary flow porometry.

### 2.2 Methods

#### 2.2.1 Coating of the membranes

The copolymer solutions were prepared by adding  $\text{EtOH}_{abs}$  to weighed amounts of copolymer and stirring the solution overnight to ensure complete dissolution. The

concentration used for these experiments was of 5 mg of copolymer per mL of ethanol.

The procedure to modify the virgin membranes was basically similar as the one presented in Chapter 2, section 2.2.1, page 45. However, in this case the modification was performed with a copolymer concentration of 5 mg/mL for different periods of time (2 h to 8 h).

The coating was performed the day before the filtration experiments, and membranes were left overnight in PBS 1x to hydrate the copolymer chains. The unmodified PVDF membrane was wetted in ethanol 30 min before the beginning of the filtration.

### 2.2.2 Water contact angle

Contact angle measurements were carried out with an angle-meter (Contact Angle Meter, DGD Fast/60, GBX). The membranes were modified according to the methodology explained before (see section 2.2.1, page 151) and they were dried at a temperature not higher than 40 °C in an oven incubator. The contact angle measurements were performed by dropping 4 µL pure-water droplets on the dry membrane surface at 25 °C. The camera installed in the equipment took the picture as soon as the droplet touched the surface and the angle was measured with the Digidrop software. This was repeated at 10 different sites of the membrane.

### 2.2.3 FTIR analysis

Fourier transform infrared spectroscopy (FTIR) technique was used to assess the presence of the coating copolymer on the membrane (FTIR-ATR, Nexus Thermo Nicolet, detector MCT-A, Diamond ATR) for the membranes modified with the random, diblock, and triblock copolymers. 16 spectra were collected at each measurement point and three points were measured for each membrane. For these spectra, the 1737 cm<sup>-1</sup> peaks were corrected against the 3020 cm<sup>-1</sup> one present in PVDF to take into account the variability in the penetration depth of the IR beam due to the nature of the acquisition method (Attenuated total reflectance - ATR).

FTIR-mapping in external reflection mode was also used to create the chemical maps of the membranes used after the filtration protocol was finished and compared

with the unmodified membrane. The membrane surfaces were scanned with an infrared spectrometer (IN10MX Thermo Scientific) under reflection mode with an analysed surface of 50 by 50  $\mu\text{m}$  for each point (one point was measured every 50  $\mu\text{m}$ ). The spectral resolution is  $8\text{ cm}^{-1}$ , and 16 scans are acquired on each measurement point. A more detailed description of the technique can be found in the previous chapter (Chapter 4, section 2, page 119).

All of the spectra and/or maps were processed using OMNIC 9 © software from Thermo Fisher Scientific Inc.

#### 2.2.4 Filtration protocol

Dead-end filtration experiments with Amicon® stirred cells (Series 8050, Merck Millipore) were carried out for the membranes modified with the different types of copolymers at a stirring speed of 200 rpm, temperature of  $20^\circ\text{C}$  and pressure of 2 bar to assess the efficiency of the coating for different coating times. The rotational Reynolds number for these conditions - and taking into account a diameter of the agitator of 0.032 m - is of about 950.

Coated membranes were left overnight with PBS 1x solution. The experiments began by performing the compaction of the membranes at 2 bar for at least 1 h, and until the fluxes were stable. Then, the initial PBS flux was recorded ( $J_{PBS,0}$ ). Afterwards, 1 g/L BSA was filtered until 20 mL of permeate was collected, and afterwards the rinsing step was performed with 20 mL of PBS 1x for 20 min and 200 rpm. The final PBS flux ( $J_{PBS}$ ) was recorded. These steps correspond to the first filtration-rinsing cycle (Cycle 1 or C1); two more cycles were performed on the same manner, yielding BSA and PBS filtration parameters for the cycles 2 and 3 (C2 and C3 respectively, see Figure 5.1).

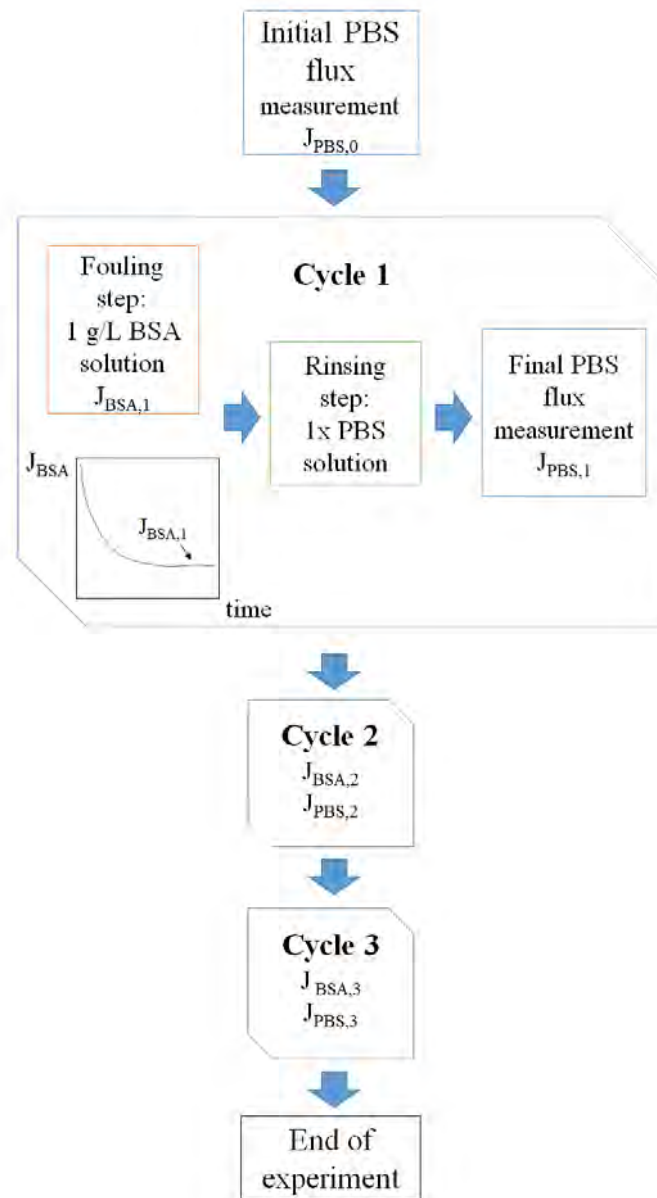


**Figure 5.1:** Diagram of the protocol for the filtration-rinsing cycles.

### Calculations

With respect to the data of fluxes, similar indexes can be calculated as in Chapter 2, 50: Reversibility index (RI), Fouling reversibility ratio (FRR), and Flux decline ratio (FDR). Their expressions are shown in the following equations.

$$RI_{C_i} = \frac{J_{PBS_f, C_i} - J_{BSA_f, C_i}}{J_{PBS_0} - J_{BSA_f, C_i}} \quad (5.1)$$

$$FRR_{C_i} = \frac{J_{PBS_f, C_i}}{J_{PBS_0}} \quad (5.2)$$

$$FDR_{C_i} = \frac{J_{BSA_f, C_i}}{J_{PBS_0}} \quad (5.3)$$

where  $J_{PBS_0}$  is the initial PBS flux,  $J_{PBS_f, C_i}$  the final PBS flux at the Cycle  $i$ , and  $J_{BSA_f, C_i}$  the final BSA flux at cycle  $i$ .

#### 2.2.5 Detection of BSA

The BSA feed solutions and final permeate samples after each filtration cycle were collected and analysed by UV spectrometry. The amount of BSA was detected by measuring the absorbance at 280 nm using an UV spectrometer (PowerWave XS, Biotech). PBS 1x was used as the reference solution and a calibration curve was constructed with BSA solutions ranging from 0.25 g/L to 2 g/L. The precision of the method was of  $\pm 0.007$  (absorbance units). Then, the observed retention ( $R_{obs}$ ) was calculated in relation with the measured concentration of BSA in the permeate and feed ( $[BSA]_{permeate}$  and  $[BSA]_{feed}$ , respectively, Eq. 5.4).

$$R_{obs} = 1 - \frac{[BSA]_{permeate}}{[BSA]_{feed}} \quad (5.4)$$

The Ferry-Renkin equation was used to estimate the theoretical retention of BSA [4]. The equation used was the following:

$$\mathbb{R} = \left[ 1 - 2 \left( 1 - \frac{a}{d} \right)^2 + \left( 1 - \frac{a}{d} \right)^4 \right] * 100 \quad (5.5)$$

where:

$\mathbb{R}$ : theoretical retention coefficient (in %),

$a$ : particle diameter (in nm),

$d$ : pore size of the membrane (in nm).

### 3 Results and Discussion

This chapter is mainly dedicated to evaluate the performance of UF membranes when subjected to filtration-rinsing cycles. As a first step, some characterisation methods have been carried out to get a better insight of the process. They include water contact angle determinations, FTIR measurements, and FEG-SEM (Field emission gun - Scanning electron microscopy) images of the membranes modified for different periods of time. Then, results for the filtrations cycles are shown, and the respective reversibility parameters calculated. Last, FTIR-mapping of some of the membranes taken after the filtration was done are presented.

#### 3.1 Characterisation of the membranes

As specified in the Materials and Methods section, the UF PVDF membranes were modified with a copolymer solution concentration of 5 mg/mL and varying the coating time. It was previously mentioned in Chapter 4 that this last parameter has not been properly addressed by membrane researchers when coating was used for the modification of membranes, particularly for our PVDF/PS-PEGMA system.

The following figure (Figure 5.2) depicts the evolution of Water contact angle (WCA) with coating time for the membranes modified with the different copolymers. It also contains a table with the chemical detection of the copolymers performed by ATR-FTIR.

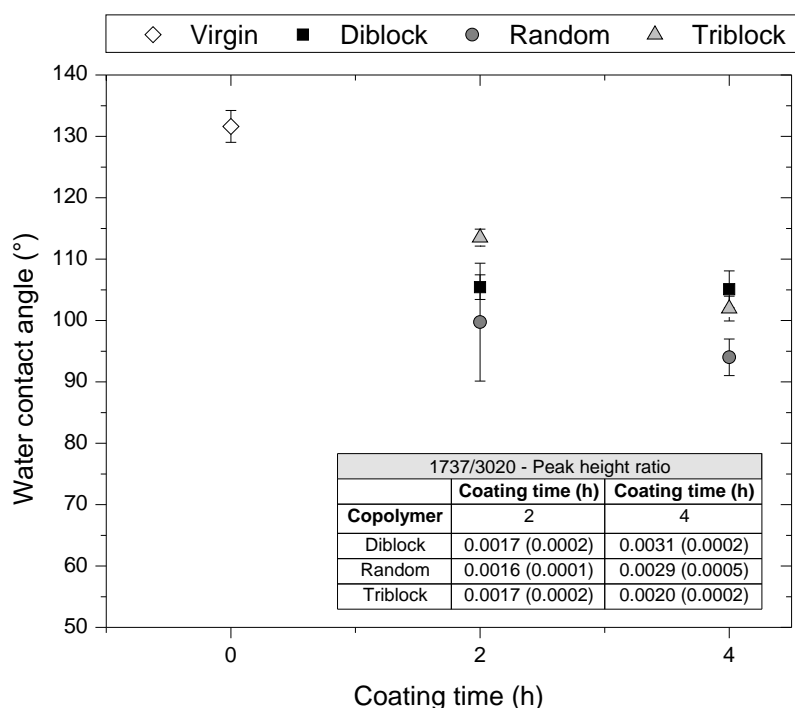


**Figure 5.2:** Variation of the water contact angle and peak height ratio with coating time for the membranes modified with 5 mg/mL of diblock, random, and triblock copolymer solutions. For the peak height ratio table: standard deviations of the measurements are presented inside the brackets).

For all the membranes modified by the copolymers the WCA were lower than the one measured for the unmodified membrane. There was a tendency to lower WCA when the coating time increased, however, due to the measurement imprecisions these changes may not be significant. It was definitely possible to conclude that the modification process yielded more hydrophilic membranes when compared to an unmodified one. The copolymers were positively detected on the membrane, since the  $1737\text{ cm}^{-1}$  peak was detected, that corresponds to the  $C = O$  group in the PEGMA chain. Generally, the longer the coating time, the more copolymer was detected in the system, which is depicted in Figure 5.3, in which the variation of WCA with peak height ratio - measured by ATR-FTIR - for the different modification conditions is represented.

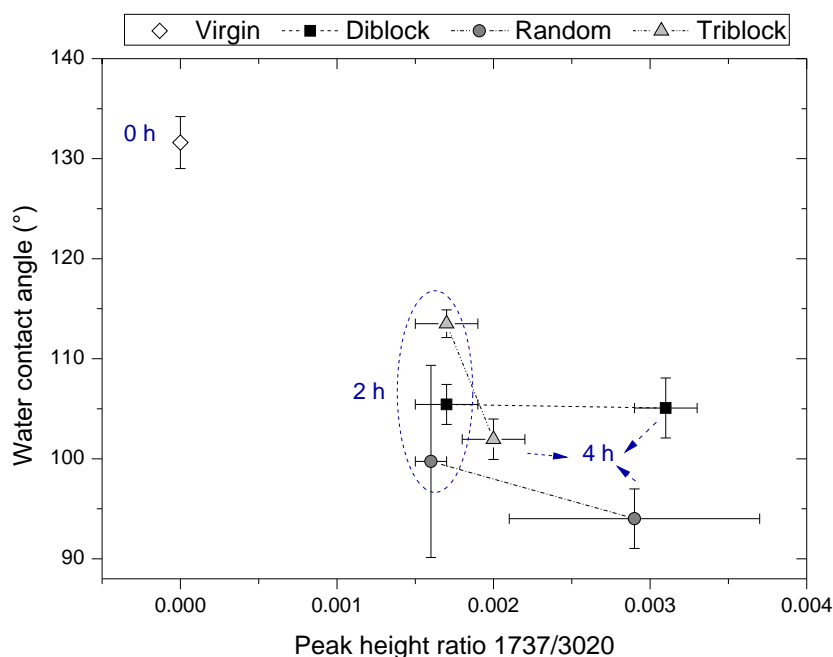


**Figure 5.3:** Variation of the water contact angle with relative peak height for the coating times of 2 and 4 hours for the membranes modified with 5 mg/mL of diblock, random, and triblock copolymer solutions. The peak heights were determined by ATR-FTIR.

Overall, the presence of copolymer increased when the WCA decreased. For the diblock copolymer, the increase in peak height ratio did not influence a change in WCA, while for the membranes modified with the triblock copolymer this tendency was more marked. It is important to note that both analytical methods for some cases showed relatively high standard deviations, that can be related to the rugosity of the membrane or imperfections on the coating process. This could be better seen on the data obtained for the random copolymer.

Limitations on the interpretation of data from contact angle measurements have been previously seen in this manuscript, and this methodology, although easy to perform and yielding an idea on hydrophilicity of the membranes, was not sensitive enough. One of the drawbacks with using conventional ATR-FTIR analysis involves the number of points taken on each membrane - in our case three to five - in that this random and limited selection of points could be hiding heterogeneities on the

distribution of the layers of interest. As seen on the previous chapter, by performing scans of a larger surface with FTIR microspectroscopy, the coating layers showed an heterogeneous distribution, so the places where measurements were randomly taken with the usual FTIR apparatus could yield different results.

The FEG-SEM images taken for the virgin membrane, and the membranes modified with the random copolymer for 4 and 6 h (Figure 5.4) clearly show that there is in fact copolymer on the membrane surface and that the longer the coating time, the more copolymer was adsorbed onto the surface of the membrane. The membranes modified for 4 h presented lower copolymer coverages, while for the membrane modified for 6 h this coverage was more homogeneous, and almost no pores could be seen.

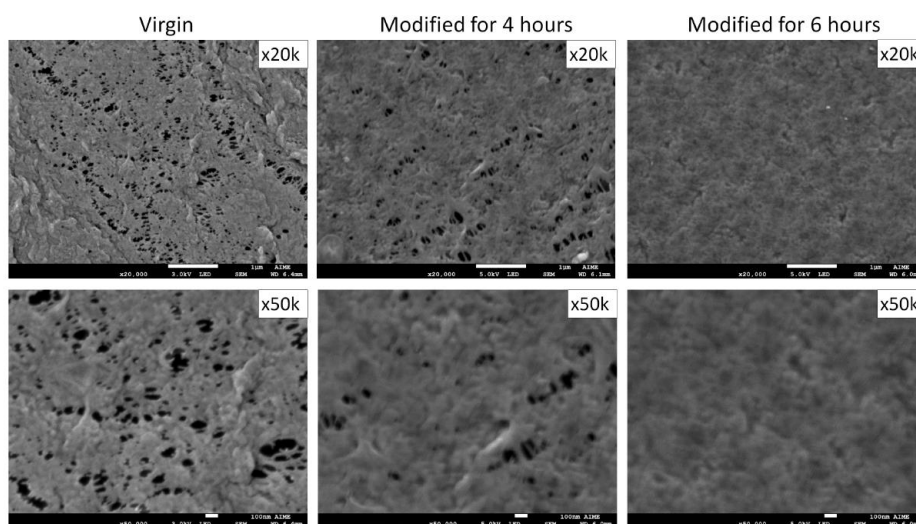


**Figure 5.4:** FEG-SEM images of the unmodified membranes and modified with 5 mg/mL random copolymer solution for 4 and 6 hours. The scale bars for the x20k and x50k magnifications correspond to 1  $\mu\text{m}$  and 100 nm, respectively. The images were taken with a Schottky Field Emission Scanning Electron Microscope (JEOL SEM-FEG JSM7800F); samples were metallised with gold.

### 3.2 Evaluation of the coating time in the filtration performance of the membranes

The optimisation of the coating time was performed using a copolymer concentration of 5 mg/mL. This concentration level was chosen since it was the one for which the copolymers generally reached the maximum coating levels - with similar mass density values -, and the copolymer solutions were stable. The different coating times used were of 2 h, 4 h and 6 h; above the coating time of 6 h the fluxes were low and the detection of the variation of fluxes was limited by the precision of the balance.

The evolution of the permeability as a function of time for the cyclic filtrations performed with the membranes modified with the different copolymers are shown in the following figure (Figure 5.5). For each condition the experiments were performed at least two times, and the variability between each experiment was found to be between 8 % and 17 %.

For all of the copolymers and coating times, the initial PBS permeability was generally the highest. Then, when BSA was filtered through the system typical filtration curves were registered, in which the permeability decreased as filtration time went by until it reached a semi-stable final value, which is decreasing in time at a very slowly rate. After the first rinsing step, the PBS fluxes were partially recovered. In the subsequent cycles, the BSA curves reached similar final permeability values and the PBS permeabilities were partially recovered. The curves for the unmodified membrane served as a comparison point to assess the effectiveness of the coating layer on the PBS and BSA permeabilities.

The initial PBS permeabilities for the membranes modified with the random copolymer for 2 h and 4 h were in the same range as for the unmodified one. This permeability was slightly lower for the membranes modified for 6 h, probably due to the presence of more copolymer on surface (see Figure 5.4). At this modification time, the final BSA permeability was smaller than for the other two and with similar values than the ones registered for the virgin membrane. The final BSA permeabilities for 2 h and 4 h were higher than the ones of the unmodified membrane.

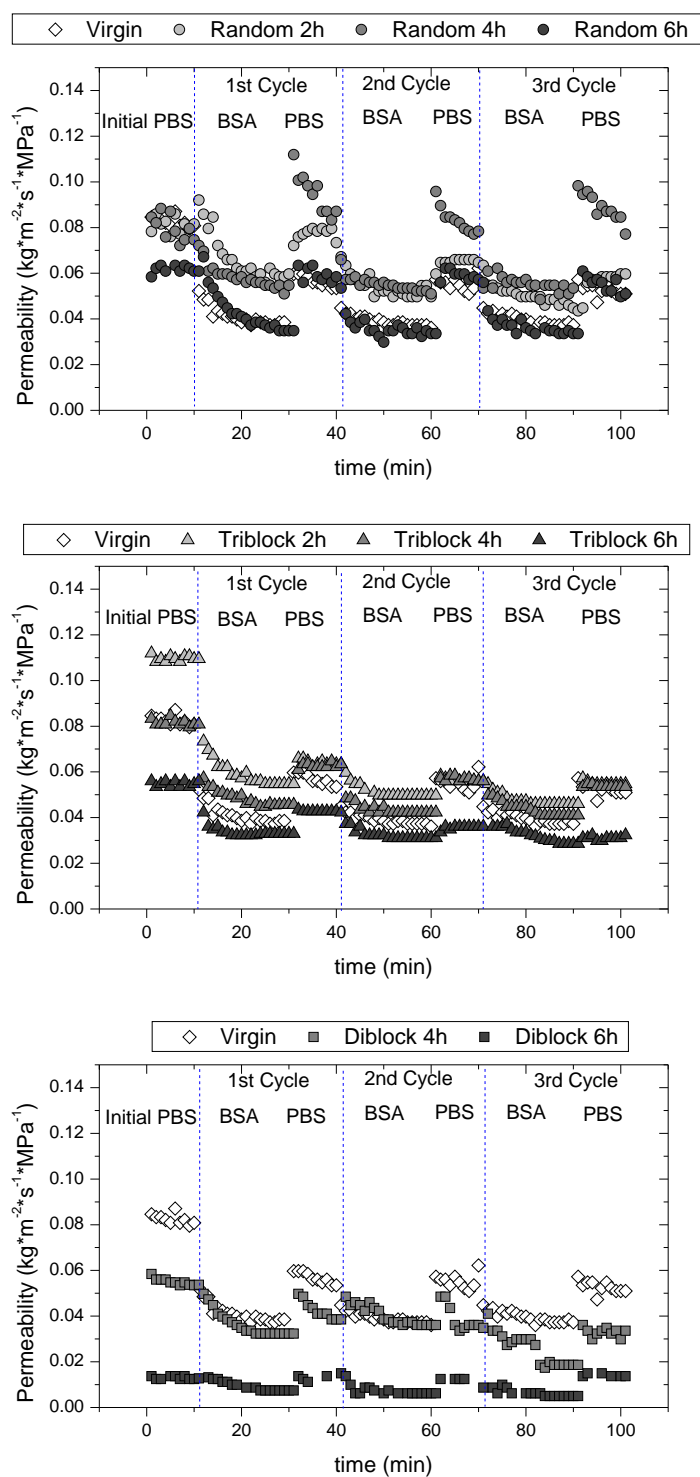


**Figure 5.5:** Evolution of the permeability with time for the unmodified membranes and modified with 5 mg/mL random, triblock, and diblock copolymer solution for 2, 4 and 6 hours.

In the case of the membranes modified with the triblock copolymer, the initial PBS permeabilities were higher for the membranes modified for 2 h and decreased with increasing coating time. The initial PBS permeabilities registered for the coating time of 6 h were lower than the one of the virgin membrane, while the ones for the membranes modified for 4 h were similar to the reference case. At the coating time of 2 h the increase in hydrophilicity seen in the variation of WCA determined previously seemed to be more important than the added resistance coming from the additional copolymer. The final BSA fluxes for the membranes modified for 2 h and 4 h were similar, and higher than the ones obtained for the membrane modified for 6 h.

The membranes modified with the diblock copolymer for 4 h and 6 h showed the lowest fluxes, for both PBS and BSA, and even lower than the ones from the unmodified membranes.

The initial PBS, and final PBS and BSA permeabilities - at the end of the third cycle of the experiment, C3 - for all of the copolymers against coating time are summarised in the following figure (Figure 5.6).

As seen before, for the unmodified membrane - coating time of 0 h - the PBS permeability decreased between the beginning and the end of the experiment, while the final BSA permeabilities remained almost unchanged.

For all of the copolymers tested, the initial PBS permeabilities decreased with an increase in coating time.

For the membranes modified with the triblock and random copolymers and a coating time of 2 h, the PBS and BSA permeabilities decreased between the first and the last filtration cycle. However, for the membranes modified with the random copolymer for 4 h the PBS permeabilities remained almost unchanged as well as the final BSA fluxes. In this case, the fouling was considered to be 100 % reversible for at least 3 filtration-rinsing cycles while maintaining the highest BSA working fluxes.

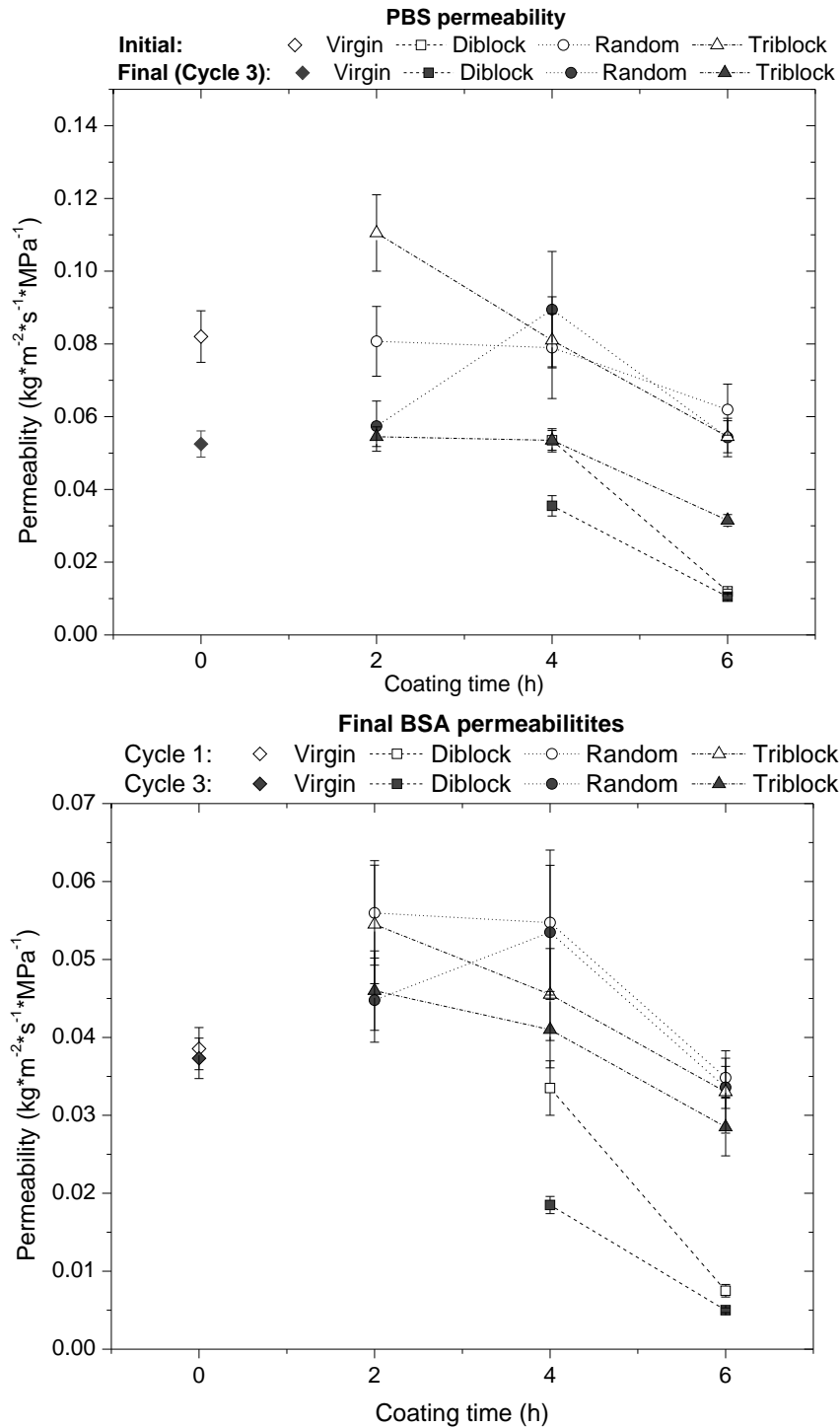


**Figure 5.6:** PBS and BSA permeabilities vs. coating time for the unmodified membranes and modified with 5 mg/mL random, triblock, and diblock copolymer solution.

In the previous figure it was again evident that the membranes modified with the diblock copolymer presented the lowest permeabilities among the tested copolymers, even though they had similar WCA and copolymer levels than the membranes modified with the random copolymer (see Figure 5.2, page 158), which has a similar MW. The only evident difference between these two copolymers is the structure: the brush in the diblock structure could be adding a higher resistance than the loops in the random copolymer. However, this should have also been evident also for the results obtained for the triblock copolymer, that has an extra PEGMA brush.

The retention of BSA at the end of each BSA filtration step for the virgin membrane and the membranes coated for 2 h, 4 h and 6 h with the random copolymer were measured. At the end of the first cycle the calculated retention percentages were of 5 %, 14 %, 8 % and 8 %, respectively, which lied very close to the estimated retention of BSA of 11 % by the Ferry-Renkin equation [4] – for a diameter of BSA of 7.9 nm and using 43 nm as a mean pore size. The results for the subsequent cycles showed some tendencies in retention percentages of BSA, for the virgin membrane the retention of BSA slightly increased to 11 %, while for the membrane modified for 6 h the final retention value reached 14 %. For the other two coating conditions the retention of BSA varied between each cycle and reached 30 %. Taking into account the expected variabilities of the process – laboratory-made membranes and the coating itself –, the modification did not significantly change the retention of BSA.

The following table (Table 5.1) sums up some the PBS and BSA permeabilities and indexes calculated from them for the unmodified and modified membranes. For the Reversibility index (RI), the values close to zero meant that the fouling was more irreversible, while a value of 1 would imply that the fouling was 100 % reversible. For the Fouling reversibility ratio (FRR), values closer to the unity meant that the PBS fluxes are closer to the initial one, while for Flux decline ratio (FDR) the BSA fluxes were higher and close to the initial PBS one.

For most of the cases, there was little variation between the calculated final indexes - on the third filtration cycle - and the ones for the first and/or second cycle (results not shown on the table). They were usually slightly higher on the first cycle and then decreased down to the third one. The highest variations were registered for

the RI of the membranes modified with the random copolymer for 2 h and the triblock copolymer for 6 h, for which the starting indexes - on C1 - were of 0.879 and 0.465, respectively.

**Table 5.1:** Main permeability values and calculated indexes for the membranes modified with 5 mg/mL of random, triblock or diblock copolymer solutions and different coating times.

Membrane	Coating time (h)	Permeability*			Index		
		PBS Initial	BSA Final**	PBS Final**	RI	FRR	FDR
Virgin	0	0.0820	0.0373	0.0525	0.34	0.64	0.45
Random	2	0.0807	0.0448	0.0574	0.35	0.71	0.55
	4	0.0790	0.0535	0.0894	1.41	1.13	0.68
	6	0.0619	0.0336	0.0543	0.73	0.88	0.54
Triblock	2	0.1105	0.0460	0.0545	0.13	0.49	0.42
	4	0.0810	0.0410	0.0535	0.31	0.66	0.51
	6	0.0545	0.0285	0.0315	0.12	0.58	0.52
Diblock	4	0.0535	0.0185	0.0355	0.49	0.66	0.35
	6	0.0120	0.0050	0.0105	0.79	0.88	0.42

\*Permeability in  $\text{kg m}^{-2} \text{s}^{-1} \text{MPa}^{-1}$ .

\*\*Final PBS and BSA permeabilities correspond to the ones registered at the end of Cycle 3.

The best performers in terms of indexes and fluxes were the membranes modified with the random copolymer. The surface coated for 2 h were protected against fouling for at least one filtration cycle. For a coating time of 4 h the membranes showed great anti-fouling properties, at least for the 3 fouling-rinsing cycles performed.

The membranes modified with the triblock copolymer did not present great reversibility indexes or other ratios, only the ones modified for 4 h showed similar values than the unmodified membranes, even though the initial permeabilities were close to the ones found for the virgin membrane. This could indicate that this copolymer coated in the conditions used was not efficient in improving the anti-fouling properties of the membrane.

Just by looking at the obtained indexes, it would seem that the membranes

modified with the diblock copolymer performed quite well, in particular for the coating time of 6 h. However, the working PBS and BSA fluxes were quite low, which could have also influenced the subsequent fouling behaviour. Thus, conclusions based solely on indexes should always be backed by raw filtration data.

FTIR maps of the membranes used for the filtrations were also acquired, and shown in Figure 5.7. After the 3-cycle filtrations were performed two pieces of the unmodified membrane and modified with the random copolymer for 2 h and 6 h were cut and the maps were acquired for the retentate and permeate side of each of them. The maps for the peaks corresponding to the copolymer ( $1737\text{ cm}^{-1}$  and  $2876\text{ cm}^{-1}$ ) and foulant ( $3300\text{ cm}^{-1}$ ) were extracted with the proprietary software and shown below.

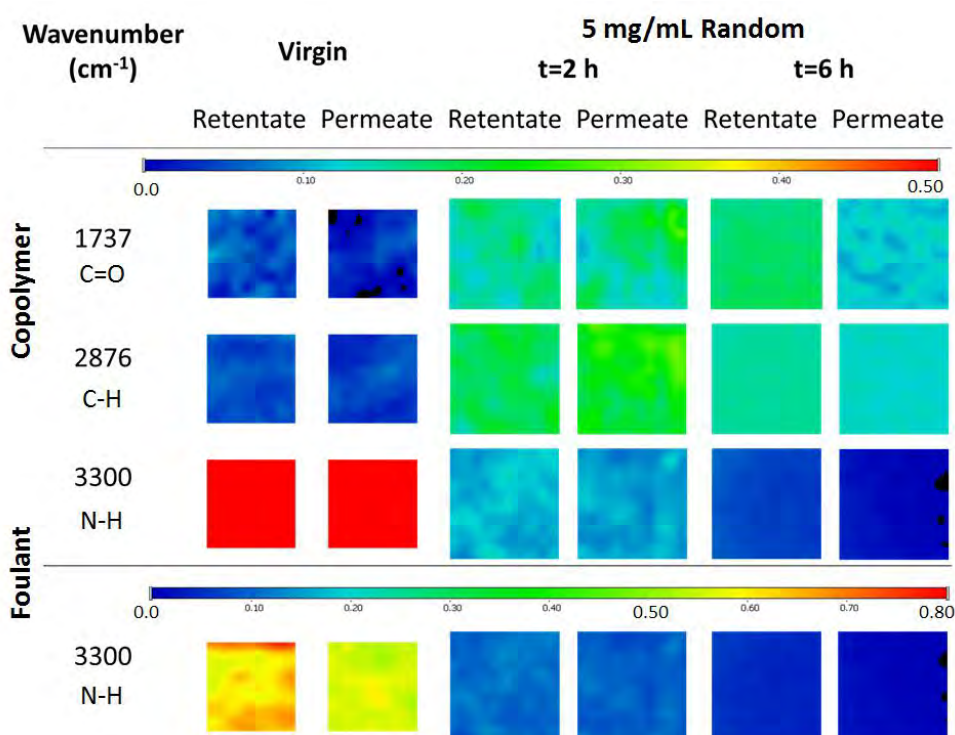


**Figure 5.7:** FTIR maps of the retentate and permeate sides for the unmodified membranes and modified with 5 mg/mL random copolymer solution for 2 h and 6 h. The maps were acquired for the membranes used on the filtration-rinsing experiments once the filtration protocol was performed. For the virgin membranes the size of the images are of  $400\text{ }\mu\text{m}$  by  $400\text{ }\mu\text{m}$ , while for the rest of the maps the size is of  $500\text{ }\mu\text{m}$  by  $500\text{ }\mu\text{m}$ .

For the virgin membrane the copolymer signals at  $1737\text{ cm}^{-1}$  and  $2876\text{ cm}^{-1}$  were, as expected, not detectable, while there was a high presence of foulant on both surfaces, even higher than the usual 0.0 to 0.5 colour scale used, thus the maps were also shown on a larger scale of 0.0 to 0.8 to appreciate the differences.

The heterogeneous distribution of the coating layer was again detected by this method. For the modified membranes, the copolymer was detected at the retentate and permeate sides, the coating probably reached the entire structure of the membrane - surface and pore walls.

BSA was present in lower quantities for the membrane modified for 6 h than for 2 h. The presence of BSA on these two membranes was much lower than the one detected for the unmodified one. The unmodified membrane and the one modified with the random copolymer for 2 h showed comparable initial PBS permeabilities, therefore, the differences in the BSA detected on the surface of these membranes could be attributed to the presence of the copolymer. Although almost no BSA was detected in the FTIR maps for the membranes modified for 6 h, the behaviour could be not fully attributed to the sole presence of the copolymer, since the fluxes were lower than for the other two.

The high presence of BSA on both sides of the virgin membrane indicated that it passed through, which was in accordance with the UV measurements presented before, and that it was highly adsorbed on - absorbed in - the membrane. This adsorption/absorption was not so evident for the modified membranes, even though the BSA was still passing through the membrane structure. This showed the effect of the coating on hindering the adsorption of the foulants.

Overall, the membranes modified with the random copolymer seemed to yield better results than the ones obtained for the diblock and triblock copolymers. This could be due to the possible distribution of these copolymers on the surface of the membrane. Figure 5.8 shows a diagram with the different types of the PS-PEGMA copolymer distributed on a membrane. All surfaces are of similar size and for the diblock and random membranes there are the same amount of molecules adsorbed on the surface of the membrane, while for the triblock this amount is cut in half to keep the same weight and molar coating densities seen in Chapter 2 (section 3.1.1, page 55).

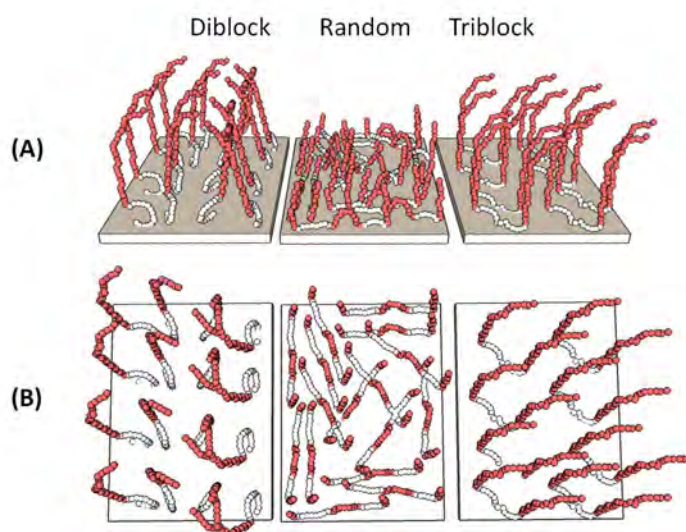


**Figure 5.8:** Diagram of the copolymers adsorbed on the surface of the membrane: (A) side view, (B) upper view.

The random copolymer has a structure that could allow a more even coverage of the surface of the membrane. The structure of the triblock copolymer guarantees a constant distance between the PEGMA brushes, and could yield a good coverage with half the amount of molecules. However this bulkier structure seriously compromised the permeability of the membrane.

Another point of discussion concerns the increase of copolymer adsorption with the coating times used. Classical Langmuir adsorption kinetics usually result in adsorption curves that reach an adsorption plateau. This plateau is generally reached within seconds or a couple of minutes after the solutions are put in contact with the surface. More complex systems, such as adsorption of large polymers for extended periods of time can be described by two-rate kinetic models [5–7]. A first step would involve the initial attachment of the polymer molecules, which could last for a few minutes, while a second step involves the rearrangement of the molecules and a possible bilayer formation. The rearrangement of "lying down" molecules could make more adsorption sites available for new molecules to adsorb onto the surface. This last process can occur in a period of a few hours, and could explain why we can

still detect an increase of the copolymer adsorbed on the surface of the membrane on long coating times.

Clearly, even if in the static adsorption tests the presence of more copolymer resulted in better anti-fouling properties, this larger amounts of copolymer critically affected the permeability of the membrane.

## 4 Conclusions

It was possible to assess the effectiveness of the coating by performing the filtration-rinsing cycles. For the membranes modified with 5 mg/mL random copolymer solution for 4 h, better anti-fouling properties and working BSA permeabilities were obtained than the ones seen for the unmodified membranes.

WCA and ATR-FTIR spectrometry measurements gave an initial outlook on the changes in the characteristics of the membrane after the modification was done. The FEG-SEM images of the surfaces showed the accumulation and distribution of the copolymer with the different coating times.

It was possible to detect the presence and distribution of the copolymer and BSA adsorbed on the surface of the membrane at the retentate and permeate side by using FTIR microspectrometry. The maps obtained with the FTIR technique also suggested that the coating was also covering the internal porous structure of the membranes, which could be protecting the internal structure of the membranes against irreversible adsorption of foulants. The obtained maps complemented the data extracted from the filtration experiments and helped in the understanding of the positive effect these copolymers have on hindering the attachment of the foulants: even though the BSA passed through the membranes it could be rinsed out in the case of the membranes modified with the random copolymer, whereas the BSA detected on both sides of the virgin membrane was much higher - with membranes showing similar flux conditions, after three filtration-rinsing cycles.

Experiments should be carried out for longer periods of time and many more fouling and rinsing cycles to provide long-term effects of the copolymers on the lifespan of the modified membranes. Tests concerning chemical cleaning of the used membranes should also be performed if we want to assess their lifespan. As commented in the previous chapter, ATR-FTIR microspectrometry could be used to try to better quantify the deposited species on the surface of the membranes.



## 5 References

- [1] Séverine Carretier, Li-An Chen, Antoine Venault, Zhong-Ru Yang, Pierre Aimar, and Yung Chang. Design of PVDF/PEGMA-b-PS-b-PEGMA membranes by VIPS for improved biofouling mitigation. *Journal of Membrane Science*, 510:355–369, 2016.
- [2] Jennifer R Du, Sigrid Peldszus, Peter M Huck, and Xianshe Feng. Modification of poly (vinylidene fluoride) ultrafiltration membranes with poly (vinyl alcohol) for fouling control in drinking water treatment. *Water research*, 43(18):4559–4568, 2009.
- [3] Antoine Venault, Yi-Hung Liu, Jia-Ru Wu, Hui-Shan Yang, Yung Chang, Juin-Yih Lai, and Pierre Aimar. Low-biofouling membranes prepared by liquid-induced phase separation of the PVDF/polystyrene-b-poly (ethylene glycol) methacrylate blend. *Journal of Membrane Science*, 450:340 – 350, 2014.
- [4] R.W. Baker. *Membrane Technology and Applications*. John Wiley & Sons, 2 edition, 2004.
- [5] Sumit Tripathi and Rico F Tabor. Modeling two-rate adsorption kinetics: Two-site, two-species, bilayer and rearrangement adsorption processes. *Journal of colloid and interface science*, 476:119–131, 2016.
- [6] Louise Deschenes, Francois Saint-Germain, and Johannes Lyklema. Langmuir monolayers of non-ionic polymers: Equilibrium or metastability? Case study of PEO and its PPO–PEO diblock copolymers. *Journal of colloid and interface science*, 449:494–505, 2015.
- [7] M Raposo, RS Pontes, LHC Mattoso, and ON Oliveira. Kinetics of adsorption of poly (o-methoxyaniline) self-assembled films. *Macromolecules*, 30(20):6095–6101, 1997.



# General conclusions and perspectives

6



---

## Conclusions and perspectives

Taking into account that the main objective of this manuscript was to study the anti-fouling properties of modified membranes, different approaches were applied on how to perform this research.

The general objective of Chapter 2 was to assess the more classical assessment techniques for the analysis of the modification success and anti-fouling properties of the membranes. To achieve this, different experiments were performed to assess the anti-fouling properties of the modified MF PVDF membranes - pore size of  $0.1 \mu\text{m}$  - with the PS-PEGMA copolymers. It was concluded that, in general, the presence of more copolymer on the surface provided an anti-fouling effect against proteins and cells when static adsorption conditions were applied. The copolymers were present on the membrane surface at comparable values than the ones found in the bibliography. However, the adsorption of the foulants never reached a value of zero, no matter how much copolymer was adsorbed on the membrane, or the type of copolymer used. The modified membranes also had better performances than the unmodified ones when filtration tests were concerned: the initial flux with respect to the unmodified membrane were not significantly affected in this case - the lowest initial fluxes were registered for the membranes modified with the triblock copolymer at  $0.6 \pm 0.1 \text{ kg m}^{-2} \text{ s}^{-1} \text{ MPa}^{-1}$  versus  $0.9 \pm 0.2 \text{ kg m}^{-2} \text{ s}^{-1} \text{ MPa}^{-1}$  for the virgin membrane. The filtration working fluxes were better for the membranes modified with the diblock and random copolymers, at around  $0.6 \text{ kg m}^{-2} \text{ s}^{-1} \text{ MPa}^{-1}$ , when the respective fluxes for the virgin and triblock cases were of approximately  $0.4 \text{ kg m}^{-2} \text{ s}^{-1} \text{ MPa}^{-1}$ . From the static adsorption tests it was evident that some foulant was still left on the membranes, which agreed with the fact that the fluxes were not quite recovered after the filtration cycle was performed, and with the fact that less amount of foulant was present in the modified membranes than for the unmodified ones.

Chapter 3 aimed to develop a system in which fouling could be directly monitored, which was achieved by developing microfluidic chips - with retentate and permeate side, as well as a membrane inserted in between - that would be integrated with fluorescence microscopy. The follow-up of the relationship between the measured grey values - accumulation of foulant - and the flux behaviour during

filtration, allowed us to detect two zones, one in which there was a direct correlation between the flux and grey value - less flux meant more accumulation - and another one in which a steady flux was reached but the grey value would continue to increase.

The objective of Chapter 4 was to apply FTIR mapping to study our system and develop the data analysis protocols to carry out this assessment. It was concluded that FTIR mapping is an important tool that can help us to complement our study of fouling phenomena by assessing chemical distribution of the different components of the system on the membrane surface at a millimetre scale.

It was also shown that it is possible to apply this technique to assess coating and fouling of the membrane – at the same time – for the surface of the sample, and the data obtained can be analysed by image analysis software, either by calculating the average signal or by defining coating/fouling levels.

The detection of the amounts of coating and copolymer layers were in agreement with other techniques: more coating detection caused less foulant to be adsorbed on the membrane.

On Chapter 5, the assessment the effectiveness of the coating by performing the filtration-rinsing cycles was performed. For the membranes modified with 5 mg/mL random copolymer solution for 4 h, better anti-fouling properties and working BSA permeabilities were obtained than the ones seen for the unmodified membranes. The initial fluxes of these membranes were be affected by the amount of copolymer adsorbed on the surface, as the FEG-SEM images of the surfaces modified for different coating times showed. The FTIR maps obtained for the membranes used in the filtration tests complemented the data extracted from the filtration experiments and helped in the understanding of the positive effect these copolymers have on hindering the attachment of the foulants. They suggested that the coating was also covering the internal porous structure of the membranes, which could indicate that the membranes modified with these copolymers could have better protection against fouling in the long-term.

Prospective work into discerning the different effect of the copolymer structure on their anti-fouling effect should involve the measurement of interaction forces by performing AFM force spectrometry measurements. This would allow the use of different probes - attaching colloids or humic acids [1, 2], and could give a better

---

view on the different effects of the copolymer structure on the adhesive properties of the probes.

Concerning the microfluidic devices, there are still some issues to overcome and improve. The way to hydrate the modified membranes needs to be solved. Perhaps more permeable membranes should be used and/or the modified membranes should be protected with glycerol prior to their insertion into the microchip - provided this glycerol can be fully removed during the set-up of the experiments. The membranes should also be kept as flat as possible during drying to avoid possible damage. The in-situ modification of the membranes when already inside the microchip by passing through the copolymer solution could also solve this issue. More work should also be performed in varying the operative conditions of the micro filtrations: variation of fluxes, concentration of BSA, and concentration of copolymer used. The observation of fouling with other type of membranes and other type of modifications (chemical grafting, blending) could be performed. Modelling also be applied to calculate kinetic parameters [3].

Further work in the field of FTIR microspectrometry should include the improvement on the image analysis to have a better understanding and analysis of the obtained data, hence improving our knowledge on the importance of the heterogeneous distribution of the coating and fouling layers and their interrelations. Fourier-transform image analysis and others could be applied in future works. The actual quantification of the species present on the surface would be of great interest, and would be a more reachable goal if the ATR acquisition mode could be used.

An interesting approach in the mapping field would be the use of infrared spectroscopy that is coupled with AFM devices [4, 5]. This would allow the determination of both physical - roughness - and chemical properties on a specific location with the possibility of measuring interaction forces as well.

Filtration experiments should be carried out for longer periods of time and many more fouling and rinsing cycles to provide long-term effects of the copolymers on the lifespan of the modified membranes. It would also be interesting to perform tests on cross-flow filtration systems. The development of optimal cleaning protocols will be a must if these membranes were to be used at pilot or industrial scale.

Overall, the PS-PEGMA copolymers improved the anti-fouling properties of the PVDF membranes. Although different copolymer structures were tested, the most

important parameter in yielding the desired anti-fouling properties was related to the coverage of the copolymer, the presence of the PEGMA polymers in that their distribution should be as even as possible. Interesting research in this area would be the combination of copolymers with different sizes - from lower to higher molecular weights - and structures - shorter, longer brushes, and loops. The addition of zwitterionic species could yield interesting results [6, 7], since it would involve a step towards the mimicking of the cellular membrane.

---

## References

- [1] Cyril Aubry, Leonardo Gutierrez, and Jean Philippe Croue. Coating of AFM probes with aquatic humic and non-humic NOM to study their adhesion properties. *Water research*, 47(9):3109–3119, 2013.
- [2] Muhammad Tariq Khan, Carmem-Lara de O. Manes, Cyril Aubry, Leonardo Gutierrez, and Jean Philippe Croue. Kinetic study of seawater reverse osmosis membrane fouling. *Environmental science & technology*, 47(19):10884–10894, 2013.
- [3] Kimberly L Jones and Charles R O’Melia. Protein and humic acid adsorption onto hydrophilic membrane surfaces: effects of ph and ionic strength. *Journal of Membrane Science*, 165(1):31–46, 2000.
- [4] Alexandre Dazzi, Craig B Prater, Qichi Hu, D Bruce Chase, John F Rabolt, and Curtis Marcott. AFM–IR: combining atomic force microscopy and infrared spectroscopy for nanoscale chemical characterization. *Applied spectroscopy*, 66(12):1365–1384, 2012.
- [5] Jocelyne E Verity, Neetu Chhabra, Koneswaran Sinnathamby, and Christopher M Yip. Tracking molecular interactions in membranes by simultaneous ATR-FTIR-AFM. *Biophysical journal*, 97(4):1225–1231, 2009.
- [6] Junsheng Liu, Tongwen Xu, Ming Gong, and Yanxun Fu. Fundamental studies of novel inorganic–organic charged zwitterionic hybrids: 3. new hybrid charged mosaic membranes prepared by modified metal alkoxide and zwitterionic process. *Journal of membrane science*, 260(1):26–36, 2005.
- [7] Ping-Sheng Liu, Qiang Chen, Shi-Shan Wu, Jian Shen, and Si-Cong Lin. Surface modification of cellulose membranes with zwitterionic polymers for resistance to protein adsorption and platelet adhesion. *Journal of Membrane Science*, 350(1):387–394, 2010.



# Appendix



Supplementary material on the  
characterisation of the modified  
membranes





## 1 Scanning electron microscopy (SEM) and Atomic force microscopy (AFM)

The scanning of the surface of the unmodified and modified membranes by SEM was performed with a Hitachi S-3000 scanning electron microscope with accelerating voltages from 7 keV to 10 keV. Samples were previously metallised by sputter-coating them with Au for 150 s.

The SEM images of the unmodified and modified membranes are shown on the following figure (Figure A.1). At this scale, it was possible to see the general structure of the membrane, and not much more. The modification performed was not intensive enough to show the differences among the different coating conditions used and copolymer types.

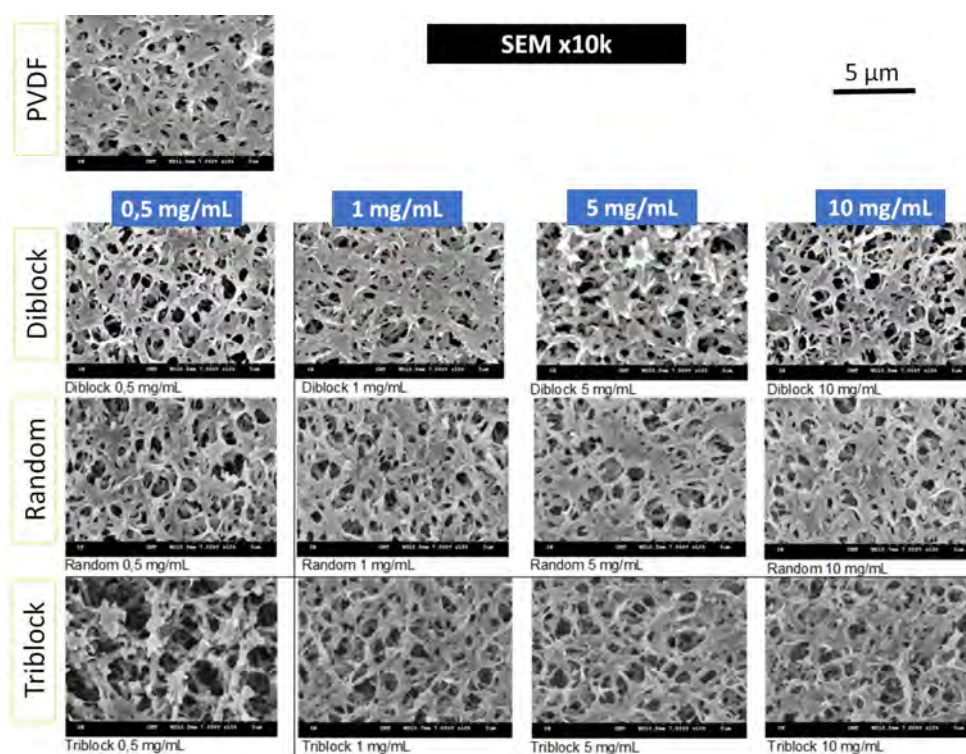


**Figure A.1:** Scanning electron microscopy images of the unmodified and modified membranes.

AFM was performed with a JPK Instruments AG multimode Nanowizard (Germany) apparatus equipped with Nanowizard scanner and operated in solution. For tapping-mode AFM, a commercial Si cantilever (TESP tip) of around 320 kHz resonance frequency from JPK instruments was used.

The AFM images were taken for the membranes modified with the different copolymers and different copolymer concentration, on a  $(x, y)$  scale of  $10 \times 10 \mu\text{m}$  and a  $z$  between 0 and  $2.8 \mu\text{m}$ . They were acquired while the membranes were hydrated with PBS solution, which could give a better insight on their properties during adsorption or filtration. RMS refers to the Root mean square roughness, that represents the standard deviation of surface heights (Figure A.2). RMS was calculated for each individual image and then the average RMS was calculated from two different images.

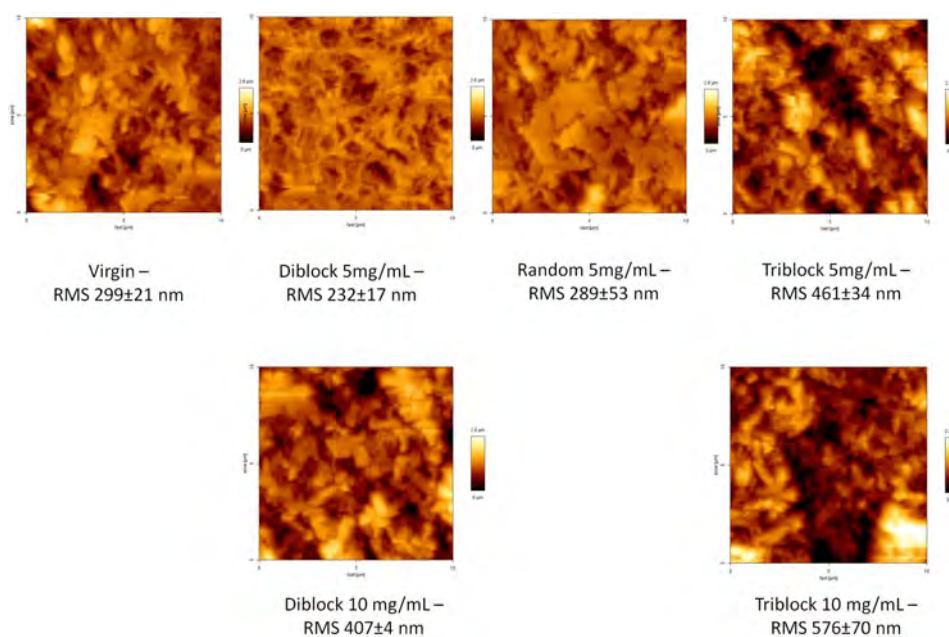


**Figure A.2:** Atomic force spectroscopy of the surface of the membranes and rugosity values. Each image was taken for an area of  $10 \times 10 \mu\text{m}$ .

The RMS seemed to be higher for the membrane modified with the triblock copolymer than for the other two. It also increased with increasing copolymer concentration. Normally, an increase in rugosity would mean that the adsorption could be higher, but there is no general consensus regarding this point.

Supplementary information on the adsorption of species and filtration performance would be required to better link these two points.



## 2 Confocal images of the WBC and PRP for the modified membranes

The following figures (Figures A.3 and A.4) correspond to the images obtained by confocal microscopy of the corresponding blood-cell type.

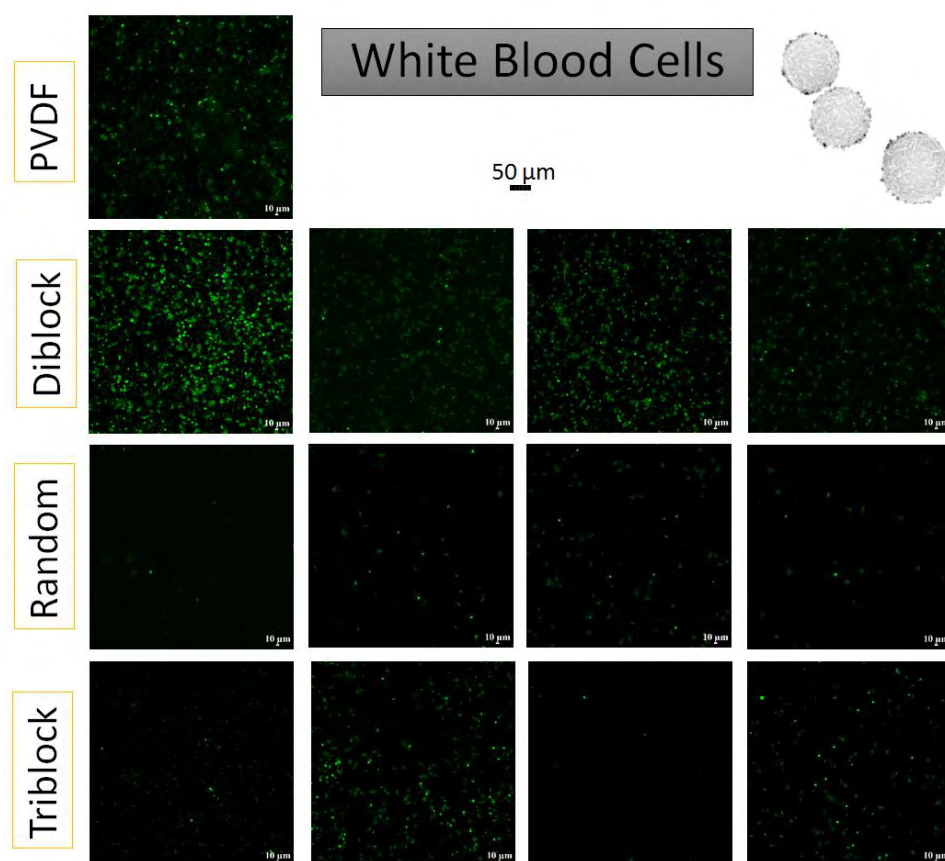


**Figure A.3:** Confocal microscopy images of WBC for the membranes coated with different concentrations of copolymers.

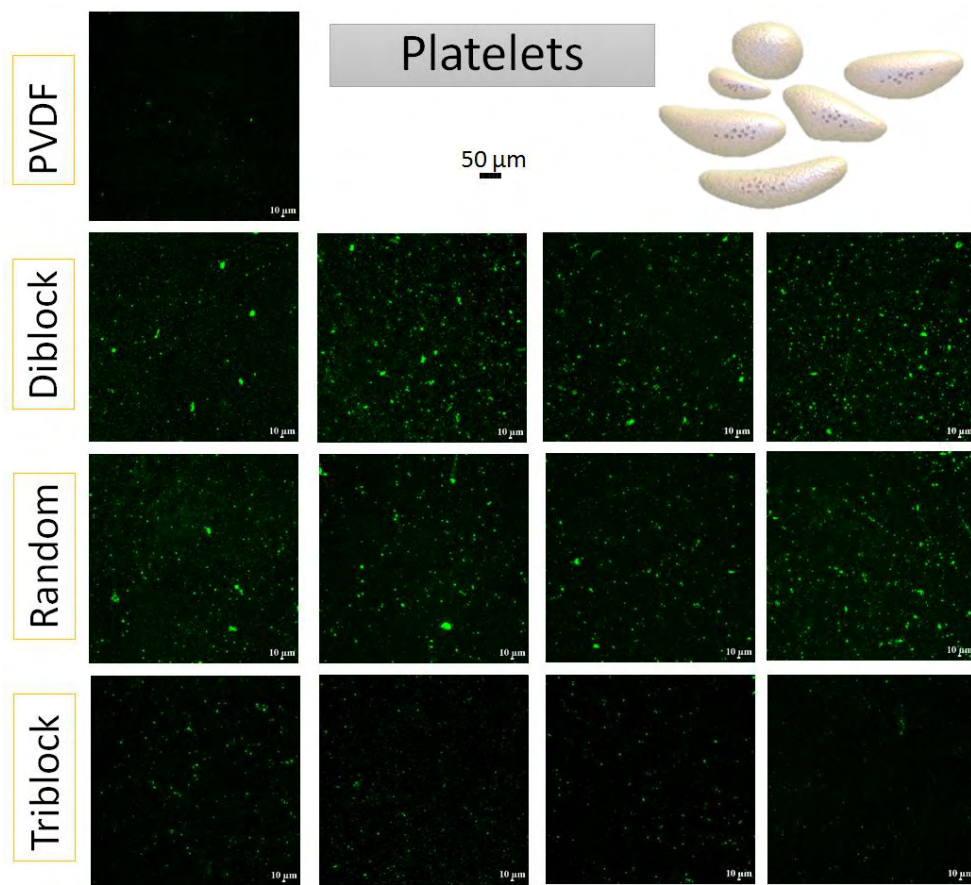


**Figure A.4:** Confocal microscopy images of PRP for the membranes coated with different concentrations of copolymers.

Supplementary information on  
the selection of the peaks of  
interest

A red square containing a white, serif capital letter 'B'.



The following figure is based on additional experiments we have run to illustrate the main differences on why it was decided to proceed with external reflection as the measurement technique for this work. In it we used PVDF membranes and of membranes modified with 5 mg/mL of PS-PEGMA random copolymer for 2 h at room temperature. One piece of each type of membrane was put in contact with 1 g/L BSA according to the protocol described in the manuscript. For these 4 samples, ATR and reflection spectra were acquired and are shown in the figure (Figure B.1).

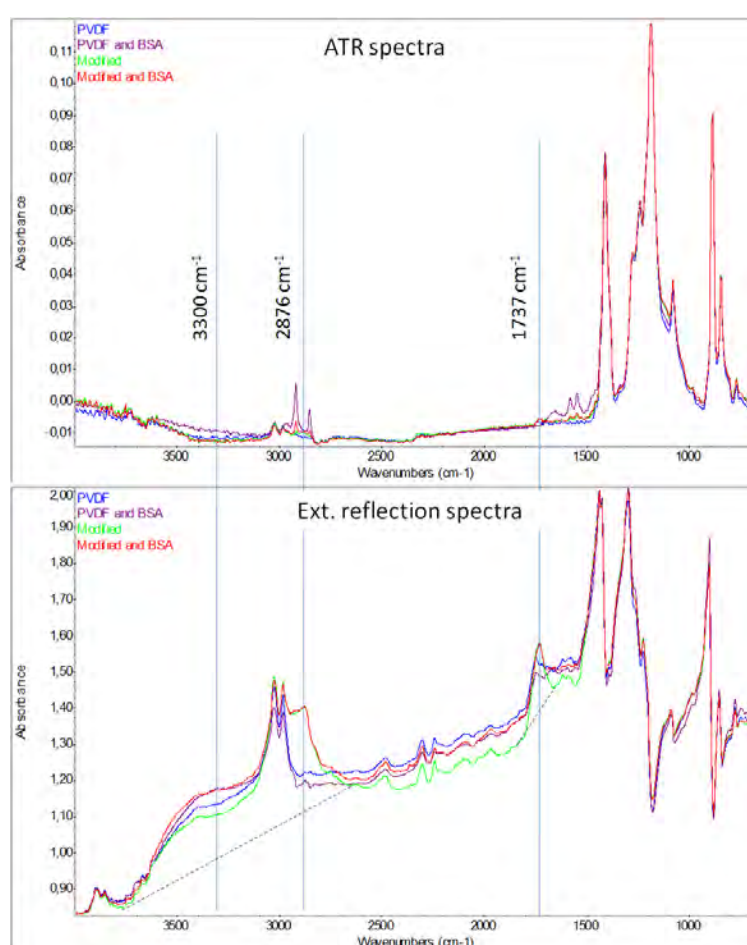


**Figure B.1:** ATR and external reflection spectra taken with the same equipment used in the experiments for unmodified and modified membranes, with and without adsorption of BSA.

On the spectra taken with ATR technique, it is hardly possible to detect a difference between the modified and unmodified membranes. The presence of BSA

can be detected for the PVDF membranes when taking into account the amine region (near wavenumbers of  $1500 - 1600 \text{ cm}^{-1}$ ). On the external reflection spectra, the peaks for the copolymer are clearly present on the external reflection spectra (at  $2876$  and  $1737 \text{ cm}^{-1}$ ). The presence of BSA was determined by following the signal at  $3300 \text{ cm}^{-1}$ . Although it was not an ideal peak, it was considered it to be a better fit for the purpose of this work. The trends measured on these peak heights were in accordance with the change in colour detected at plain sight (BSA was orange) and by the performance results of the filtrations performed.

The height of the BSA peak – and all of the other peaks - was measured by taking the baseline at similar wavenumbers (shown in the figure – dashed grey line), and the presence of the other peaks in the vicinity did not greatly interfere on their results (see Figure B.2). One end of this baseline was taken at a wavenumber of  $3700 \text{ cm}^{-1}$ , while the other end was chosen in a region where other peaks would not interfere (at a wavenumber of  $2600 \text{ cm}^{-1}$ ).

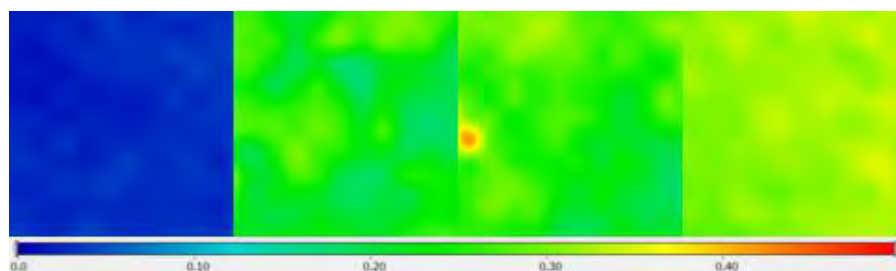


**Figure B.2:** BSA adsorbed on a PVDF membrane at different times. From left to right: 10 minutes, 1 h, 2 h and 8 h.

Scientific communication





## Publications



FTIR mapping as a simple and powerful approach to study membrane coating and fouling



Lucia Benavente<sup>a</sup>, Clémence Coetsier<sup>a</sup>, Antoine Venault<sup>b</sup>, Yung Chang<sup>b</sup>,  
Christel Causserand<sup>a</sup>, Patrice Bacchin<sup>a</sup>, Pierre Aimar<sup>a,\*</sup>

<sup>a</sup> Laboratoire de Génie Chimique, Université de Toulouse, CNRS, INPT, UPS, 118 Route de Narbonne, 31062 Toulouse, France

<sup>b</sup> R&D Center for Membrane Technology and Department of Chemical Engineering, Chung Yuan Christian University, 200 Chung Pei Rd., Chung-Li 32023, Taiwan

## Conference communication

### 12<sup>th</sup> World Filtration Congress, Taipei, Taiwan, April 2016

#### Oral presentation

##### FTIR MAPPING ADAPTED TO ASSESS COATING AND FOULANT DISTRIBUTION ON MODIFIED MEMBRANES

L. Benavente<sup>a,b</sup>, C. Coetsier<sup>a,b</sup>, A. Venault<sup>c</sup>, C. Causserand<sup>a,b</sup>, Y. Chang<sup>c</sup>, P. Bacchin<sup>a,b</sup>,  
P. Aimar<sup>a,b</sup>

<sup>a</sup> Université de Toulouse, INPT, UPS, Laboratoire de Génie Chimique, 118 Route de Narbonne, F-31062 Toulouse, France.

<sup>b</sup> CNRS, Laboratoire de Génie Chimique, F-31062 Toulouse, France

<sup>c</sup> R&D Center for Membrane Technology and Department of Chemical Engineering, Chung Yuan Christian University, 200 Chung Pei Rd., Chung-Li 32023, Taiwan

#### Poster

**LABORATOIRE DE GÉNIE CHIMIQUE**  
TOULOUSE - UMR 5503

**12th WORLD FILTRATION CONGRESS**  
WFC 12  
APRIL 11-15, 2016 - TAIPEI

**Direct observation of fouling with modified membranes integrated into microfluidic chips**

L. Benavente<sup>a\*</sup>, C. Coetsier<sup>a</sup>, A. Venault<sup>b</sup>, C. Causserand<sup>a</sup>, Y. Chang<sup>b</sup>, P. Bacchin<sup>a</sup>, P. Aimar<sup>a\*\*</sup>

<sup>a</sup> Laboratoire de Génie Chimique, Université de Toulouse, CNRS, INPT, UPS, 118 Route de Narbonne, 31062 Toulouse, France

<sup>b</sup> R&D Center for Membrane Technology and Department of Chemical Engineering, Chung Yuan Christian University, 200 Chung Pei Rd., Chung-Li 32023, Taiwan

\* benavente@chimie.ups-tlse.fr, \*\* aimar@chimie.ups-tlse.fr

## Euromembrane 2015, Aachen, Germany, September 2015

### Oral presentation

#### FTIR mapping for membrane modification assessment

L. Benavente<sup>a,b</sup>, C. Coetsier<sup>a,b</sup>, A. Venault<sup>c</sup>, C. Causserand<sup>a,b</sup>, Y. Chang<sup>c</sup>, P. Bacchin<sup>a,b</sup>, P. Aimar<sup>a,b</sup>

<sup>a</sup> Université de Toulouse, INPT, UPS, Laboratoire de Génie Chimique, 118 Route de Narbonne, F-31062 Toulouse, France.

<sup>b</sup> CNRS, Laboratoire de Génie Chimique, F-31062 Toulouse, France

<sup>c</sup> R&D Center for Membrane Technology and Department of Chemical Engineering, Chung Yuan Christian University, 200 Chung Pei Rd., Chung-Li 32023, Taiwan

**Keywords:** membrane modification, FTIR, fouling resistance

### Poster

The poster features a light blue background with a grid pattern. On the left is the logo for 'LABORATOIRE DE GÉNIE CHIMIQUE TOULOUSE • UMR 5503'. The main title is 'In-situ monitoring of fouling dynamics with microfluidic chips integrating membranes'. Below the title is the author list: 'L. Benavente<sup>a,b,\*</sup>, D. Snisarenko<sup>a,b</sup>, C. Coetsier<sup>a,b</sup>, A. Venault<sup>c</sup>, C. Causserand<sup>a,b</sup>, Y. Chang<sup>c</sup>, P. Bacchin<sup>a,b</sup>, P. Aimar<sup>a,b,\*\*</sup>'. At the bottom, there are three footnotes: <sup>\*</sup>Université de Toulouse, INPT, UPS, Laboratoire de Génie Chimique, 118 Route de Narbonne, F-31062 Toulouse, France; <sup>\*\*</sup>CNRS, Laboratoire de Génie Chimique, F-31062 Toulouse, France; and <sup>\*\*\*</sup>R&D Center for Membrane Technology and Department of Chemical Engineering, Chung Yuan Christian University, 200 Chung Pei Rd., Chung-Li 32023, Taiwan. Email addresses are provided for L. Benavente and P. Aimar.



## Low Fouling Membranes for Water and Bio tech Applications

Water scarcity has become one of the key issues to solve, and efficient water treatment is paramount to treat water sources. In recent decades membrane technology has become one of the promising solutions for water treatment. Nevertheless, membranes are prone to fouling phenomena - the deposition, adsorption, and absorption of particles in the membrane structure -, which hinders their life-span and productivity, and raise operative costs. One approach to minimize this issue is to modify the already mechanically and chemically stable hydrophobic membranes with amphiphilic materials. The main aim of this work is to characterise the anti-fouling properties of PVDF (Polyvinylidene fluoride) membranes modified with different types of PS-PEGMA (Polystyrene – Poly(ethylene glycol) methacrylate) copolymers, firstly by using classical techniques, and then, by developing and/or adapting new ones: microfluidic devices coupled with fluorescence microscopy, and the use of Fourier Transform Infrared microspectroscopy (FTIR mapping). FTIR mapping allowed the local detection of the coating layer and showed its heterogeneous distribution on the surface of the membrane. These maps, that represent the importance of the coating on the membrane, were correlated with the deposit of proteins on the surface. Microfluidic systems were also developed to characterise the adsorption of fluorescent proteins on the membrane under a fluorescent microscope in the presence of a flow. This study allowed the in-situ and dynamic follow-up of the adsorption – during filtration cycles – and of the desorption – during rinsing cycles – of the proteins on the membrane. These local measurements were compared against permeability measurements during the filtration/rinsing cycles evidencing the anti-fouling role of the copolymers used for the modification of the membranes, particularly for the triblock and random copolymers.

*Keywords: fouling, water treatment, adsorption, membrane modification, PVDF, PS-PEGMA*

---

## Membranes à faible colmatage pour des applications de traitement des eaux et biotechnologiques

La pénurie d'eau est devenue un des problèmes clés à résoudre, et pour y faire face, il est nécessaire de disposer d'unités de traitement de l'eau efficaces. Au cours des dernières décennies la technologie des membranes est devenue l'une des techniques les plus prometteuses pour le traitement de l'eau. Néanmoins, les membranes ont une durée de vie limitée et sont, par ailleurs, sujettes à des phénomènes de colmatage - le dépôt, l'adsorption et l'absorption de particules dans la structure de la membrane -, ce qui réduit leur productivité, et augmente les coûts opérationnels. Une approche pour minimiser ce problème consiste à modifier des membranes hydrophobes, mécaniquement et chimiquement stables, en y greffant des matériaux amphiphiles afin de réduire le colmatage. L'objectif principal de ce travail est de caractériser les propriétés anti-colmatage des membranes de PVDF (Polyvinylidene fluoride) modifiées avec différents types de copolymères PS-PEGMA (Polystyrene – Poly(ethylene glycol) methacrylate), tout d'abord par l'utilisation de techniques classiques, puis, par le développement et / ou l'adaptation de techniques microfluidiques couplés à la microscopie à fluorescence et l'utilisation de la cartographie par microspectroscopie infrarouge à transformée de Fourier (IRTF). La cartographie IRTF a permis de quantifier localement le greffage et de mettre en évidence l'hétérogénéité du greffage sur la membrane. Ces cartes, représentant l'importance du greffage sur la membrane, ont par ailleurs été corrélées au dépôt de protéines sur la surface. Des systèmes microfluidiques ont également été développés pour caractériser sous microscope à fluorescence l'adsorption de protéines fluorescentes sur une membrane en présence d'un débit. Cette étude permet de suivre in situ et en dynamique l'adsorption (lors de cycles de filtration) et la désorption (lors de cycles de rinçage) de protéines sur la membrane. Ces mesures locales ont été mises en regard avec des mesures de perméabilité lors de cycles filtrations/rinçage mettant en évidence un rôle anti-fouling en particulier pour les copolymères tri-blocs ou pour les copolymères à enchaînement aléatoire.

*Mots clés: colmatage, traitement des eaux, adsorption, modification des membranes, PVDF, PS-PEGMA*